Calorimetric and Molecular Acoustic Study of Phospholipid-Sterol and Phospholipid-Peptide Interactions

DISSERTATION

zur Erlangung des Academischen Grades
Doktor der Naturwissenschaften
(Dr. rer. nat.)

eingereicht beim
Fachbereich Chemie
der Technischen Universität Dortmund

von

Linus Ndubuike Okoro M.Sc.

aus Mbaise, Nigeria

Dortmund, 2008

Erstgutachter: Prof. Dr. R. Winter

Zweitgutachter: Prof. Dr. H. Rehage

To the Almighty God

Acknowledgement

TABLE OF CONTENTS

1. INTRODUCTION

1.1 LIPIDS

Lipids are broadly defined as any fat-soluble (lipophilic), naturally occurring molecule, such as fats, oils, waxes, sterols, monoglycerides, diglycerides, phospholipids and others. Lipids are a diverse group of compounds that have many key biological functions, such as structural components of cell membranes, energy storage sources and intermediates in signaling pathways. For example, in recent years, evidence has emerged showing that lipid signaling is a vital part of the cell signaling [Wang 2004]. Lipid signaling may occur via activation of GPCR's or nuclear receptors, and members of several different lipid categories have been identified as signaling molecules and cellular messengers [Eyster 2007]. Lipids play diverse and important roles in nutrition and health [Spiller ed. 2006]. Many lipids are absolutely essential for life. However, there is also considerable awareness that abnormal levels of certain lipids, particularly cholesterol (in hypercholesterolemia) and trans fatty acids, are risk factors for heart disease amongst others. Lipids are small amphiphilic molecules. Many different lipid species can be found in biological cell membranes. Cell membranes are dynamic, fluid structures where the molecules are able to diffuse rapidly in the plane of the membrane.
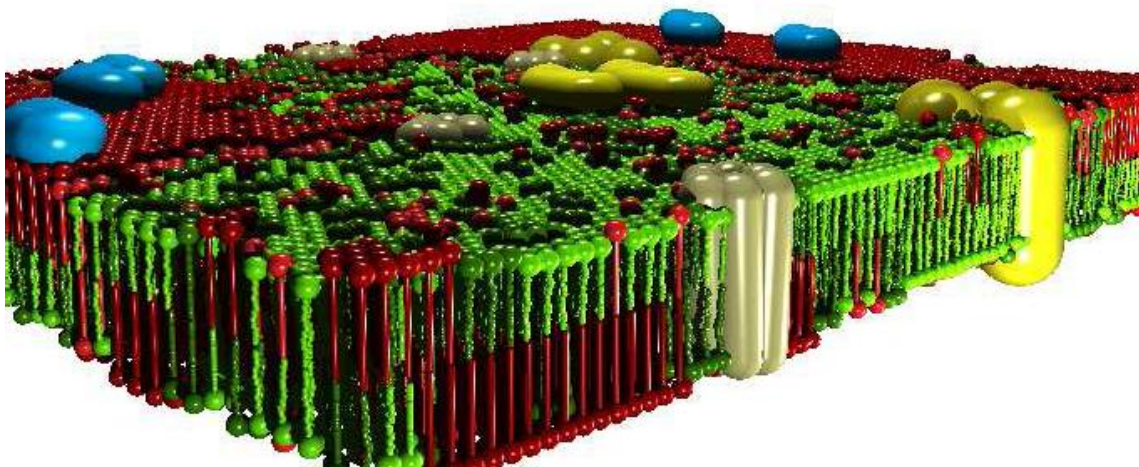
Figure 1.1: A modern picture of a biological cell membrane. The different colors of the smaller objects represent lipids with an ordered (red) or disordered (green) configuration. Lipid domains with different physical properties are formed. The aggregation of proteins (rigid, big objects) is allowed. Proteins might

prefer ordered or disordered lipids. This model allows the control of biological function because of the physics of the lipid membrane (*picture generated by H. Seeger, NBI Copenhagen*).

Membranes of eukaryotic cells have a complex composition consisting of hundreds of different lipids and proteins, plus cholesterol or closely related sterols (fig. 1.1).

Three particular families of lipids, which have a special status in biological membranes are phospholipids, glycolipids and sterols [Israelachvili 1980].

1.2   PHOSPHOLIPIDS

Glycerophospholipids, also referred to as phospholipid, are ubiquitous in nature and are key components of the lipid bilayer of cells, as well as being involved in metabolism and signaling. Glycerophospholipids (Ivanova 2007) may be subdivided into distinct classes, based on the nature of the polar headgroup at the *sn*-3 position of the glycerol backbone in eukaryotes and eubacteria or the *sn*-1 position in the case of archaebacteria. Examples of glycerophospholipids found in biological membranes are phosphatidylcholine (also known as PC and lecithin), phosphatidylethanolamine (PE) and phosphatidylserine (PS). In addition to serving as a primary component of cellular membranes and binding sites for intra- and intercellular proteins, some glycerophospholipids in eukaryotic cells, such as phosphatidylinositol and phosphatidic acids are either precursors of, or are themselves, membrane-derived second messengers.

Phospholipids are major components of the cell membrane. They are similar to fats, but have only two fatty acids rather than three. The third hydroxyl group of glycerol is joined to a phosphate group, which is negative in electrical charge. In other words, the phospholipid molecule consists of a phosphate-containing polar headgroup attached to two hydrophobic hydrocarbon chains (fig. 1.2). Additional small molecules, usually charged or polar, can be linked to the phosphate group to form a variety of phospholipids. Phospholipids are described as being amphipathic, having both a hydrophobic and a hydrophilic region. Their tails, which consist of hydrocarbons, are hydrophobic and are excluded from water. Their heads, however, which consist of the phosphate group and its attachments, are hydrophilic, and have an affinity for water.
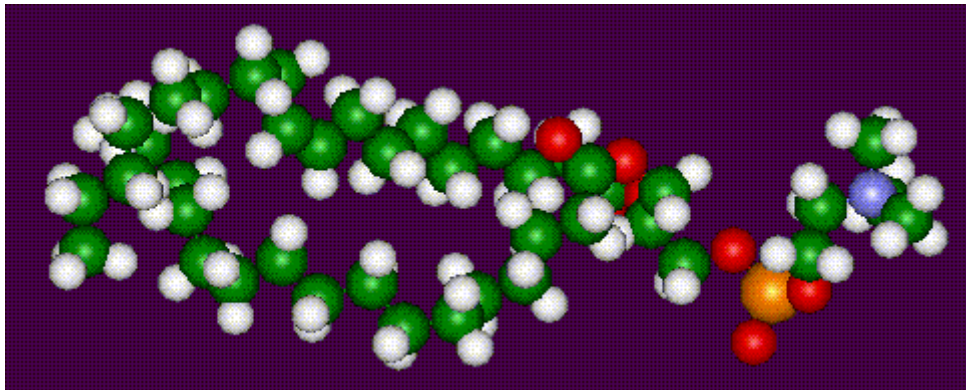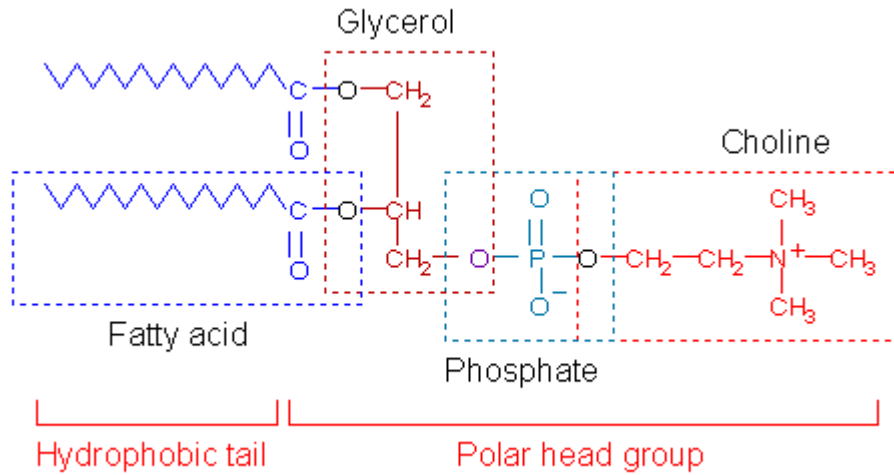
Figure 1.2: Structure of a phospholipid (phosphatidylcholine): (a) The chemical structure (b) The computer model.

Due to their structure, when phospholipids are added to water, they self-assemble into aggregates so that the phosphate heads make contact with the water and the hydrophobic hydrocarbon tails are restricted to water-free areas. Differences in the length and saturation of the fatty acid tails are important because they influence the ability of phospholipid molecules to pack in the bilayer, a factor that influences the fluidity of the bilayer.

1.3 STEROLS

Sterols, such as cholesterol, are important for the structural, dynamical as well as functional properties of biological membranes [Mouritsen 2004, Finegold 1993, Vance 2000]. They are found in high concentrations (even up to about 50 mol%) in plasma membranes of animal and higher plant cells, but in markedly lower concentrations in intracellular membranes where they are synthesized. Although sterols are classified chemically as lipids, they are synthesized by complex pathways independent of the pathways for the synthesis of other common lipids. Their biosynthetic pathways are long, complicated and energetically expensive. As an example, in order to synthesize cholesterol from acetyl-CoA about 30 enzymatically catalyzed steps are required. Along the biosynthetic path of cholesterol, a large number of sterols are synthesized as intermediates [Risley 2002]. The first sterol to be produced from squalene is lanosterol and from that point another 18 sterols will be made until cholesterol is synthesized. Thus, considerable cellular energy is spent on producing the specific structure of cholesterol. Cholesterol must therefore fulfil some important functions in higher vertebrate cells that cannot be fulfilled by any other sterol structure. Cholesterol performs a wide range of roles in human cells. It is the precursor for the synthesis of hormones and numerous other biologically important molecules [Russell 1992, Schoonjans 2000]. It has also been shown to influence the physical properties of membranes, such as their fluidity [Kusumi 1983, Bloch 1985] and also play other membrane-associated roles, such as in signal transduction [Simons 2000] and ion permeation [Haines 2001]. Mammalian cells die in the absence of cholesterol or if substituted with a plant sterol or with lanosterol or ergosterol. Cholesterol also cannot substitute for ergosterol in yeast and fungi. This observation leads to the conclusion that sterols are important for cell survival and also that only a particular sterol structure is suited for a particular cell type.

Ergosterol is the major sterol in many fungi and protozoans, where they fulfil various functions, including growth and regulating and maintaining membrane elasticity, permeability and integrity. A considerable amount of research has been devoted to elucidate the different biological functions of sterols and to understand the physical basis for their evolution by investigating the role of sterols in modulating physical properties of artificial and biological membranes, and to unravel the relationship between their function and molecular structure [Demel 1976, Yeagle 1985, Finegold 1993].

1.3.1   Lipid – Sterols Interaction

Cholesterol (see Figure 1.3) has a hydrophobic and planar fused tetracyclic ring structure with two β-oriented methyl groups at positions 10 and 13, a branched extended iso-octyl side chain at position C17, and a hydrophilic β-oriented hydroxyl group at position C3. The sterol ring orients itself parallel with the acyl chains of the membrane phospholipids, with its 3 β-OH group in proximity to the phospholipid ester carbonyl oxygen at the lipid−water interface. Van der Waals interactions between the lipid acyl chains and the sterol ring as well as its branched side chain seem to be the most important contributions stabilizing cholesterol−phospholipid interactions. It has been demonstrated by a variety of physical techniques [Zuckermann 2004], that cholesterol has a "condensing" (ordering) effect on the packing of phospholipids in their fluid-like (liquid-crystalline) state, because the rigid ring structure of the sterol limits the possibility for *cis-trans* isomerizations and kink formation of neighboring lipid chains, and a disordering effect below the chain-melting transition, i.e., in the gel state of the lipid bilayer.
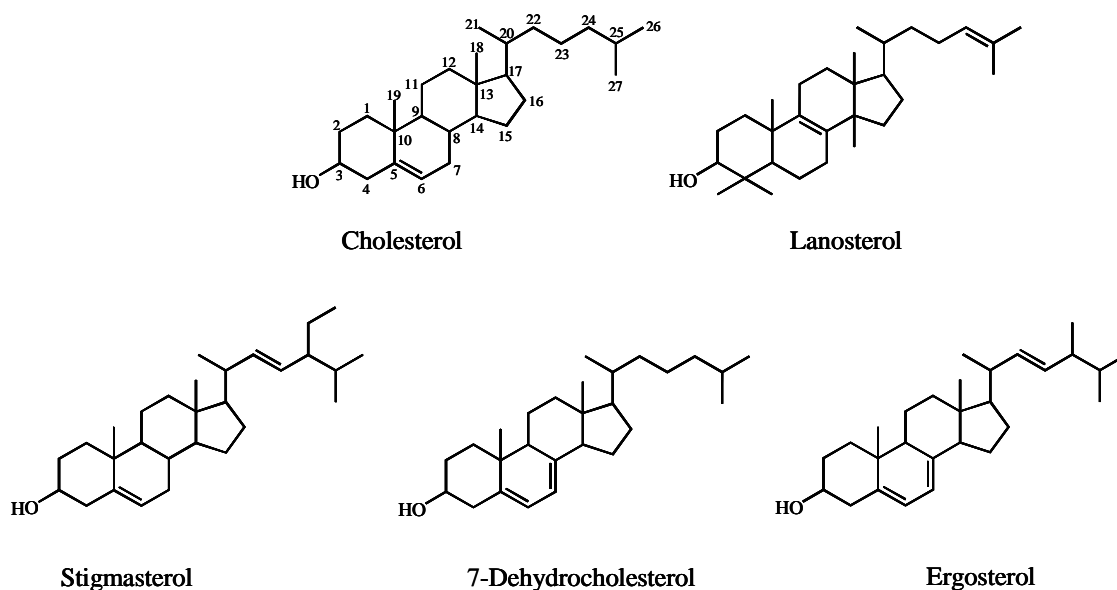
Figure 1.3: The chemical structures of the sterols used in this study. The formula of cholesterol includes the numbering of the carbon atoms.

The extent of these effects depends on the detailed molecular structure of the lipid, but probably also on the sterol conformation and stereochemistry [Bernsdorff 1996, Bernsdorff 1997, Miao 2002, McMullen 1994]. Whereas structural and dynamical properties of these systems have been studied to a significant extent, there is a lack of knowledge of thermodynamic functions of these systems [Melchior 1980, Böttner 1993, Seemann 2003]. Bacia et al [Bacia 2005] has shown also that a different sterol structure may induce a different curvature of giant unilamellar vesicles of model raft mixtures. Recently, Bernsdorf et al. investigated the influence of the sterol side chain and ring structure on the acyl chain orientational order of lipid bilayers by measuring the steady-state fluorescence anisotropy of the fluorophore 1-(4-trimethylammonium-phenyl)-6-phenyl-1, 3, 5-hexatriene (TMA-DPH) to establish the molecular basis underlying the changes in order parameter of the lipid bilayer system [Bernsdorff 2003]. Sterols with the bulkiest unsaturated side chains or sterol nuclei (stigmasterol, β-sitosterol and lanosterol) induce the smallest order parameter increase of the fluid bilayer at high sterol concentrations (> 30 mol%) and hence become less potent rigidifiers at high sterol levels. At the highest sterol levels, cholesterol and - even more pronounced - the plant sterol ergosterol have the most profound ordering effect on fluid DPPC bilayers [Bernsdorff 2003].

In this study, we investigated volumetric properties of lipid vesicles of the common phospholipid 1,2-dipalmitoyl-*sn*-glycero-3-phosphatidylcholine (DPPC), containing different amounts of various sterols up to 36 mol% sterol.

One of the very important features of phospholipid bilayers is their thermotropic phase behavior. Fully hydrated bilayers composed of a single phospholipid species undergo a well-defined gel to fluid phase transition. Each lipid has a characteristic transition temperature. Studies of the changes taking place at the phase transition provide a very valuable method of characterizing the properties of the fluid state, which is probably the most relevant to biological membranes. The fluid state is relevant to biological membranes because at body temperature a big proportion of the membrane lipids are above their main phase transition, *i.e.* in the fluid phase. The temperature at which the phase transition occurs in phospholipids depends on the hydrophobic tail structure of the specific lipid. A long tail length increases the tendency of the hydrocarbon tails to interact with each other and this in turn increases the transition temperature. If the hydrocarbon chain is unsaturated, then this produces a kink in the chain that makes it more difficult to pack with the rest of the lipid acyl chains. This results to lowering the transition temperature.

DPPC phospholipid bilayers exhibit two principal thermotropic lamellar phase transitions, corresponding to a gel-to-gel ($L_{\beta'}$-$P_{\beta'}$) pretransition and a gel to liquid-crystalline ($P_{\beta'}$-L_α) main transition at $T_m \approx 41.5$ ^{o}C [Cevc 1987]. In the fluid-like L_α phase, the hydrocarbon chains of the lipid bilayer are conformationally disordered, whereas in the gel phases, the hydrocarbon chains are more extended and relatively ordered. In general, sterol molecules are, in contrast to phospholipids, essentially rigid and relatively smooth in their hydrophobic parts. They prefer to have next to them lipid acyl chains that are ordered. On the other hand, because the sterols have different molecular shapes from conformationally ordered lipid chains, they tend to break the lateral packing of solid-ordered (s_o) phases. This can lead to the emergence of a physical state of lipid-sterol membranes, which has characteristics intermediate between a solid-ordered and liquid-disordered (l_d), the liquid-ordered (l_o) state (fig.1.4). In recent years, cholesterol-rich liquid ordered (l_o) structures have received much attention in membrane biophysics [Brown 1998, Baumgart 2003, Silvius 2003].

gel (s_o)   liquid disordered (l_d)   liquid ordered (l_o)
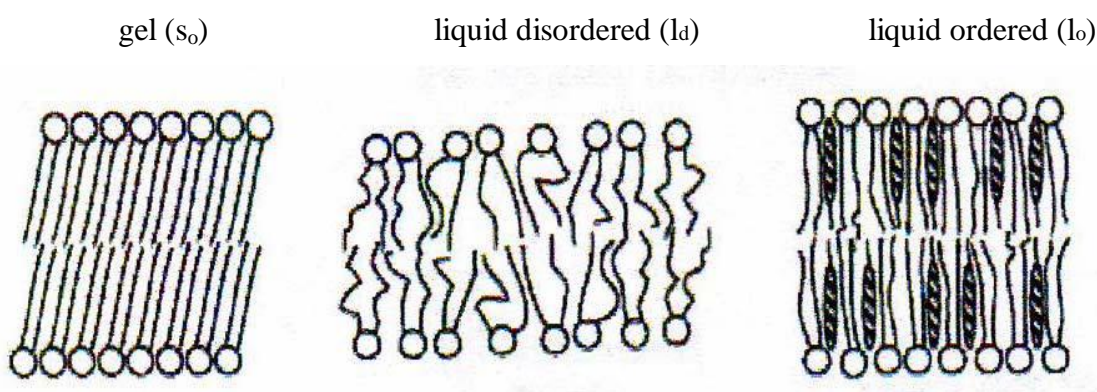
Figure 1.4: Membrane phases of the lipids of the plasma membranes. The gel phase melts above T_m to form a fluid phase (liquid-disordered (l_d)), sometimes referred to as "liquid-crystalline"). The presence of cholesterol (hatched ovals) forms an intermediate phase between gel and l_d, for which the term liquid-ordered (l_o) was coined (Munro, 2003).

 A hypothesis has been put forward that so-called rafts, which are liquid-ordered domain structures enriched in cholesterol and sphingolipids, exist in cell membranes and have potential functional importance in processes such as intracellular membrane sorting and signal transduction at the cell surface [Edidin 2003]. Only for selected phospholipid-sterol systems, temperature-concentration phase diagrams are available [Zuckermann 2004, Ipsen 1990, Vist 1990, Hsueh 2005]. They exhibit the one-phase regions l_d (liquid-disordered), s_o (solid-ordered), and l_o (liquid-ordered). In

addition, l_o+s_o and l_o+l_d two-phase coexistence regions – separated by a three-phase line - are found in the intermediate sterol concentration range at low and high temperatures, respectively. (The terms 'solid' and 'liquid' characterize mainly the fluidity of a phase, whereas 'ordered' and 'disordered' indicate the conformational state (order parameter) of the lipid acyl chains.) At sufficiently high temperatures, the l_o+l_d two-phase regions seem to be terminated in a critical point.

The focus of our study was to identify and characterize the differential effects of various sterols (Fig. 1.3) including cholesterol, ergosterol (which is essential in some fungi or protozoan cells), the plant sterol stigmasterol, *trans*-7-dehydrocholesterol (7-DHC), and lanosterol, the evolutionary precursor of cholesterol, on equilibrium volumetric properties of the DPPC bilayer membrane and to relate these effects to the difference in their molecular structure. To this end, pressure perturbation calorimetry (PPC) has been used, which allows determination of the temperature dependence of the coefficient of expansion coefficient, α, as well as volume changes accompanying lipid phase transitions. The PPC measurements were carried out over a wide temperature range in order to cover all relevant phase regions of these DPPC-sterol mixtures. Complementary DSC thermograms were also recorded to reveal temperature-dependent phase changes.

1.4 GRAMICIDIN D

In 1939 the French-American microbiologist Rene Dubos isolated the substance tyrothricin and later showed that it was composed of two substances, gramicidin (20%) and tyrocidine (80%). These were the first antibiotics to be manufactured commercially. Gramicidin is a heterogeneous mixture of antibiotic compounds, Gramicidins A, B and C, making up 80%, 6%, and 14% respectively [Bourinbaiar 1997], all of which are obtained from the soil bacterial species *Bacillus brevis* and called collectively Gramicidin D. Gramicidin D are linear pentadecapeptides; that is chains made up of 15 amino acids [Burkhart, 1999]. This is in contrast to gramicidin S, which has a cyclic peptide chain. Gramicidin is active against Gram-positive bacteria, except for the Gram-positive bacilli, and against selected Gram-negative organisms, such as Neisseria bacteria.

Gramicidin has the general formula: formyl-L-**X**-Gly-L-Ala-D-Leu-L-Ala-D-Val-L-Val-D-Val-L-Trp-D-Leu-L-**Y**-D-Leu-L-Trp-D-Leu-L-Trp-ethanolamine. X and Y depend upon the gramicidin molecule. There exists valine and isoleucine variants of all three gramicidin species

and 'X' can be either valine or isoleucine. Y determines which is which; in the place of Y, Gramicidin A contains Tryptophan, B contains Phenylalanine and C contains Tyrosine. Also note the alternating stereochemical configurations (in the form of D and L) of the amino acids: this is vital to the formation of the β-helix. The chain assembles inside of the hydrophobic interior of the cellular lipid bilayer to form a β-helix. The helix itself is not long enough to span the membrane but it dimerises to form the elongated channel needed to span the whole membrane.

1.4.1   Lipid – Gramicidin Interaction

The primary interest of gramicidin lies in its ability to form ion channels in lipid membranes. Gramicidin has been reported to form specific channels across the cell membrane and to enhance the transport of cations [Woolf 1994]. Gramicidin has no charged or hydrophilic side chains, and its aqeous solubility is low. As both the amino and carboxy termini of the molecule is blocked, gramicidin has been found to partition strongly into the hydrophobic region of phospholipid membranes and to maintain the liquid - crystalline state [Short 1987, Glowka 2005]. Extensive studies have been made on the influence of gramicidin on lipid polymorphism and of the ordering effects on the lipid chains [Killian 1992, Rice 1979, Kharakoz 1993, Szule 2003]. Gramicidin S has been found to progressively decrease the phase transition of DMPC vesicles as well as to decrease the degree of cooperativity of the main phase transition and to increase the volume compressibility of the vesicles [Krivanek 2001, Lewis 1999]. The PFG-NMR method has been used in microscopically oriented bilayers to investigate the effect of the Gramicidin D on the lateral diffusion of DMPC [Orädd 2004]. No evidence of linear aggregate of gramicidin in the gel phase was found. Aggregation of gramicidin A in phospholipids has been reported [Ivanova 2003].

It has also been observed that gramicidin insertion into the DMPC bilayer structure has significant influence on the lipid bilayer structure and temperature, pressure phase behaviour [Zein 2000, Eisenblätter 2006]. In his study, a small fluid-gel co-existence region and two pressure-induced gel phases, different from those of the pure lipid bilayer system, and which separate at low temperature/high pressure, upon gramicidin insertion was reported. Direct evidence of head-to head dimer formation has been observed in spin-labeled gramicidin A using double-quantum coherence electron spin resonance (DQC-ESR) [Ge 1999]. Further, the interaction between integral proteins and lipids has been found to depend on the relative length of

their hydrophobic core, a concept known as the 'hydrophobic matching' (Woolf 1996). In another study on the influence of drugs on the relaxation process in lipid membranes, Seeger et al, reported that gramicidin A decreased the temperature-dependence of the heat capacity as well as the magnitude and temperature-dependence of the relaxation time [Seeger 2007]. Gramicidin modulates the spontaneous curvature properties of the phospholipid assemblies [Szule 2003]. The effect of gramicidin D on the conductance and electroporation thresholds of planar bilayer membranes has been examined and was found to change their mechanical properties [Troiano 1999]. The vibrational circular dichroism (VCD) and absorption spectra of Gramicidin D in three model membranes (dioctadecyldimethylammonium chloride vesicles, dimyristoyl-phosphatidylcholine vesicles and sodium dodecyl sulfate micelles) have been studied. The study revealed that the presence of cations does not change the membrane-bound conformation of gramicidin D [Zhao 2001].

The structural basis for the reduction in channel conductance of single tryptophan analogues of gramicidin with three Trp→hydrophobic substitutions has been explored. It was reported that gramicidin analogues containing single a tryptophan residue adopt a mixture of non-channel and channel conformations, as evident from the analysis of the membrane penetration depth using size exclusion chromatography and backbone CD data [Chattopadhyay 2008]. It is known from calorimetry that peptides and proteins influence the chain melting transition of lipids. Usually, transition profiles are broadened and /or shifted to either lower or higher temperature. The small cyclic peptide gramicidin S has been reported to induce a shift of the heat capacity events to lower temperature [Lewis 1999]. It has been shown as well, that the presence of peptide or proteins in the membrane can significantly affect the dynamic structure of the bulk lipid [Ge 1994].

The goal of this study is to incorporate different gramicidin D concentrations into DPPC bilayer, and to determine the effects of increasing concentrations of gramicidin D on the lipid bilayer membrane compressibility and volume changes / fluctuations in their different transition phases. To this end, we have used molecular acoustics (ultrasound velocity and densitometry) and calorimetry (pressure perturbation calorimetry and differential scanning calorimetry). This is the first time that such a multi-technique approach could be employed for the study of DPPC – gramicidin interactions, to the best of our knowledge. In this study we have

been able to reveal a considerable influence of gramicidin D on the thermodynamic, mechanical, volume and compressibility properties of DPPC bilayer.

1.5 MELITTIN

Melittin, the principal toxic component in the venom of the European honeybee, *Apis mellifera*, is a cationic hemolytic peptide [Sessa 1969, Habermann 1972, Tosteson 1985]. It constitutes 50% of the dry weight of the bee venom. The active peptide melittin is released from its precursor, promelittin, during its biosynthesis in honey bee and later gets formylated [Habermann 1972]. It is composed of 26 amino acids (NH2-G-I-G-A-V-L-K-V-L-T-T-G-L-P-A-L-I-S-W-I-K-R-K-R-Q-Q-CONH2) in which the amino-terminal region (residues 1–20) is predominantly hydrophobic whereas the carboxy-terminal region (residues 21–26) is hydrophilic due to the presence of a stretch of positively charged amino acids. Melittin amphiphilic property makes it water soluble and yet it spontaneously associates with both natural and artificial membranes [Dempsey 1990]. The crystal structures of melittin have been resolved by X-ray crystallography [Terwilliger 1982]. In an aqueous solution of high peptide concentration, high pH value, or high ionic strength, tetrameric melittin of high symmetry is formed readily [Dempsey 1990]. The hydrophobic surface of each amphipathic α-helical monomer is essentially completely removed from solvent exposure upon tetramerization.

1.5.1   Lipid – Melittin Interaction

Melittin causes bilayer micellization and membrane fusion and has also been observed to form voltage-dependent ion channels across planar lipid bilayers [Bechinger 1997, Monette 1996]. The characteristic action of melittin is its hemolytic activity (Habermann 1972, DeGrado 1982, Rudenko 1995, Raghuraman 2005]. It is commonly believed that multimeric pore formation is the mode of action of many naturally produced peptides such as antimicrobial peptides and toxins [Allende 2005, Rapaport 1996, Rex 1996]. Few studies have been attempted to monitor the structure and function of such pores and their results show that melittin forms pores that have a rather wide distribution of sizes. For example, the sizes of the melittin pores that are characterized by the inner pore diameter have been reported to be in the range of 10–60 A°, 13–

24 A° and 25–30 A° [Rex 1996, Matsuzaki 1997] from vesicle leakage experiments. The diameter of these pores is expected to increase when the peptide concentration is increased.

Under certain conditions, melittin molecules insert into the lipid bilayer and form multiple aggregated forms that are controlled by temperature, pH, ionic strength, lipid composition and the lipid-to-peptide ratio. Lipid composition and phase separation appears to play a critical role in melittin-induced pore formation. The action of melittin on membrane proteins has been studied and apart from its ability to disrupt lipid bilayers, melittin affects the dynamics of membrane proteins. For instance, it has been shown that lytic concentrations of melittin dramatically reduce the rotational mobility of band 3 protein in human erythrocyte membranes [Clague 1988, Hui 1990].

Melittin oligomers appear to be involved in membrane permeabilization, which supralinearly depends on the peptide concentration in both voltage-gated ion channel experiments [Pawlak 1991]. The orientation of melittin in a phospholipid bilayer has been explored (including molecular dynamics simulation studies) and was found to be sensitive to the experimental conditions [Bachar 2000, Bradshaw 1994, Lin 2000]. The aggregation state of melittin in membranes is an important issue since this property is presumed to be associated with the function of melittin. This can be appreciated by the fact that melittin forms voltage-gated channels [Tosteson 1981] which may require self association of melittin monomers to form pores in membranes. It is not known whether pore-forming melittin aggregates pre-exist in the membrane in the absence of an applied membrane potential.

Membrane fusion between liposomes composed of acidic phospholipids and neutral phospholipids induced by melittin has been studied using DSC [Higashino 2001], in which the roles of hydrophobic and electrostatic interactions were investigated in membrane fusion induced by melittin. These results indicate that a peptide containing hydrophobic and basic regions can mediate membrane fusion between neutral and acidic liposomes by hydrophobic and electrostatic interactions. Teng et al. have explored the effect of high pressure on the association of melittin to membrane. They discovered that the increase in lipid chain parking induced by pressure does not alter the association of bound complexes [Teng 1993]. Light scattering and ^{31}P-NMR have been used to monitor the effects of melittin on phosphatidylcholine (PC) bilayers of variable acyl chain length (from C16:0 to C20:0). From the experiment it was observed that melittin interacts with all lipids provided the interaction is initiated in the lipid fluid phase [Faucon 1995]. Unger et al. has studied the effect of cyclization of melittin analogues on the structure, function, and model

membrane interactions. It was found that cyclization altered the binding of melittin analogues to phospholipid membranes and had increased the antibacterial activity but decreased the hemolytic activity [Unger 2001]. The interaction of melittin and phospholipids has been extensively studied partly because it has a secondary amphiphilic property [Terwilliger 1982, Ladokhin 1999] as well as a model for this class of peptides. Interestingly, the role of melittin–lipid interactions has also been shown to be responsible, along with more specific binding of melittin with membrane proteins, for the inhibition of the Ca^{2+}-ATPase [Baker 1995] and protein kinase C [Raynor 1991]. The dependence of melittin aggregation on temperature [Iwadate 1998] and its thermodynamics, as determined by circular dichroism spectroscopy, has been reported [Wilcox 1992].

Melittin has been a source of inspiration for the development of novel antiviral and antibacterial agents that act at the membrane level to cause leakage in their lethal mechanism [Baghian 1997]. The interaction of melittin with membranes in general, and with cholesterol-containing membranes in particular has been explored, with possible relevance to its interaction with the erythrocyte membrane [Raghuraman 2004]. In an experiment to investigate the lipid-binding behavior of three peptides: melittin, magainin II, and cecropin P1, Lad et al. observed that melittin binding to lipids was 50% greater for either magainin or cecropin [Lad 2007].

The lytic activity of melittin has been reported to strongly depend on the membrane composition. Whereas zwitterionic lipids are more affected by the melittin lytic activity [Monette 1995], membranes with longer hydrocarbon chains are less affected [Bradrick 1995]. Although cell lysis by melittin has been extensively studied, the molecular mechanism of its hemolytic activity is still not well understood. In particular, the role of specific lipids on melittin-induced hemolysis is not yet clear. Detailed volumetric properties and thermodynamic information on melittin in membranes is important due to the widespread occurrence of the motif in host-defense peptides and membrane proteins. DPPC, one of the best studied phospholipids is a zwitterionic phospholipid with a medium tail consisting of 16 carbons and has a length appropriate for the study of melittin action on lipids.

In this study, we have been able to obtain a more detailed volumetric, thermodynamic and mechanical picture of melittin-DPPC bilayers around the phase transition temperature as revealed by calorimetry and molecular acoustic, and to gain more insight into the molecular mechanism of the lytic and fusion activity of melittin on DPPC membranes.

2.   MATERIALS, SAMPLE PREPARATIONS AND METHODS

2.1 MATERIALS

1, 2-dipalmitoyl-*sn*-glycero-3-phosphocholine (DPPC)	Avanti Polar Lipids
Cholesterol	Sigma-Aldrich
7-dehydrocholesterol (7-DHC)	Sigma-Aldrich
Lanosterol	Sigma-Aldrich
Stigmasterol	Sigma-Aldrich
Ergosterol	Fluka
Gramicidin D (gD)	Sigma-Aldrich
Melittin	Calbiochem (Germany)

All chemicals were used without further purification.

All other materials were reagent grade and obtained from commercial sources.

2.2 DATA ANALYSIS

The analysis of the acquired data and their eventual representation as thermograms was carried out using the program Origin 7.0 Software for Windows, version 7.0, Microcal, USA.

2.3 SAMPLE PREPARATIONS

2.3.1 Multilamellar vesicles for calorimetric studies

Multilamellar vesicles (MLV) of DPPC and model sterols / peptides with designated mole ratios were mixed in a chloroform-methanol mixture (3:1 v/v) and dried as a thin film under a stream of nitrogen and then freeze-dried in a freeze-dryer (Christ, Osterode, Germany) under high vacuum overnight. The lipid films were hydrated in a Tris buffer (10 mM Tris-HCl, 100 mM NaCl, pH 7.4), followed by vortexing at ~62°C (above the main phase transition temperature, T_m, of DPPC (~41.5°C [Cevc 1987]), and five freeze-thaw cycles, resulting in homogeneous multilamellar vesicles (MLVs). The final DPPC concentration used in the calorimetric measurements was 10 mg/ml for sterols, 10 mg/ml for gramicidin D, and 5 mg/ml for melittin.

2.3.2 Large unilamellar vesicles for the ultrasonic velocity and density study

Large unilamellar vesicles (LUVs) of uniform shape and size used in the ultrasound velocity and the density measurements were prepared from the MLVs by extrusion [MacDonald 1991] using a Mini-Extruder (Avanti Polar Lipids Inc., Alabaster, AL, USA), and passing them through 100 nm Nuclepore® Polycarbonate Track-Etch™ Membranes (Whatman GmbH, Dassel, Germany) at ~60°C. The final DPPC concentration used in the ultrasound velocity and the density measurements for both gramicidin D and melittin was 5 mg/mL.

2.4   METHODS

2.4.1 Extruder

By extruding multilamellar vesicles it is possible to obtain unilamellar vesicles which only consist of one lipid bilayer. Unilamellar vesicles do not sink to the bottom of the solution, but stay in solvent, because of their small size and mass. The extruder consists of two syringes pushing the solvent through a polycarbonate filter with a pore size of 100 nm (see fig. 2.1)

Figure 2.1: The extruder.

The extrusion was done at least 20 times, to make sure that all the vesicles were unilamellar, and slowly so that the filter did not break. The extrusion was done above the melting temperature of the lipid membranes, because the membranes are then softer and easier to extrude. A sample of extruded vesicles is more transparent than a sample of multilamellar vesicles and has a hazy blueish colour.

2.4.2   Calorimetric measurements

2.4.3   Differential scanning calorimetry

Pressure perturbation calorimetry and differential calorimetry measurements were performed with a MicroCal (Northampton, USA) VP-DSC micro-calorimeter, equipped with a pressurizing system from the same manufacturer.

The reference cell was filled with the Tris buffer solution. Both buffer and sample solutions were degassed before being injected into the respective cells. Included in the standard VP-DSC instrument is a pressuring cap that allows application of 1.8 bars to the cells in order to avoid air bubbles at elevated temperatures. The instrument was operated in the high gain mode at a scanning rate of 40 $^{\circ}$C h^{-1}. Baseline subtraction (pure buffer) and normalization with respect to scan rate and concentration were performed by the instrument software, yielding the temperature-dependent apparent (excess) molar heat capacity of the vesicles, C_p, with respect to the buffer solution.

2.4.4   Pressure perturbation calorimetry (PPC)
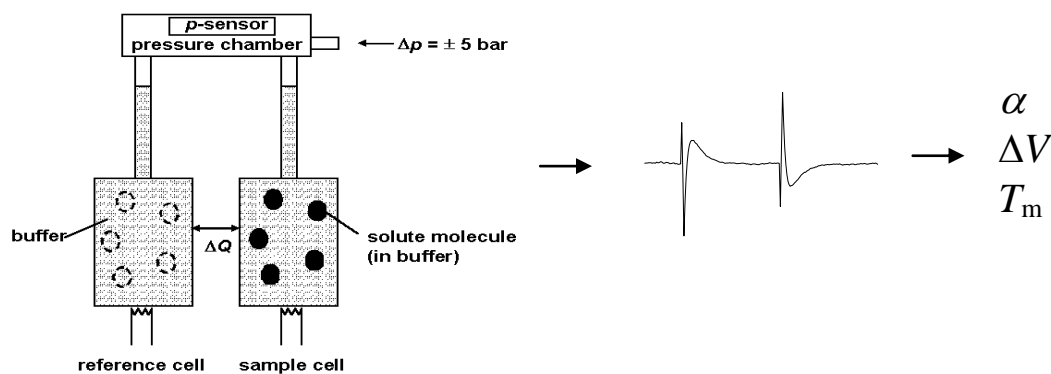
Figure 2.2: Schematic diagram of PPC describing the measurement curves and the derived thermodynamic parameters (*Microcal user note, 2000*).
.

Pressure perturbation calorimetry (PPC) measurements were carried out on the VP-DSC calorimeter equipped with MicroCal's (Northampton, MA, USA) PPC accessory.

This novel method allows to measure heat effects induced by small periodic changes of gas pressure ($\Delta p = \pm 5$ bar) above the solution [Heerklotz 2002, Ravindra 2003, Dzwolak 2003, Mitra 2006]. The physical principle is the same as in a heat-induced thermal expansion, although the measurable is ΔQ - the heat released upon a pressure change of Δp at temperature T. Three control and calibration measurements were performed, namely water (sample cell) versus water (reference cell), buffer versus water and buffer versus buffer. The results of these control experiments were fit by second-order polynomials and were used for the evaluation of the coefficient of thermal expansion α (T) of the measured system. From the relative volume changes $\Delta V/V$, the absolute volume changes ΔV can be determined when the specific volume and the molar mass of the sample are known [Seemann 2003, Krivanek 2008]. Knowing the thermal expansion coefficient of the solvent, α_0, mass, m, and partial specific volume of the solute, V_s, through a series of reference measurements, one can calculate the apparent thermal expansion coefficient of the dissolved particles:

2.4.4.1 Theory

The basic theory of pressure perturbation calorimetry is outlined below:

The heat of a reversible process, dQ_{rev}, is related to the entropy change, dS, at the temperature T.

$$dQ_{rev} = TdS \tag{1}$$

Differentiation with respect to pressure, p, yields

$$\left(\frac{\partial Q_{rev}}{\partial p}\right)_T = T\left(\frac{\partial S}{\partial p}\right)_T \tag{2}$$

From $dG = Vdp - SdT$, it follows that

$$\left(\frac{\partial S}{\partial p}\right)_T = -\left(\frac{\partial V}{\partial T}\right)_p \tag{3}$$

Eqn. (2) can thus be rewritten as

$$\left(\frac{\partial Q_{rev}}{\partial p}\right)_T = -T\left(\frac{\partial V}{\partial T}\right)_p \qquad (4)$$

The thermal expansion coefficient of volume V is defined as

$$\alpha_v = \frac{1}{V}\left(\frac{\partial V}{\partial T}\right)_p \qquad (5)$$

and can thus be determined from an isothermal measurement of the heat consumed or released upon a small pressure change:

$$\alpha_v = -\frac{\Delta Q_{rev}}{TV\Delta p} \qquad (6)$$

Moreover, the relative volume change $\Delta V/V$ at a phase or structural transition, taking place in the temperature range from T_o to T_e can be obtained by

$$\frac{\Delta V}{V} = \int_{T_o}^{T_e} \alpha(T)\,dT \qquad (7)$$

For two-component systems, such as biopolymer solutions, one has to extend these equations [Lin 2002, Kujawa 2001]. If the sufficiently dilute solution is composed of m_s grams of a solute dissolved in m_0 grams of solvent, the total solution volume V may be expressed as

$$V = m_0 V_0 + m_s \overline{V_s} \qquad (8)$$

where V_0 is the specific volume of the pure solvent, and V_s is the partial specific volume of the solute in the solution. The partial volume of the solute includes not just its intrinsic volume, but also any volume changes induced as a result of interactions with the solvent. Differentiating Eqn. (8) with respect to temperature at constant pressure yields

$$\left(\frac{\partial V_{total}}{\partial T}\right)_p = m_0\left(\frac{\partial V_0}{\partial T}\right)_p + m_s\left(\frac{\partial \overline{V}_s}{\partial T}\right)_p \tag{9}$$

and after substituting the right hand side of Eq. (9) into Eq. (4) and (5), we obtain

$$\left(\frac{\partial Q_{rev}}{\partial p}\right)_T = -T\left[m_0\left(\frac{\partial V_0}{\partial T}\right)_p + m_s\left(\frac{\partial \overline{V}_s}{\partial T}\right)_p\right] = -T\left[m_0 V_0 \alpha_0 + m_s \overline{V}_s \overline{\alpha}_s\right] \tag{10}$$

$\alpha_0 = (1/V)(\partial V_0 / \partial T)_p$, is the α of the solvent volume and $\overline{\alpha}_s = (1/\overline{V}_s)(\partial \overline{V}_s \partial T)_p$ is the α of the solute partial volume. The heat arising from pressure perturbation of the solution can thus be viewed as the sum of that arising from the perturbation of the solvent and from the perturbation of the solute in solution. Integration of Eqn. (10) over a small pressure range Δp leads to

$$\Delta Q_{rev} = -T\left[m_0 V_0 \alpha_0 + m_s \overline{V}_s \overline{\alpha}_s\right]\Delta p \tag{11}$$

In a differential PPC experiment, with sample solution in the sample cell and buffer in the reference cell, both cells are subjected to the same Δp so that the net heat change ΔQ_{rev} will be equal to the difference between Eqn. (11) for the sample cell and that for the reference cell. If the cells have an identical volume, then ΔQ_{rev} arises because the volume occupied by the solute in the sample cell, is replaced by solvent in the reference cell, *i.e.*,

$$\Delta Q_{rev} = -T(m_s \overline{V}_s \overline{\alpha}_s - m_s \overline{V}_s \alpha_0)\Delta p \tag{12}$$

which then rearranges to

$$\overline{\alpha}_s = \alpha_0 - \frac{\Delta Q_{rev}}{Tm_s \overline{V}_s \Delta p} \tag{13}$$

where the total mass of solute, m_s, is obtained by multiplying its concentration, c_s [g/mL] with the cell volume, V_{cell} [mL].

2.4.5   Ultrasonic resonator technology (URT)

Ultrasonic Resonator Technology (URT) is a novel method based on the high-resolution measurement of ultrasonic velocity and absorption. Unlike other techniques that characterize a sample's electromagnetic properties, sound propagation compresses and expands the sample, thus determining with very high sensitivity the sample concentration, structure, and, in particular, intermolecular forces and their change over time or temperature. URT uniquely provides information on the sample's dynamic properties and their effect on physical stability. URT complements current methodologies by extending label-free physical characterization to a new dimension, saving time and increasing confidence in producing more stable products. This label-free approach as well results in facile analysis and rapid analysis times under real conditions. With URT, one can directly probe the mechanical properties of samples and their surrounding media. This provides incremental information about the sample which allows one to quantify both inter- and intra- molecular forces as they change over time or with temperature.

URT detects minute changes at the molecular level within a liquid sample by creating a standing field of acoustic waves between two parallel transducers. The methodology is different from other sound-based techniques, such as those used in medical imaging; it uses two high-precision transducers opposite one another to produce a standing sound wave in a temperature controlled sample chamber. URT can detect changes in the speed of sound (ultrasonic velocity, u) and energy attenuation (ultrasonic attenuation, A) that occur when the properties (e.g., lipid melting transition) of the sample change over time or with varying temperature. The power levels employed in URT are so low that they leave the samples unchanged and the sample can be recovered and analysed further. The use of sound has several advantages over spectroscopic methods including the analysis of opaque samples from low to high viscosity. Dr. Theodor Funck and his colleagues first developed the technology at the Max Planck Society in Germany in the 1970s. Today, URT and related ultrasonic technologies are used by various industries for the characterization of liquid samples, including polymers, nucleic acids, lipids and proteins at low and high solute concentration. In a surprising discovery in 2002, TF instruments demonstrated that the URT is applicable to the diagnosis of human diseases: ultrasonic measurements using body fluids of patients suffering from various neurological diseases and of healthy individuals revealed distinct differences between the various samples.

Using the URT the intrinsic physical properties of a liquid samples are characterized with unmatched resolution and accuracy. The URT permits insights into important properties and interactions down to molecular dimension.
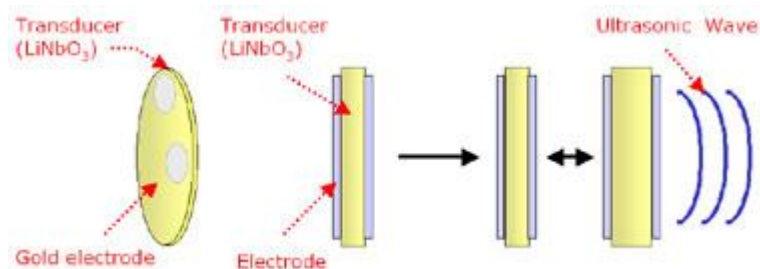
Figure 2.3: Sound generator made of a monocristaline LiNbO3 disc (*TF Instruments*).

The sound wave is produced by a sound generator, which in the case of the ResoScan is a monocristaline LiNbO3 disc (fig. 2.3) coated on two surfaces with gold serving as electrodes. It acts as a transducer (as it converts oscillation of electrical voltage into mechanical vibration generating the ultrasonic wave) as well as a piezoelectric material (it changes its thickness when an electrical voltage is applied).
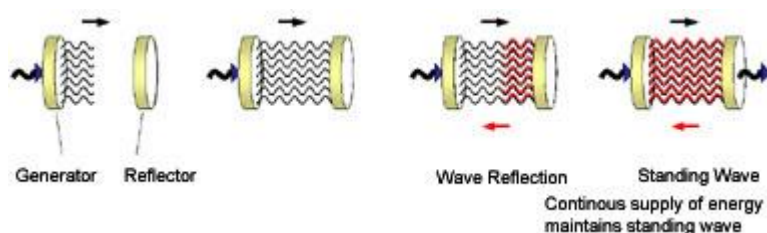
Figure 2.4: Establishing standing waves between transducers (*TF Instruments training course*).

The generated ultrasonic wave is reflected by a reflector (fig. 2.4). Friction and other processes on the molecular level lead to a conversion of energy of the sound wave into heat. The continuous supply of energy maintains the wave field within the resonator (standing wave). The (resonance) frequency of the standing wave amplifies any subtle change within the sample and therefore provides high resolution.

2.4.5.1   Ultrasonic resonator with fixed transducers

If sound waves generated by an oscillating wall (transducer) are reflected by a solid wall (reflector), then in the space between transducer and wall the sound waves are subjected to

interference phenomena. If the reflector is at a fixed distance D from the transducer and precisely parallel, acoustical resonances can be observed in the space between transducer and reflector. It is evident from Fig. 2.5 that sound waves of certain wavelengths, i.e. of certain frequencies, are enhanced by reflection and interference. In these cases the sound waves form a field of standing waves at defined resonance frequencies. The lowest resonance frequency, the so-called fundamental resonator frequency f, corresponds to a half wavelength of sound and permits the calculation of the sound velocity u from the distance D and the observed fundamental resonance frequency f.
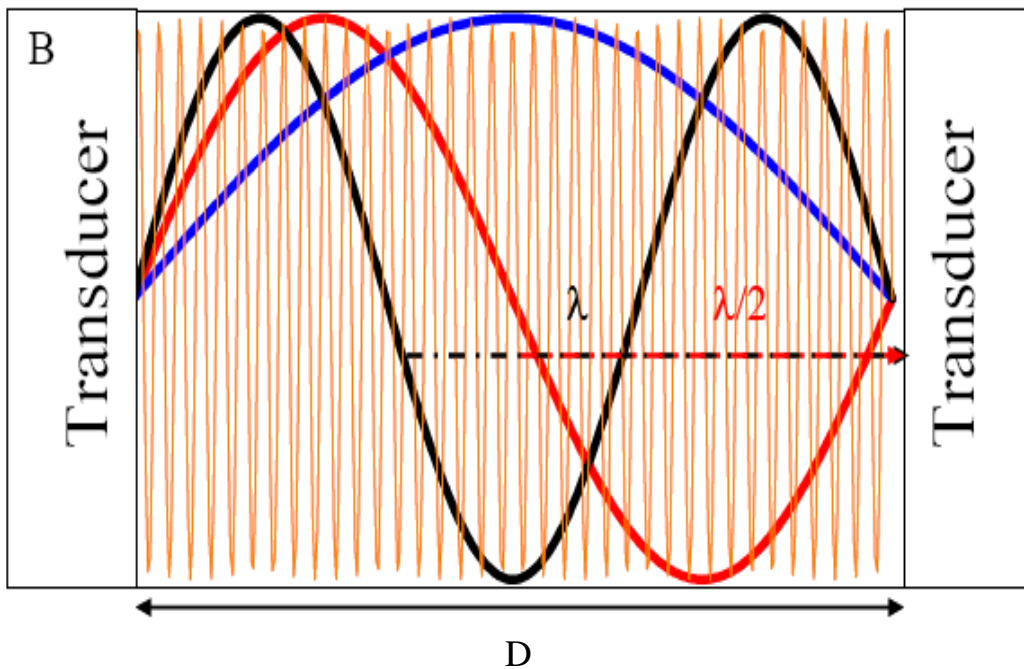
Fig. 2.5: Standing wave pattern (*adapted from TF Instruments training course*).

2.4.5.2   The physical features of sound

The propagation of sound, which is a longitudinal compressional wave, is determined by the properties of the medium. The phenomena of sound are well described by Newton's second law, which describes the force acting on an element of the material and accelerates it. Hence, the sound velocity u is determined by the mass of the material and the elastic forces hindering the movement of the material elements (Wood equation or Newton-Laplace equation).

2.4.5.3   Propagation of sound waves

 If a sample is compressed by a single shift of a solid wall of its container, the movement of the elements of the sample is transferred to neighboring elements due to the elastic forces in the sample, in other words this compression pulse propagates through the sample with the speed of sound. If the wall moves periodically back and forth at the position $x = 0$ with a frequency f, a uniform field of compressional waves is generated as shown in Fig. 2.5. The characteristic magnitudes of the compressional sound wave are described by the wave equation (Eq. 14):

$$f = u/\lambda \tag{14}$$

Where λ is the wavelength of the sound waves. The sound velocity u can be considered in most practical cases as frequency independent. It is characteristic for any material and depends on the density and the elastic forces in the material. Typical values for the velocity of sound in different materials are: Vacuum: 0 m/s, Air: 330 m/s, Liquids: 800-2000 m/s, Water: 1500 m/s, Solids: 5000-10000 m/s. It is evident from Fig. 2.5 that in the compressional longitudinal sound wave the elements of the material move back and forth in the direction of the propagation of the sound wave. The amplitude of this movement is on the order of 0.1 nm.

2.4.5.4   Ultrasound velocity measurement of lipid-peptide mixtures

The ultrasound velocity u of the vesicles was determined simultaneously using a differential ultrasonic resonator device ResoScan (TF Instruments, Heidelberg, Germany, operating in a frequency range of 7.2 – 8.5 MHz: see figure 2.6) [Eggers 1969, Eggers 1973, Stuehr 1965].
Ultrasonic measurements are extremely sensitive to temperature changes. Reproducibility and accuracy is therefore crucially dependent on TFI's Ultra-high Precision Peltier-Thermostat that reaches temperature constancy better than 1 mK (0,001 °C), and features a fast heating, cooling and equilibration time between 5 and 85 °C.

Figure 2.6: The picture of TF Instruments Ultrasonic Resonator in our laboratory.

The sound velocity of the lipid dispersion was determined relative to that in the buffer solution at the same temperature in terms of the velocity number, $[u]$, defined as [Stuehr 1965].

$$[u] = (u - u_0)/u_0 c \tag{15}$$

Where u and u_o denote the sound velocity in the solution and in the solvent, respectively, and c is the solute concentration in mol/L.

2.4.6 Densitometry

The densities, ρ and ρ_0, of the lipid solution and the solvent, respectively were measured by a high-precision density meter DMA 5000 (Anton Paar, Graz, Austria) (Fig. 2.7) based on the mechanical oscillator principle [Kratky 1973], corrected for viscosity-induced errors.
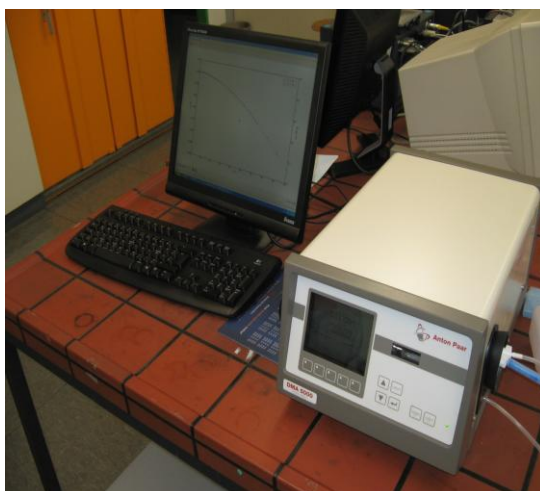
Figure 2.7: The Picture of the Anton Paar DMA 5000 Densitometer in our laboratory.

The determination of density is a well-established tool for product monitoring and quality control. Knowledge of the density is required for many complex applications, including research and development projects. Several methods can be used to measure the density of a liquid. The pycnometer and the hydrometer are traditional instruments for density determination, to name a few. The demand for an instrument that provides increased precision as well as fast results led to the development of the DMA 5000 density meter.

The first digital density meter ever, the DMA 02C, was introduced in 1967. The measuring principle of the DMA 02C was based on the U-tube method which revolutionized density determination as it allowed fast and reliable results with much better repeatability. Soon this method, developed by H. Stabinger and H. Leopold, was established worldwide and became the acclaimed standard method for density determination.

Over the years, this technology was further improved. The result is the DMA 5000 developed by Anton Paar which is regarded as among the best and accurate high-precision density meter in the market.

The DMA 5000 has the following specifications: measuring range 0 to 3 g/cm^3, accuracy density: ± 0.000005 g/cm^3, temperature: ± 0.01 °C, repeatability, specific density: 0.000001 g/cm^3, temperature: 0.001 °C, measuring temperature 0 to +90 °C, pressure range 0 to 10 bar (0 to 145 psi), and minimum amount of sample, approx. 1 mL.

The DMA 5000 density meter combines the well known Anton Paar U-tube measuring principle with the patented reference oscillator built into the measuring cell that eliminates long-term drift, and a high-precision Platinum thermometer seen as the most accurate temperature sensor available. The viscosity of a sample affects the density determination. The DMA 5000 automatically corrects the viscosity influence on density over the whole viscosity range, whether the samples have high or low viscosity.

2.4.6.1 The measuring principle

A U-shaped glass tube of known volume and mass is filled with the liquid sample and excited electronically by a Piezo element. The U-tube is kept oscillating continuously at the characteristic frequency f. Optical pick-ups record the oscillation period T as:

$$T = 1/f \tag{16}$$

This frequency is inversely proportional to the density ρ of the filled-in sample. The reference oscillator speeds up the measurements when aiming at various measuring temperatures. Once the instrument has been adjusted with air and water, the density of a sample can be determined. Hence, related parameters, e.g. concentration, are calculated from the density.
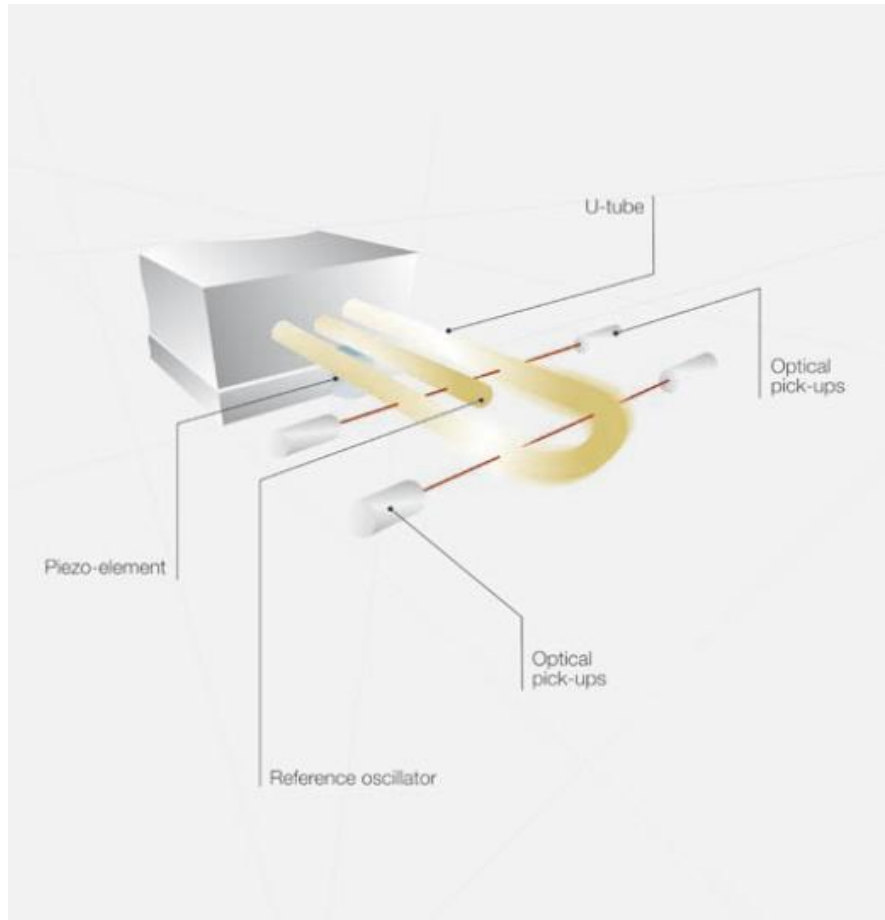
Figure 2.8: The Densitometer U-shaped tube (*Anton Paar*).

The Anton Paar DMA 5000 wide range of applications not only includes research purposes, but also in government and standardization organizations, institutions with the need for accurate results, which includes the Beverage industry for the determination of sugar content in soft drinks and fruit among other uses, the Pharmaceutical industry and medical science for the determination of specific gravities of medical preparations.

The density meters determine the density ρ of liquids and gases by measuring the period of oscillation. To this end, the sample is introduced into a system which can oscillate and whose "natural frequency" is influenced by the mass of the sample. This system is a U-shaped tube which is excited to undamped oscillations by electronic means. Both straight sections of the U-shaped tube form the spring element of the oscillator. The direction of the oscillation is perpendicular to the plane of the U-shaped tube. The oscillating volume V is limited by the

mounting points which are fixed. If the oscillator has been filled with the sample at least up to the mounting points, then the same known volume V of the sample also oscillates. The mass of the sample can therefore be considered as proportional to its density. If the oscillator has been filled beyond the mounting points, this has no effect on the measurement. For this reason, the oscillator can also measure the densities of samples flowing through it.

Assuming that the temperature is held constant, the density can be calculated from the period by considering a hollow body with mass M suspended on a spring constant s. The volume V of the hollow body is then filled with a sample of density ρ. The natural frequency of this spring mass system is:

$$f = \frac{1}{2\pi} \sqrt{\frac{s}{M + \rho V}} \qquad (17)$$

The period T is:

$$T = 2\pi \sqrt{\frac{M + \rho V}{s}} \qquad (18)$$

The density dependent on the period T is:

$$\rho = \frac{T^2 s}{4\pi^2 V} - \frac{M}{V} \qquad (19)$$

Using the abbreviations $A = c/4\pi^2 V$ and $B = M/V$, we arrive at:

$$\rho = AT^2 - B \qquad (20)$$

The constants A and B comprise the spring constant of the oscillator, the mass of the empty tube and the volume of the sample involved in the oscillation. A and B are therefore device constants for each individual oscillator. They can be derived from two period measurements when the oscillator has been filled with substances of known density [User manual, Anton Paar].

The partial molar volume, V^0, of the lipid is evaluated from the density data by the given relation:

$$V^o = \left(\frac{\partial V}{\partial n}\right) \cong \frac{M}{\rho_0} - \frac{\rho - \rho_0}{\rho_0 c} \tag{21}$$

where V is the volume, n the number of solute molecules in moles, and M is the molar mass of the solute. The very right term is valid only for diluted lipid suspensions as used in this study.

The adiabatic compressibility coefficient, $\beta_S = -1/V \, (\partial V/\partial p)_S$ (V, p and S are the volume, the pressure and entropy, respectively), the speed of sound propagation, u, in the medium, and the density, ρ are related by the expression:

$$\beta_S = 1/u^2 p \tag{22}$$

2.4.7 Calculation of Compressibilities

In molecular acoustics, due to the additivity of all components of the system, the partial molar adiabatic compressibility, K_S^o, is generally used, which is given by;

$$K_S^o = \left(\frac{\partial K_S}{\partial n}\right) = \left(\frac{\partial V^o}{\partial p}\right)_S \cong \beta_{S,0}\left(2(V^o - [u]) - \frac{M}{\rho_0}\right) \tag{23}$$

Where $K_S = \beta_S V$ is the adiabatic compressibility and $\beta_{S,0}$ is the adiabatic compressibility coefficient of the solvent. Here again, as in the case of the partial molar volume, the right term is valid only for diluted lipid samples. By dividing the partial molar quantities V^o and K_S^o by the molar mass of the solute, we obtain the partial specific values, i.e., the partial specific volume, v^o, and the partial specific adiabatic compressibility, k_S^o. Accordingly, the concentration, c, in Eqn. 15 becomes c/M, which is than expressed in mg/mL.

The sound velocity was determined with a relative error better than 10^{-3} %, corresponding to a precision higher than 5×10^{-5} mL/g in [u]. The density values were measured with relative error smaller than 10^{-3} %, so the accuracy in v^o is better than 10^{-4} mL/g. Therefore, considering the relative errors of [u] and v^o, the certainty in k_S^o taken from Eq. 23 is within 10^{-12} mL/gPa. In both methods, the corresponding values were measured at discrete temperatures (read with an accuracy of 10^{-3} °C), resulting in an average temperature scan rate of ~12 °C/h.

The adiabatic compressibility of the lipids, β_S^{lipid}, is defined as

$$\beta_S^{\text{lipid}} = -\frac{1}{v^o}\left(\frac{\partial v^o}{\partial p}\right)_S \tag{24}$$

which is related to the partial specific adiabatic compressibility, k_S^o, by

$$k_S^o = v^o \beta_S^{\text{lipid}} \tag{25}$$

β_S^{lipid} can thus be directly obtained from combined ultrasound velocity and density measurements. Lipid bilayer thermotropic main phase transitions are considered to be of weak first-order, i.e., they show typical features of first-order phase transitions, such as abrupt changes in specific volume or a peak in the enthalpy and entropy, but also significant fluctuations in volume and lamellar d-spacing, which are typical for a second-order phase transition. The isothermal compressibility, K_T, is directly proportional to the volume fluctuations of the system [Wilson 1957, Hill 1960]. In a system exhibiting a first-order transition, K_T diverges at the phase transition temperature, whereas it exhibits a power-law behavior ($K_T \propto |T\text{-}T_c|^{-\gamma}$), with a particular critical exponent ($\gamma = 1.24$ for 3D systems) in the critical-point region of a second-order phase transition [Stanley 1971, Winter 1999]. By the ultrasound velocity and the density measurements, however, only the adiabatic compressibility, K_S, can be determined (see Eqn. 22 and 23). The isothermal compressibility can be calculated from [Hill 1960]

$$K_T = K_S \frac{C_p}{C_V} \tag{26}$$

where C_p and C_V are the heat capacities at constant pressure and volume, respectively, which, using Maxwell relations, can also be expressed as

$$K_T = K_S + \frac{T}{C_p}\left(\frac{\partial V}{\partial T}\right)_p^2 = K_S + \frac{TE^2}{C_p} \tag{27}$$

with the thermal expansion $E = (\partial V/\partial T)_p$. Hence, the isothermal compressibility can be obtained from the adiabatic one when the thermal expansion and the heat capacity data are available. Differentiating Eqn. 27 yields the exact differential of K_T, $\mathrm{d}K_T$, which is given as:

$$\mathrm{d}K_T = \mathrm{d}K_S + \frac{E^2}{C_p}\,\mathrm{d}T + 2\frac{TE}{C_p}\,\mathrm{d}E - \frac{TE^2}{C_p^2}\,\mathrm{d}C_p \tag{28}$$

For convenience, Eqn. 27 is adapted through Eqn. 28 by thermodynamic treatment to a form where the corresponding partial specific quantities are taken [Chalikian 2003]:

$$k_T^o = k_S^o + \frac{T\alpha_0^2}{\rho_0 c_{p,0}}\left(2\frac{e^o}{\alpha_0} - \frac{C_p^o}{\rho_0 c_{p,0}}\right) \tag{29}$$

k_T^o is the partial specific isothermal compressibility, α_0 ($\alpha = E/V$) and $c_{p,0}$ are the thermal expansion coefficient and the specific heat capacity of the solvent, respectively; e^o and C_p^o are the partial specific expansivity and the partial specific heat capacity of the lipid, respectively; the latter is given by [Privalov 1980]

$$C_p^o = \frac{\Delta C_p}{m} + \frac{v^o}{v_0^o}c_{p,0} \tag{30}$$

where m is the mass of the solute.

The corresponding isothermal compressibility of the lipid, $\beta_T^{\text{lipid}} = k_T^o/v^o$ (please note that β_T^{lipid} differs from the partial specific isothermal compressibility coefficient, β_T^o, which is defined as $\beta_T^o = 1/M\ (\partial\beta_T/\partial n) = \beta_T\ v^o/V$), can be obtained from Eqn. 29 and is given as:

$$\beta_T^{\text{lipid}} = \beta_S^{\text{lipid}} + \frac{T\alpha_0^2}{v^o\rho_0 c_{p,0}}\left(2\frac{e^o}{\alpha_0} - \frac{C_p^o}{\rho_0 c_{p,0}}\right) \tag{31}$$

For simplification, we denote in Eqn. 31 the second and third term as β_e^{lipid}, and β_C^{lipid}, respectively:

$$\beta_T^{\text{lipid}} = \beta_S^{\text{lipid}} + \beta_e^{\text{lipid}} - \beta_C^{\text{lipid}} \tag{32}$$

Hence, the isothermal compressibility coefficient, β_T^{lipid}, is given as a sum of the adiabatic compressibility, β_S^{lipid}, an expansion term, β_e^{lipid}, and a heat capacity term, β_C^{lipid}. Interestingly, as can be seen from Eqs. 29 and 31, the heat capacity term has a compensating effect, balancing that of the thermal expansion on the adiabatic compressibility.

The thermodynamic parameters C_p, K_T and E are directly related to corresponding fluctuation parameters [Cooper 1984]: i) the square average of the enthalpy fluctuations, its variance, $\langle\Delta H^2\rangle$, is determined by the heat capacity, C_p, of the system, ii) the square average of the volume fluctuations $\langle\Delta V^2\rangle$ as given by the respective isothermal compressibility, K_T, and iii) the covariance between H and V, $\langle\Delta H\ \Delta V\rangle$, is related to the thermal expansion, E:

$$\langle\Delta H^2\rangle = RT^2 C_p \tag{33a}$$

$$\langle\Delta V^2\rangle = RTK_T \tag{33b}$$

$$\langle\Delta H\ \Delta V\rangle = RT^2 E = RT^2 V\alpha \tag{33c}$$

As seen from Eqn. 33c, the thermal expansion couples contributions from the heat capacity and the isothermal compressibility.

3.0   RESULTS AND DISCUSSION

3.1   LIPID – STEROL INTERACTION

For all lipid mixtures studied, DSC and PPC scans have been measured for a series of sterol concentrations, ranging from 5 to 36 mol%. Figure 3.1a shows the DSC scans (as stacked plot) of DPPC dispersions containing different concentrations of cholesterol. Pure DPPC displays a sharp transition at the main gel-to-fluid transition at $T_m = 41.5$ ^{o}C, and a small endothermic peak due to the $L_{\beta'}$-$P_{\beta'}$ pretransition which appears around 35 ^{o}C. For 5 mol% cholesterol, the transitions broaden and shift towards lower temperatures. The transition enthalpies ΔH also decrease concomitantly. As the cholesterol concentration increases to 12 mol% and higher, the main transition peak intensity decreases and broadens drastically, producing a multicomponent DSC endotherm consisting of a sharp component (arising from the fairly cooperative melting of domains enriched on DPPC) that is progressively reduced in temperature, enthalpy and cooperativity (width), and a broad component that increases in both temperature and enthalpy, but decreases in cooperativity, in agreement with literature data [McMullen 1995, McMullen 1993, Mannock 2006].
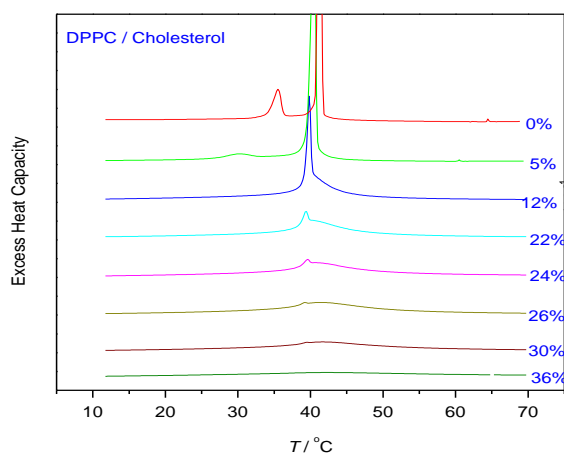
a)   b)
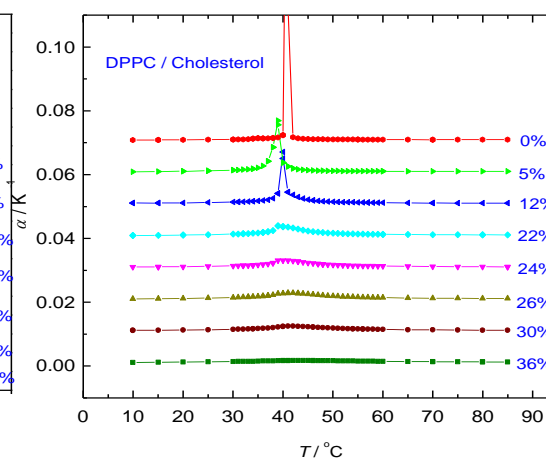
Figure 3.1: a) DSC thermograms (heating scans only) of pure DPPC and DPPC/cholesterol mixtures in excess water. The thermograms were acquired at the sterol concentrations (in mol%) indicated and have all

been normalized against the mass of DPPC used. b) Temperature dependence of the coefficient of thermal expansion, α, of pure DPPC and DPPC/cholesterol mixtures (pH 7.4, 10 mM Tris buffer, scan rate 40 ^{o}C/h). To facilitate better visibility, the curves are displaced along the *y*-axis (from bottom to top by 0.01 units).

The DSC thermogram can be interpreted in terms of a transition from a s_o+l_o two-phase region to an all-fluid l_d phase at high temperatures (above ~55°C), thereby passing through a l_o+l_d two-phase region above about 40°C [Sankaram 1991, Hsueh 2005]. Whereas at 30 mol% cholesterol a weak and broad DSC endotherm is still observed, at 36 mol% cholesterol, no phase transitions seem to be visible anymore.

Figure 3.2a shows the DSC data for DPPC-ergosterol. In agreement with data from Hsueh et al. [Hsueh 2005], at 5 mol% ergosterol, the main transition becomes broadened and shifts toward lower temperature, indicating a s_o and l_d phase coexistence region. As the ergosterol concentration increases to 22 mol%, the intensity of the main DSC peak decreases, and the peak position seems to remain essentially unchanged.

a)   b)

Figure 3.2: a) DSC scans (heating only) of pure DPPC and DPPC/ergosterol mixtures in excess water. b) Temperature dependence of the coefficient of thermal expansion, α, of pure DPPC and DPPC/ergosterol mixtures (pH 7.4, 10 mM Tris buffer, scan rate 40°C/h).

A broad shoulder appears on the high-temperature side of the sharp peak, also suggesting a l_d+l_o two-phase region. Where the broad peak ends, the transition to the l_d phase occurs. At ergosterol concentrations of 30 mol% and above, a very broad residual endotherm is observed only, similar to that seen in DPPC-cholesterol MLV.

a)   b)

Figure 3.3: a) DSC scans (heating only) of pure DPPC and DPPC/stigmasterol mixtures in excess water. b) Temperature dependence of the coefficient of thermal expansion, α, of pure DPPC and DPPC/stigmasterol mixtures (pH 7.4, 10 mM Tris buffer, scan rate 40 ^{o}C/h).

The DSC thermograms of the systems DPPC/stigmasterol and DPPC/7-DHC exhibit a similar concentration dependent behavior (Figs. 3.3a, 3.4a). For stigmasterol, no sharp component is observed in the DSC thermograms above 12 mol% sterol, rather a broad DSC peak centered around 40-41°C, only. However, there are significant differences in the pattern of thermal events observed for the system DPPC/lanosterol (Fig. 3.5a) at concentrations above 12 mol%, indicating that the phase behavior of this system is qualitatively different at high sterol concentrations. A pronounced l_d+l_o phase coexistence region above T_m seems to be lacking (see also [Mannock 2006]). Also for 5 mol% lanosterol, no pretransitional peak is observed, indicating that lanosterol is more

effective at abolishing the pretransition than cholesterol on a molar basis, in agreement with literature data [Zuckermann 2004, Mannock 2006].

a)

b)
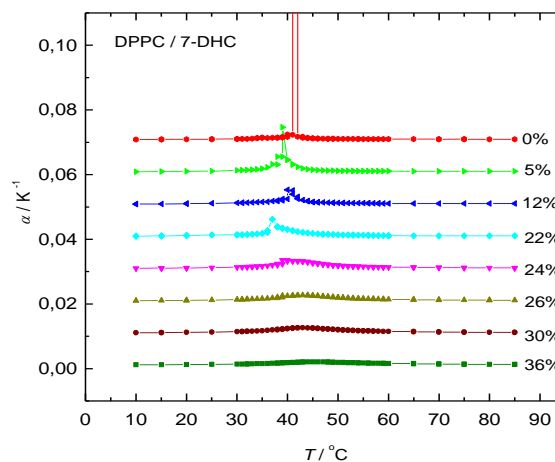
Figure 3.4: a) DSC scans (heating only) of pure DPPC and DPPC/7-dehydrocholesterol (7-DHC) mixtures in excess water. b) Temperature dependence of the coefficient of thermal expansion, α, of pure DPPC and DPPC/7-dehydrocholesterol (7-DHC) mixtures (pH 7.4, 10 mM Tris buffer, scan rate 40 ^{o}C/h).

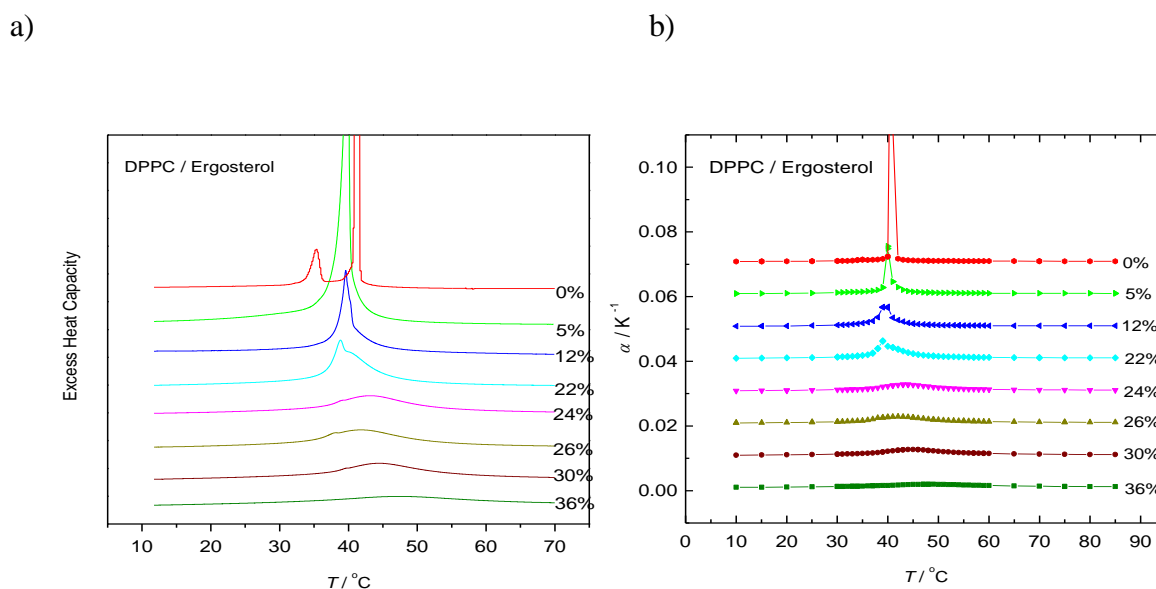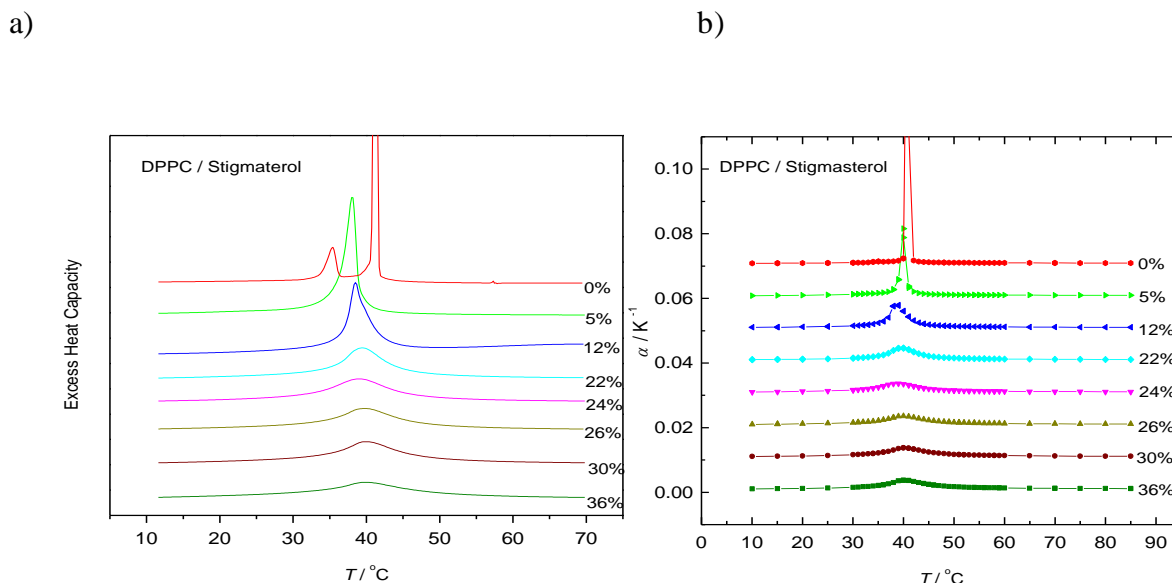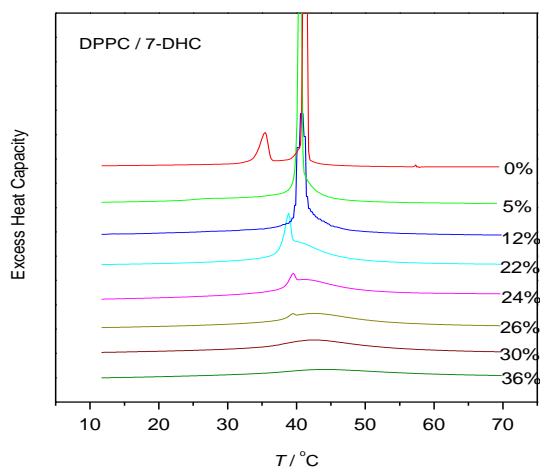a)   b)
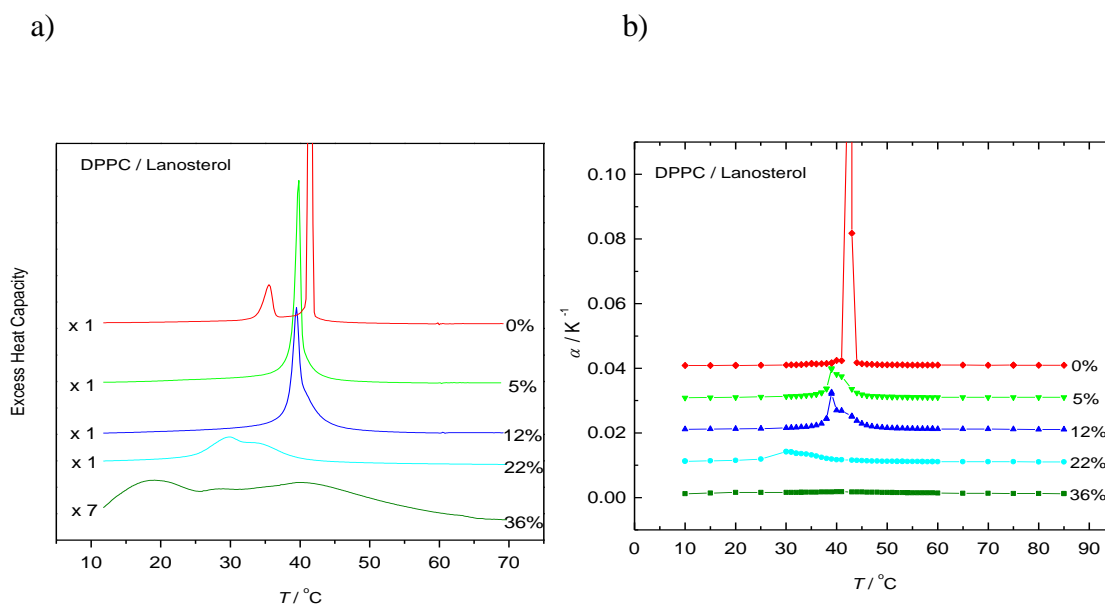
Figure 3.5: a) DSC scans (heating only) of pure DPPC and DPPC/lanosterol mixtures in excess water. b) Temperature dependence of the coefficient of thermal expansion, α, of pure DPPC and DPPC/lanosterol mixtures (pH 7.4, 10 mM Tris buffer, scan rate 40 ^{o}C/h). Eventually, y-axis scaling factors are used and indicated on the left-hand side of the thermogram.

Generally, the thermodynamic variables C_p and α are directly related to fluctuation parameters. The square average of the enthalpy fluctuations, $\langle \Delta H^2 \rangle$, is determined by the heat capacity, C_p, of the system, and the covariance between H and V fluctuations, $\langle \Delta H \Delta V \rangle$, is related to the thermal expansion [Smirnovas 2006]: See eqns. 33a & 33c.

Figure 3.1b reveals the corresponding coefficient of thermal expansion for the system DPPC/cholesterol as obtained from the PPC data. Notably, the $\alpha(T)$ curves exhibit a similar shape as the $C_p(T)$ data, an indication of the membrane enthalpy and volume fluctuations being governed by the same molecular origin. Below the main phase transition temperature of pure DPPC, α increases slightly with increasing temperature. Around the main phase transition temperature, α undergoes a rather sharp increase, reaches a maximum of about 0.15 K^{-1} at T_{m} (41.5^{o}C), and then rapidly decreases with increasing temperature, to reach a value close to that obtained below the transition temperature (α is ~0.9·10^{-3} K^{-1} below the pretransition (20 ^{o}C) and ~1.0·10^{-3} K^{-1} above the main transition (65 ^{o}C)). The observed α-value of pure DPPC is in the same range as that of other phospholipids [Melchior 1980, Böttner 1993, Heerklotz 2002, Heerklotz 2006],

and similar to the thermal expansivity of pure liquid hydrocarbons, such as tetradecane (α = 0.9 10^{-3} K^{-1}), but an order of magnitude larger than that of water [Heerklotz 2002]. Nagle and Wilkinson dilatometry measurement determined the α value for DPPC as $dV/dT = 0.83$ X 10^{-3}K^{-1}(lipid density of 1.0 g/ml) below the pretransition and 0.94 x 10^{-3} K^{-1} above the main transition (Wilkinson 1978). Osmotic gradient application across bilayer membranes has been used to determine α with a similar result. Pressure perturbation calorimetry, among the other above mentioned techniques is seen as the easiest and fastest.

With increasing cholesterol concentration, α increases slightly below and – notably, despite the condensing effect cholesterol imposes on fluid bilayers – also above T_m (for example, $\alpha = 1.25 \cdot 10^{-3}$ K^{-1}at 20 ^{o}C and $\alpha = 1.4 \cdot 10^{-3}$ K^{-1} at 65 ^{o}C for 30 mol% cholesterol in DPPC), whereas the main peak height of α in the transition region decreases and broadens markedly.

a)   b)
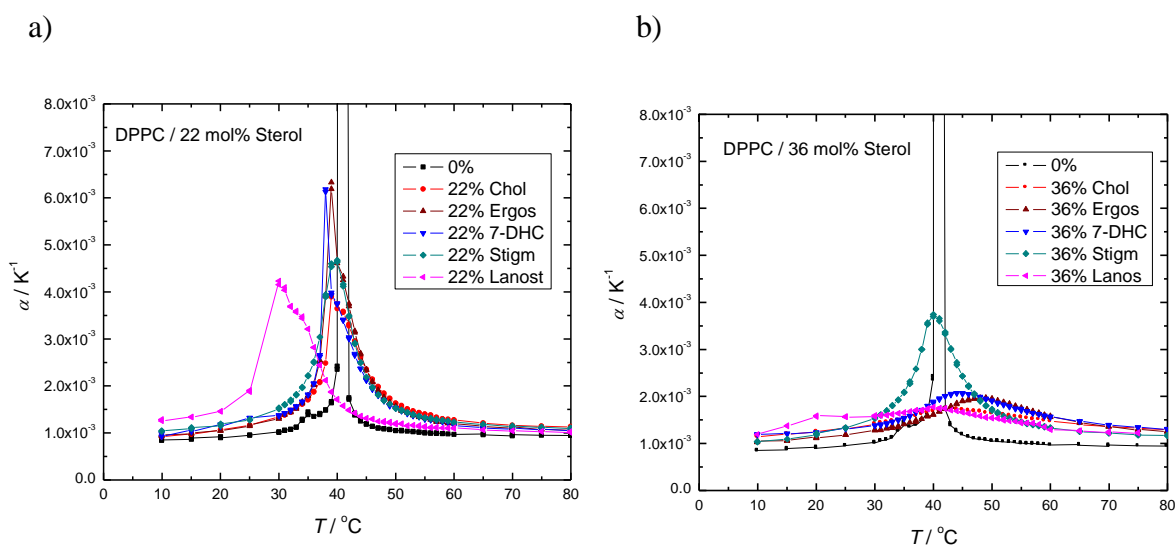
Figure 3.6: Temperature dependence of the coefficient of thermal expansion, α, of the various DPPC/sterol mixtures for 22 and 36 mol% sterol.

Figures 3.6 a, b display the $\alpha(T)$-data in an expanded scale for all sterols at a concentration of 22 and 36 mol%, respectively. Besides lanosterol, a qualitatively similar

behavior of $\alpha(T)$ is observed for all sterols at a sterol concentration of 22 mol% (Fig. 3.6a). The only significant differences are somewhat larger α-values at the transition maxima. For the system DPPC/lanosterol, the asymmetric peak is broadened and shifted to a ~8 ^{o}C lower temperature, however, and the coefficient of thermal expansion is the largest one below T_{m}. Figure 3.6b displays the corresponding PPC data for 36 mol% sterol. As expected, the α-values have further decreased in the phase transition region. For 7-DHC and ergosterol, the broad transition maxima have shifted to slightly higher temperatures if compared to cholesterol, whereas for lanosterol, again, a shift towards lower temperatures is observed. Notably, no such suppression of the transition is observed for DPPC/36 mol% stigmasterol. The PPC data for both sterol concentrations indicate that cholesterol is most efficient in suppressing the chain-melting transition of the phospholipid bilayer system.

From an integration of the PPC data over the temperature range where the phase transitions occur, the relative volume changes, $\Delta V/V$, of pure DPPC and the DPPC/sterol mixtures have also been determined (Fig. 3.7). $\Delta V/V = 0.04 \pm 0.007$ (4 %), corresponding to an absolute volume change of 29 mL/mol, for pure DPPC, $\Delta V/V$ is 0.032 ± 0.003 for 5 mol%, 0.03 ± 0.002 for 12 mol%, 0.013 ± 0.005 for 26 mol% cholesterol, and continues to decrease with increasing sterol concentration, finally reaching $\Delta V/V = 0.002 \pm 0.001 \approx$ 0 around 36 mol% cholesterol. The corresponding width of the overall transition, $\Delta T_{1/2}$, increases from about 1 ^{o}C for the main transition of pure DPPC to about 13 ^{o}C for the DPPC/36 mol% cholesterol mixture. The volume change associated with the pretransition of pure DPPC is a factor of about 10 smaller than that of the main transition.

Tables 1-4 summarize the calculated volumetric properties of all DPPC/sterol mixtures studied, whereas figure 3.7 represents graphically, the relative volume changes, $\Delta V/V$, of pure DPPC and all DPPC/sterol mixtures as a function of sterol concentration.

Table 1: DPPC+Cholesterol- 20mg/ml, 10mM Tris-NaCl.

Sample	T_m (^{o}C)	$\Delta V/V$ (%)	ΔV (mL/mol)	$T_{1/2}$ (^{o}C)
DPPC	41.00 ± 0.01	4.000 ± 0.70	29.36 ± 5.0	1.01 ± 0.025
DPPC+5 mol% Chol	39.02 ± 1.00	3.190 ± 0.30	23.00 ± 2.0	2.01 ± 0.100
DPPC+12 mol% Chol	40.02 ± 0.00	2.960 ± 0.20	21.98 ± 1.5	1.99 ± 0.000
DPPC+22 mol% Chol	39.01 ± 0.00	1.799 ± 0.30	13.10 ± 2.2	5.99 ± 0.000
DPPC+24 mol% Chol	39.01 ± 1.00	1.474 ± 0.10	10.69 ± 0.6	7.99 ± 0.010
DPPC+26 mol% Chol	42.00 ± 0.00	1.344 ± 0.50	9.7 ± 3.6	10.00 ± 1.000
DPPC+30 mol% Chol	42.00 ± 0.00	0.963 ± 0.20	6.9 ± 1.4	9.99 ± 1.010
DPPC+22 mol% Chol	40.99 ± 2.00	0.220 ± 0.10	1.5 ± 0.6	12.98 ± 1.000

Table 2: DPPC+Ergosterol- 20 mg/1 ml, 10 mM Tris-NaCl.

Sample	T_m (^{o}C)	$\Delta V/V$ (%)	ΔV (mL/mol)	$T_{1/2}$ (^{o}C)
DPPC	41.00 ± 0.01	4.000 ± 0.70	29.36 ± 5.0	1.01 ± 0.025
DPPC+5 mol% Ergos	39.0 ± 1.00	2.850 ± 0.20	19.83 ± 1.4	1.99 ± 0.010
DPPC+12 mol% Ergos	40.0 ± 0.00	2.390 ± 0.10	16.83 ± 0.7	2.99 ± 0.000
DPPC+22 mol% Ergos	39.01 ± 0.00	1.799 ± 0.30	16.22 ± 1.4	7.00 ± 0.000
DPPC+24 mol% Ergos	43.0 ± 1.00	1.467 ± 0.30	10.33 ± 2.1	7.99 ± 0.900

DPPC+26 mol% Ergos	42.0 ± 0.00	1.380 ± 0.10	9.72 ± 0.7	9.99 ± 0.000
DPPC+30 mol% Ergos	42.0 ± 1.00	1.227 ± 0.10	8.65 ± 0.7	10.00 ± 0.000
DPPC+36 mol% Ergos	44.0 ± 1.00	0.446 ± 0.20	3.20 ± 1.4	14.00 ± 1.000

Table 3: DPPC+Stigmasterol-20 mg/1 ml, 10 mM Tris-NaCl.

Sample	T_m (°C)	$\Delta V/V$ (%)	ΔV (mL/mol)	$T_{1/2}$ (°C)
DPPC	41.00 ± 0.01	4.000 ± 0.70	29.36 ± 5.0	1.01 ± 0.025
DPPC+5 mol% Stg	38.0 ± 0.00	3.858 ± 0.30	27.18 ± 2.1	1.99 ± 0.000
DPPC+12 mol% Stg	39.0 ± 0.00	3.131 ± 0.10	21.6 ± 0.7	1.99 ± 0.000
DPPC+22 mol% Stg	40.0 ± 0.00	2.219 ± 0.20	15.31 ± 1.4	5.01 ± 0.000
DPPC+24 mol% Stg	39.0 ± 0.01	1.664 ± 0.10	11.36 ± 0.7	7.98 ± 0.900
DPPC+26 mol% Stg	40.0 ± 0.00	1.692 ± 0.10	11.20 ± 0.7	7.99 ± 1.000
DPPC+30 mol% Stg	40.0 ± 0.00	1.757 ± 0.20	11.20 ± 1.3	7.00 ± 1.000
DPPC+36 mol% Stg	40.0 ± 0.10	1.801 ± 0.10	11.23 ±0.6	6.99 ± 0.100

Table 4: DPPC+7-Dehydrocholesterol-20 mg/ml, 10 mM Tris-NaCl.

Sample	T_m (^{o}C)	$\Delta V/V$ (%)	ΔV (ml/mol)	$T_{1/2}$ (^{o}C)
DPPC	41.00 ± 0.01	4.000 ± 0.70	29.36 ± 5.0	1.01 ± 0.025
DPPC+5 mol% 7DHC	39.0 ± 0.01	2.968 ± 0.20	21.7 ± 1.4	2.00 ± 1.000
DPPC+12 mol% 7DHC	40.0 ± 0.01	1.983 ± 0.10	14.3 ± 0.7	3.98 ± 0.004
DPPC+22 mol% 7DHC	39.0 ± 0.00	2.063 ± 0.20	14.2 ± 1.4	3.00 ± 0.000
DPPC+24 mol% 7DHC	39.0 ± 0.00	1.717 ± 0.20	12.1 ± 1.4	8.00 ± 1.000
DPPC+26 mol% 7DHC	42.0 ± 0.50	1.266 ± 0.30	8.9 ± 2.1	10.00 ± 1.000
DPPC+30 mol% 7DHC	42.0 ± 0.01	1.187 ± 0.10	8.3 ± 0.7	10.99 ± 1.000
DPPC+36mol% 7DHC	44.0 ± 0.5	0.604 ± 0.07	4.2 ± 0.7	11.98 ± 1.010

Table 5: DPPC+Lanosterol- 20 mg/ml, 10 mM Tris-NaCl.

Sample	T_m (^{o}C)	$\Delta V/V$ (%)	ΔV (ml/mol)	$T_{1/2}$ (^{o}C)
DPPC	41.00 ± 0.01	4.000 ± 0.70	29.36 ± 5.0	1.01 ± 0.025
DPPC+5 mol% Lan	39.01 ± 0.00	2.575 ± 0.2	18.43 ± 1.4	3.00 ± 0.010
DPPC+12 mol% Lan	39.01 ± 0.00	3.320 ± 0.10	23.76 ± 0.7	1.98 ± 0.000
DPPC+22mol% Lan-Peak 1	30.03 ± 0.01	0.26 ± 0.20	1.90 ± 1.4	11.99 ± 0.000
DPPC+24mol% Lan-Peak 2	20.02 ± 0.01	0.161 ± 0.00	1.15 ± 0.00	5.00 ± 0.000

a)   b)
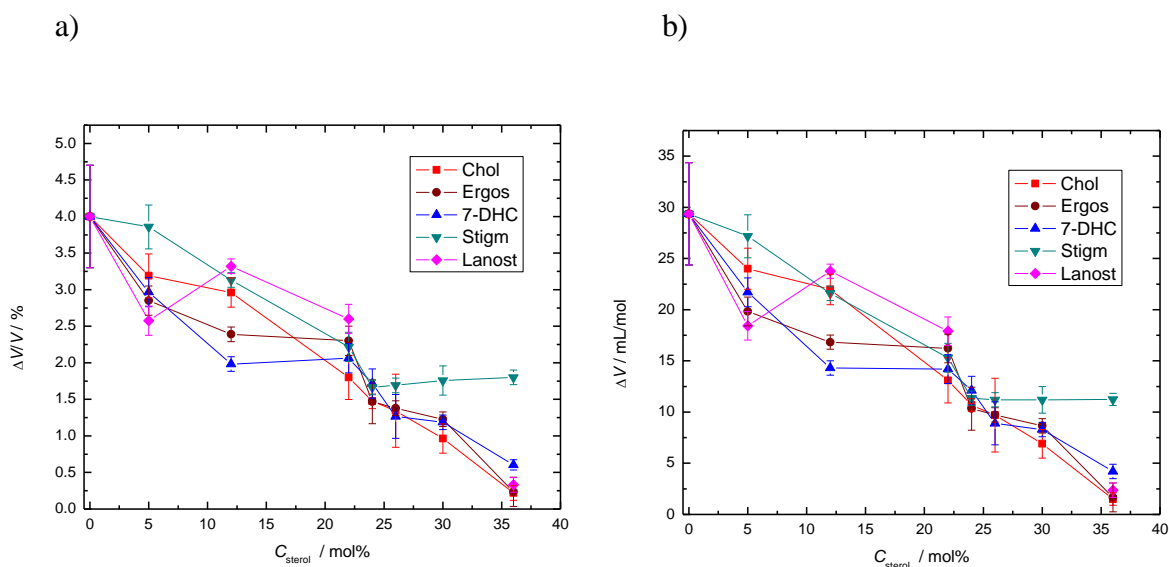
Figure 3.7: Temperature dependence of the overall relative volume changes, $\Delta V/V$, and of the absolute volume change, ΔV, of the various DPPC/sterol mixtures undergoing their chain-melting transitions.

Qualitatively, a similar, essentially linear behavior is observed for $\Delta V/V$ as a function of sterol concentration for all DPPC/sterol mixtures. Only for the system DPPC/stigmasterol, a saturation behavior seems to occur above 24 mol%. Notably, a similar behavior has been found for the order parameter profile of DPPC/stigmasterol as a function of sterol concentration [Bernsdorff 2003]. Generally, the transition half width $T_{1/2}$, increased with increase in sterol content (due to peak broadening).

3.1.1   Concluding Remarks

The focus of this study was to identify and characterize the differential effects of various sterols, including cholesterol, the plant sterols ergosterol and stigmasterol, *trans*-7-dehydrocholesterol (7-DHC), and lanosterol, the evolutionary precursor of cholesterol, on the volumetric properties of the DPPC bilayer membrane and to relate these effects to the difference in their molecular chemistry (Fig. 1.3). To this end, PPC experiments have been carried out that allow determination of the temperature dependence of the coefficient of expansion coefficient as well as volume changes accompanying lipid phase transitions.

Recent measurements of the lipid acyl chain order parameter revealed that with increasing side-chain volume of the sterol, the conformational order of the lipid acyl chains decreases, and an increase in alkyl chain volume has the most drastic effect on the condensing capacity of sterols [Bernsdorff 2003]. The introduction of a double bond in the side chain counteracts this effect, owing to the decreased volume fluctuations in the steroid alkyl chain region. Introduction of a double bond in the ring system leads at low and medium high sterol levels (up to ~40 mol%) to a drastic increase in conformational order of the lipid acyl chains (compare, e.g. *trans*-7-dehydrocholesterol with cholesterol), which can indeed be substantially higher than that induced by cholesterol. Additional methyl groups in the ring system of the sterol markedly counteract this rigidifying effect (compare lanosterol with ergosterol). Sterols with the bulkiest unsaturated side chains or sterol nuclei (stigmasterol, lanosterol) induce the smallest order parameter increase of the fluid bilayer at high sterol concentrations (> 30 mol%), and hence become less effective rigidifiers at high sterol levels. The difference might also be due to a different solubility/partitioning in the bilayer. Lanosterol is a sterol precursor. Owing to its additional methyl groups in the ring system, its partitioning is much less effective than that of cholesterol at high sterol levels. An important conclusion has been that cholesterol, with its streamlined molecular structure, interacts more effectively with lipid chains and stabilizes the liquid-ordered state. Interestingly, from an evolution point of view, cholesterol seems to be very efficient in suppressing the chain-melting transition of the phospholipid bilayer system. A marked limitation of the condensing effect is observed for the stigmasterol system having a rather bulky alkyl chain [Bernsdorff 2003], which is also reflected in volumetric parameters as discussed above.

As shown here, alterations in the sterol structure are also reflected in their thermodynamic properties. Though the overall thermodynamic features of all sterols besides lanosterol seem to be qualitatively similar, minor differences are found, such as in abolishing the pretransition and in the extension of the phase space of the two-phase regions, as indicated by the differences observed in the corresponding DSC and PPC thermograms. For lanosterol, differences in the miscibility and temperature-concentration phase behavior and hence the thermodynamic functions $C_p(T)$ and $\alpha(T)$ are most obvious when compared to cholesterol and the other sterols. The changes in $C_p(T)$ are found to

precisely mirror the corresponding $\alpha(T)$ data, an indication of the membrane enthalpy and volume fluctuations (Eqns. 33a, 33c) being governed by the same molecular origin. Increases in $C_p(T)$ and $\alpha(T)$ at phase changes are mainly linked to cooperative fluctuations of large numbers of lipid molecules in their physical state [Krivanek 2008, Edel 2001]. The sharpness of the transition peaks is related to the correlation lengths of these fluctuations, namely the domain sizes of the coexisting phases. With increasing sterol concentration, the widths of both thermodynamic parameters at the chain-melting transitions increase drastically, indicating coupled enthalpy and volume fluctuations with low amplitude by large correlation lengths over an extended temperature region.

The large cross-sectional area of the steroid ring system of lanosterol makes it a more effective spacer than DPPC molecules in the gel-state bilayer, thus relieving the mismatch in the cross-sectional areas of the acyl chains and the DPPC polar headgroups at lower sterol concentrations more efficient than cholesterol. Also, the rougher surface of the lanosterol molecule would be expected to produce a greater amount of orientational disorder in the adjacent phospholipid's acyl chains, thus further augmenting the expansion of the DPPC gel-state bilayer, and leading to the markedly larger α-values observed for this system.

3.2   LIPID – PEPTIDE INTERACTIONS

3.2.1   Lipid – gramicidin D interaction

3.2.1.1   Calorimetric measurements on DPPC – gramicidin D mixtures

The DSC and PPC measurements were carried out at concentrations 0, 1, 2.5, 5, 7.5, and 10 mol% of gramicidin, in the temperature range $10 – 70^o$C for DSC scans (Fig.3.8a) and $10 – 85\ ^o$C for PPC scans (Fig. 3.8b). The shape of the heat capacity profile contains thermodynamic information on the mode of interaction between peptides and lipids, as regards to their spatial organization [Ivanova 2001]. Figure 3.8a shows the DSC heat capacity traces (as stacked plot) of DPPC dispersions containing different concentrations of gramicidin. Pure DPPC displays a sharp main transition (s_o to l_d transition) at $T_m =$

41.0 ^{o}C, as well as a small endothermic peak due to the L_β' - P_β' pretransition, appearing at 35 ^{o}C.

At 1% gramicidin concentration, we observe peak broadening (with a small asymmetry at the low temperature end) of the transition and a shift to a lower temperature. The asymmetry of the profile could result from the change in mixing behavior (Morrow 1986). Again the intercalation of the peptide between gel and the fluid domains lead to the lowering of the cooperativity of the melting transition. The transition peak intensity as well as the enthalpy equally decrease. At higher gD concentration, within the main transition region, a two phase region is induced, probably a gD-rich and a gD-poor lipid phase, which might be linked to the increasing hydrophobic mismatch between the lengths of the lipid chains and the polypeptide upon temperature increase.

At 2.5% and higher concentrations, the main peak position remains essentially unchanged. The main transition gets more broadened, but the center of the transition stays at approximately the same temperature for all concentrations. Additionally, a broad shoulder at the low-temperature side of the sharp peak is observed, which may suggest a (l_o to l_d) two-phase region.

Another interesting observation is the reappearance of a pre-transition peak at a much lower temperature near 24 ^{o}C at the 5% gramicidin concentration. A similar low-temperature transition has been observed in a different system of DMPC and gramicidin D in methanol (Orädd 2004). This may possibly be attributed to some rearrangements in the hydrocarbon region of the bilayer in the gel phase. It could as well be a result of the reported gD formation of linear aggregates in the gel phase of DPPC (Ivanova 2003). From his analysis, Ivanova et al. predicted the aggregation of Gramicidin A in both lipid phases of DMPC and DPPC. A shoulder at the low temperature end of the heat capacity profile indicates unfavorable partitioning in the low temperature phase.

a)   b)
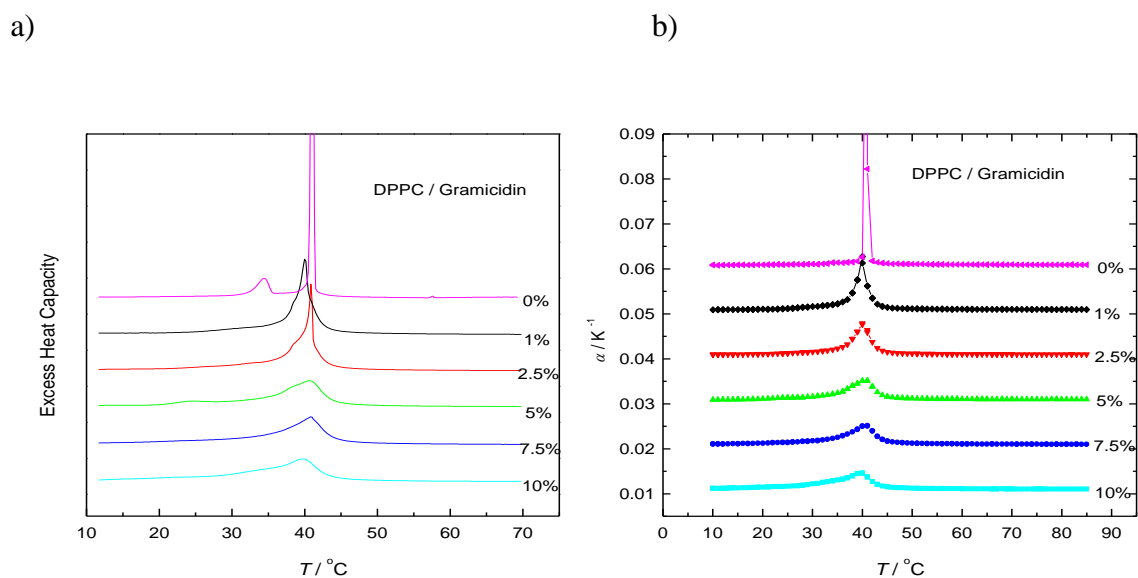
Figure 3.8: a) DSC thermograms (heating scans, only) of pure DPPC and DPPC/gramicidin mixtures in excess water. The thermograms were acquired at the gramicidin concentrations (in mol%) indicated. b) Temperature dependence of the coefficient of thermal expansion, α, of pure DPPC and DPPC/gramicidin mixtures (pH 7.4, 10 mM Tris buffer, scan rate 40°C/h). To facilitate better visibility, the curves are displaced along the *y*-axis (from bottom to top by 0.01 units).

Figure 3.8b reveals the PPC stacked plot of the coefficient of thermal expansivity versus temperature curve of the DPPC/ mol% gramicidin D mixtures. Again, PPC peaks exhibit almost perfectly the same shape (Ebel 2001, Heerklotz 2002, Okoro 2008), which as already stated, is an indication of the membrane enthalpy and volume fluctuations being governed by the same molecular parameters. Concerning T_m values, similar results as from DSC were obtained for PPC. C_p and α are directly related to the fluctuation parameters (eqns. 33a and 33c).

PPC scans were carried out with solutions of DPPC/gramicidin D in Tris buffer yielding the changes with temperature of the thermal expansion coefficient, α, shown in figure 3.8b. Around the phase transition temperature, α for pure DPPC undergoes a sharp increase, reaching a maximum of about 0.12 K^{-1} at T_m (41 °C), and then rapidly decrease with increasing temperature, to reach a value nearly equal to that obtained below the transition temperature (α is $\sim$0.93 x 10^{-3} K^{-1} below the pretransition (20 °C) and $\sim$1.0 x 10^{-3} K^{-1} above the main transition (65 °C)).

We observe a slight increase in α, below the pretransition with increase in gramicidin concentration. As an example, $\alpha = 1.12 \times 10^{-3}$ K^{-1} for 5 mol%, and $\alpha = 1.25 \times 10^{-3}$ K^{-1} for 7.5 mol% at 20 ^{o}C, while at 65 ^{o}C, there is no significant change in α. for the concentrations.

From the integration of α over the temperature range where the transitions occur, we obtain the relative volume changes, $\Delta V/V$, for the pure DPPC and each of the DPPC / gramicidin concentrations (Fig.3.8b). $\Delta V/V = 0.04 \pm 0.007$ (4 %), corresponding to an absolute volume change of 29 mL/mol, for pure DPPC, $\Delta V/V$ is 0.028 ± 0.001 for 1 mol%, 0.026 ± 0.002 for 2.5 mol%, 0.023 ± 0.002 for 5 mol% gramicidin, and continues to decrease with increasing gramicidin concentration, finally reaching $\Delta V/V = 0.013 \pm 0.0002 \approx 0$ at 10 mol% gramicidin. The corresponding width of the overall transition, $\Delta T_{1/2}$, increases from about 1 ^{o}C for the main transition of pure DPPC to about 4 ^{o}C for the DPPC / 10 mol% gramicidin mixture.

Figure 3.9 shows the relative volume changes, $\Delta V/V$, and absolute volume changes, ΔV of pure DPPC and all DPPC/gramicidin mixtures as a function of gramicidin concentration at the main phase transition.
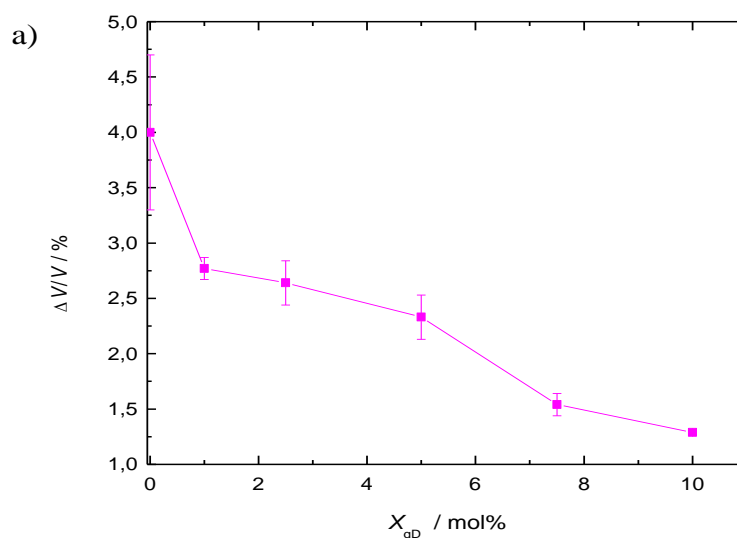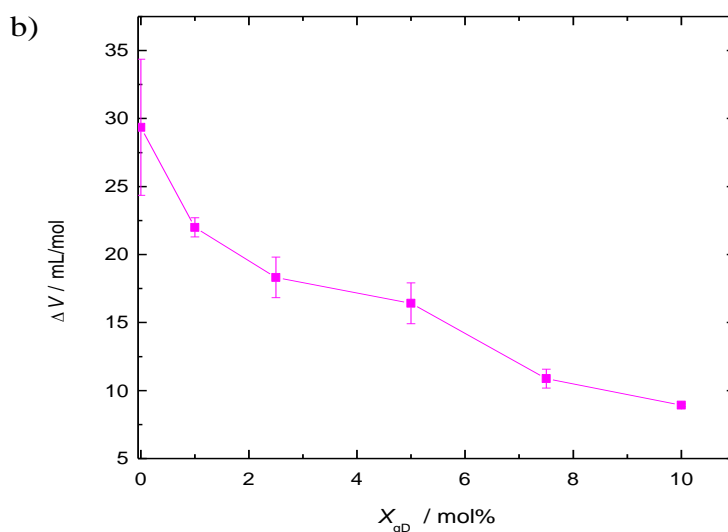
Figure 3.9: Temperature dependence of (a) the overall relative volume changes, $\Delta V/V$, and (b) the absolute volume change, ΔV, of the DPPC/gramicidin mixtures undergoing their chain-melting transitions.

The plot reveals a sharp decrease in both $\Delta V/V$ and ΔV upon addition of 1.0mol% gramicidin, followed by a gradual decrease with increase in gramicidin concentration.

3.2.1.2   Ultrasound and Density Measurements on DPPC – Gramicidin Mixtures

Sound velocimetry and densitometry are sensitive tools to study the mechanics and thermodynamics of biomolecules and biocolloids. When the two methods are used simultaneously to study the phase transition peculiarities of lipid bilayers, they enable one to determine the degree of phase transition cooperativity. In addition to the thermodynamic properties and the volumetric properties of the lipid phase transition obtained by differential scanning calorimetry (DSC), and pressure perturbation calorimetry (PPC), these methods allow one to study the mechanical properties of lipid bilayer membranes. This advantage is most useful in the study of protein/peptide-lipid interactions, since the determination of mechanical parameters is crucial for an evaluation of the size of distorted membrane structure around proteins or peptides (Hianik 1995).

We used ultrasound and densitometry techniques to measure the velocity number, $[u]$, and the partial specific volume, v^o, of the DPPC-gramicidin mixtures. From equation 23, we determined the partial specific adiabatic compressibility, k_S^o, of the lipid dispersion. Figure 3.10a shows the temperature dependent velocity number $[u]$ for the DPPC – gramicidin mixtures. At points distant from the lipid main phase transition temperature, T_m, $[u]$, a gradual decrease of $[u]$ with rise in temperature is observed, leading to the typical anomalous dip (Mitaku 1978, Kharakoz 1993, Schrader 2002, Krivanek 2008) in the vicinity of T_m for pure lipids. The lowest value of $[u]$ at T_m is ~- 0.15mL/g for pure DPPC, which is consistent with Mitaku and co-workers data (Mitaku 1978). It should be noted, however, that the size and the width of the dip in $[u]$ depends on the sample preparation [Mitaku 1978], which is related to the different degree of cooperativity of the main phase transition, on the lipid concentration [Kharakoz 1993], and on the ultrasound frequency applied for the measurement itself [Mitaku 1982], which is related to the heat exchange within the period of the sound wave [Osdol 1989, Heimburg 1996]. The dip in the ultrasonic number profiles will be more pronounced at lower frequencies, because C_p assumes higher values, leading to an increase of the adiabatic compressibility at lower frequencies. The frequency dependence of the ultrasonic absorption coefficient of DPPC suspensions has been measured. The excess absorption data has been described by a relaxation term with a discrete relaxation time, displaying some evidence of critical slowing down near the phase transition [Heimburg 1996].

In addition, inadequately high temperature scan rates might induce a slight shift in the dip minimum position toward higher temperatures [Kaatze 2006], since lipid bilayers are not able to thermally equilibrate rapidly due to molecular processes slowing down during the main phase transition.

a)   b)
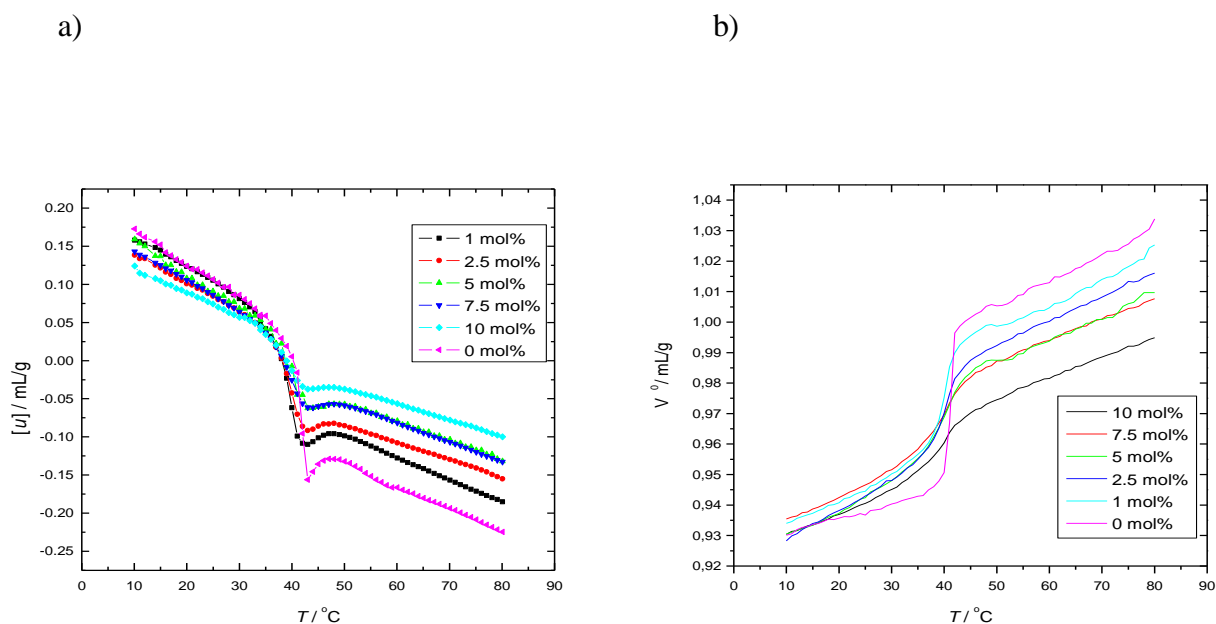
Figure 3.10: The temperature dependence of the ultrasound velocity number, [*u*], and partial specific volume, *v*° for DPPC-gramicidin D mixtures.

Addition of 1 mol% gramicidin produced a significant change in [*u*], and a peak broadening is observed leading to a comparatively increased [u] at T_m with a dip of ~-0.1mL/g. The dip continues to decrease with increase in gramicidin concentration, with the highest value and broadest peak at 10 mol%. In the gel phase, in general, we observe that [*u*] is smaller below T_m and larger above T_m for both DPPC – gramicidin mixtures than for the pure DPPC LUVs. In addition, for the DPPC – gramicidin mixtures in the gel phase, there is no clearly defined trend in [*u*] unlike in the transition region. It is of interest to note that the minimum in the [*u*] value generally reflects effects from changes in heat capacity, C_p, [*u*] and the isothermal compressibility β_T upon approaching Tm.

The temperature dependence of the partial specific volume, v^o, is shown in figure 3.10b. An increase of v^o with temperature is observed throughout the whole melting transition regime. A step-like change at the transition temperature T_m is observed for pure DPPC and for DPPC – gramicidin concentrations of 1 and 2.5 mol%. Changes in [*u*] and v^o with increase in gramicidin concentration are clearly observed at T_m and above the T_m region indicating, increased volume fluctuations in this temperature region. The Δv^o for

pure DPPC at the gel/fluid transition was found to be ~0.045, which corresponds to an ~4% bilayer volume increase. The partial specific volume ν^o is larger below T_m and smaller above T_m for the DPPC – gramicidin mixtures, similar to the behavior of [u].

Figure 3.11: The temperature dependence of the partial specific adiabatic compressibility, k_S^o, of DPPC-gramicidin mixtures at different gramicidin mole fractions, X_{gD} and the adiabatic compressibility coefficient, β_S^{lipid}, of DPPC LUVs at various gramicidin mole fractions.
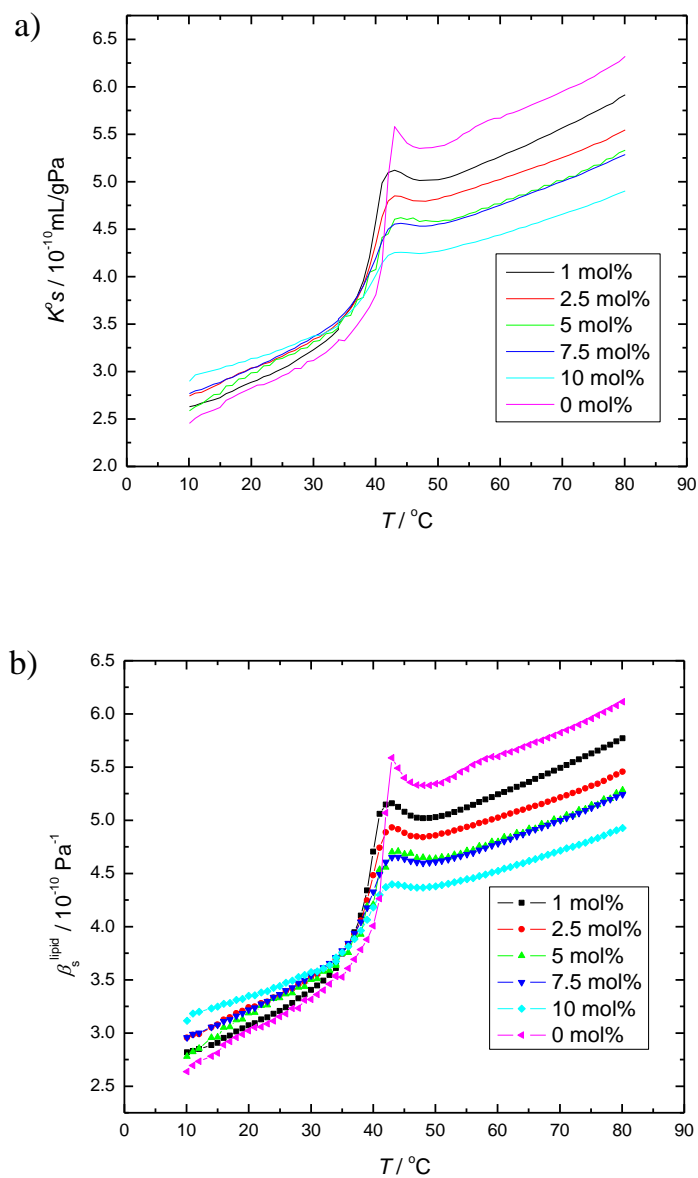
The partial specific adiabatic compressibility, k_S^o, has been determined from equation 23. Figure 3.11a gives the temperature dependence of k_S^o for the DPPC – gramicidin mixtures. As expected, the k_S^o for pure DPPC has the highest value increasing from 2.35 mL/gPa at 10 ^{o}C and abruptly reaching 5.5 mL/gPa (57%) at T_m. It shows a slight drop right beyond T_m, and finally continues to increase with increasing temperature to reach its maximum value of 6.3 mL/gPa at 80 ^{o}C.

Generally, we observe a significant broadening of the transition peak, a shift to lower temperatures and a decrease of k_S^o in the lipid melting transition region with increasing gramicidin concentration. Increase in compressibility of the lipid vesicle with increasing gramicidin concentration below T_m suggests a dencrease in the lipid bilayer order. The opposite holds true for $T > T_m$, where k_S^o decreases with increasing gD concentration.

The temperature dependence of β_S^{lipid} for the DPPC – gramicidin mixtures is displayed in figure 3.11b. As can be seen it has the same shape as k_S^o (Eqn. 25), which includes the anomalous peak at the main phase transition.

At 25 and 60 ^{o}C, β_S^{lipid} for pure DPPC is 3.2×10^{-10} Pa^{-1} and 5.6×10^{-10} Pa^{-1}, respectively. The value for β_S^{lipid} of 3.4×10^{-10} Pa^{-1} at 30 $^\circ$C is in good agreement with $\beta_S^{lipid} = 3.5 \times 10^{-10}$ Pa^{-1} obtained by Mitaku and coworkers (Mitaku 1978), but 5.3×10^{-10} Pa^{-1} at 50 $^\circ$C is higher compared to the literature value of 4.6×10^{-10} Pa^{-1}, which might be due to different vesicle preparations (LUV in our study and MLV in the reference mentioned (Mitaku 1978)). Alike for k_S^o, the anomalous increase of β_S^{lipid} around T_m is still significant at 1 and 2.5 mol% of gramicidin and markedly diminishes for higher gramicidin concentrations.
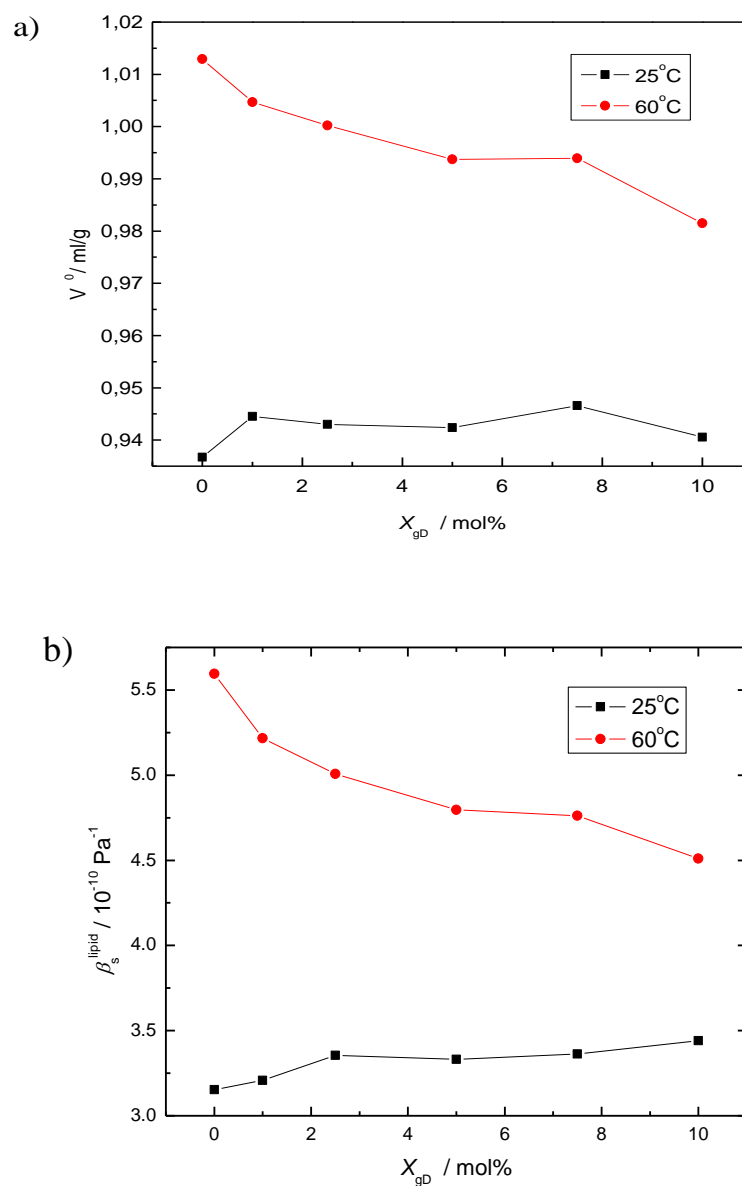
Figure 3.12: The partial specific volume and the adiabatic compressibility coefficient of DPPC-gD mixtures as a function of gD concentration at 25 ^{o}C and 60 ^{o}C.

A summary of the effects of increasing gramicidin concentration on v^o and β_S^{lipid} of the bilayer at 25 and 60°C is shown in figures 3.12a & 3.12b, respectively. The data reveal a

continuous decrease in ν^o and β_S^{lipid} with gD concentration in the fluid phase (except between 5 and 7.5%, where we observe only a very slight decrease) and a slight increase with concentration in the gel phase. The increase of β_S^{lipid} with increasing gD concentration, in the gel phase probably reflects the disordering effect which gD imposes on ordered phospholipid bilayers in this phase region. The data thus clearly show that incorporation of gD also drastically changes the temperature-dependent gel phase behavior of DPPC. It has been reported that incorporation of gD leads to a decrease of the molecular order of the acyl chains in the gel phases, whereas in the fluid phase, the mean order parameter increases (Eisenblätter 2006). Incorporation of gD into fluid-like DPPC has been shown to have a significant rigidifying effect on the conformational order in a cooperative manner along the entire acyl chain. Furthermore, it can be seen that, as expected, both ν^o and β_S^{lipid} generally increase with increasing temperature, and the slope of $\beta_S^{\text{lipid}}(T)$ decreases with increase in gD concentration.

3.2.1.3   Pure DPPC Bilayer Volume Fluctuations

Lipid bilayers show significant volume fluctuations as can be seen in the abrupt change in ν^o at the main phase transition. The isothermal compressibility, K_T, is directly proportional to the volume fluctuations of the system (Hill 1960, Krivanek 2008). We can only determine the adiabatic compressibility from the ultrasound velocity and density measurements. However, the isothermal compressibility can be calculated (see Eqn. 26)

A comparison of the compressibilities of the DPPC LUVs reveals, as expected from Eqn.26, that $\beta_T^{\text{lipid}} > \beta_S^{\text{lipid}}$ by ~11% in the whole temperature range. However around the T_m region, β_T^{lipid} differs distinctly, attributable to the absence of heat transfer between the lipid bilayer and the buffer solution within the time window of the ultrasound wave period (~ 14 µs in our experiments) for the adiabatic compressibility. This means that slow relaxation processes around T_m are not revealed from β_S^{lipid} measured by ultrasound velocity. Hence, β_S^{lipid} derived by means of the ultrasound velocity measurements is not able to capture the slow relaxation processes around T_m. In fact, a drastic slowing down of the relaxation time has been observed approaching the

DPPC main phase transition (Osdol 1991, Grabitz 2002) and was found to be as slow as 20-45 s in MLVs and ~3 s in LUVs.

The DPPC LUV values of β_T^{lipid} in the gel phase and fluid phase are found to be $3.8\pm0.2 \times 10^{-10}$ Pa^{-1} and $5.5\pm0.2 \times 10^{-10}$ Pa^{-1} respectively, which are in good agreement with the previously determined values from measurements of the partial volume as a function of pressure (Seemann 2003). At the main phase transition we found β_T^{lipid} to be 9.0×10^{-9} Pa^{-1}, which differs from the literature values available (Seemann 2003). This discrepancy probably arises from the different widths of the chain melting transition (which, in turn, depends on the vesicle preparation) and the fact that the ultrasound velocity, the density as well as the thermal expansion coefficient measurements were carried out with larger steps around T_m, only. The data are also in reasonable agreement with theoretical calculations by Heimburg et al. (Heimburg 1998), which rely on a linear proportionality between the excess heat capacity and the thermal volume changes, which has been shown to be valid for different lipid bilayer compositions (Edel 2001). Differences in absolute values might also be due to the fact that in their measurements the entire lipid solution and not partial quantities are considered.

3.2.1.4   Isothermal Compressibility and Volume Fluctuations of DPPC – Gramicidin Mixtures

Figure 3.13a displays the temperature dependences of the isothermal compressibility of DPPC-gD LUVs at different gD concentrations. We observed that the isothermal compressibility peak at the main transition drops drastically (~ 75 %) upon addition of gramicidin concentrations as low as 1 mol%. This decrease in β_T^{lipid} corresponds to a similar strong decrease (80 %) of the thermal expansion coefficient (Fig. 3.8b), again indicating the close relationship between the corresponding fluctuations ($\langle\Delta V^2\rangle$ *vs.* $\langle\Delta H\Delta V\rangle$) (Krivanek 2008).
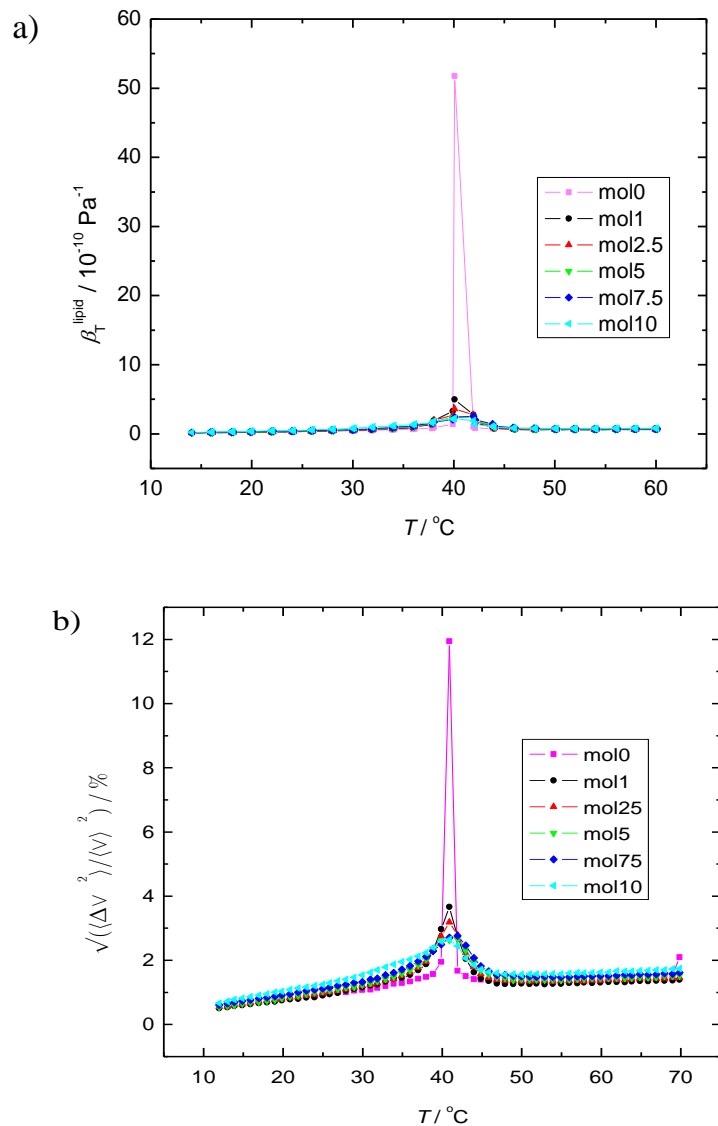
Figure 3.13: The temperature dependence of (a) the isothermal compressibility coefficient of the lipids β_T^{lipid} and (b) the calculated relative volume fluctuations for DPPC-gD mixtures at different gD mole fractions, X_{gD}.

Between 1 and 10 mol% gD, we observe only a slight decrease in β_T^{lipid} at the main transition region with increasing gD concentration, and almost no change between 5 and 7.5 mol%, as already observed in β_S^{lipid}. At gramicidin D concentrations higher than 5

mol%, β_T^{lipid} is greater than β_S^{lipid} at the gel-fluid region by $\sim$ 10 - 20% in the whole temperature range covered. Significant differences in β_T^{lipid} and β_S^{lipid} are seen in the gel and fluid phases of the lipid bilayer, as the solvent and lipid membranes are adiabatically uncoupled in the MHz region in the ultrasound experiment.

These differences become dramatic in the gel-fluid transition region, indicating a significant degree of slow relaxational processes in the μs time range in the transition region. β_T^{lipid} in both the gel phase (25 ^{o}C) and in the fluid phase (60 ^{o}C) of the DPPC-gD mixtures between 1 and 10 mol% reveal continuous increase with increase in gD concentration (fig. 3.13c). Above the main transition, at 60 ^{o}C, only the β_T^{lipid} value of 10 mol% gramicidin surpasses the value for pure DPPC.
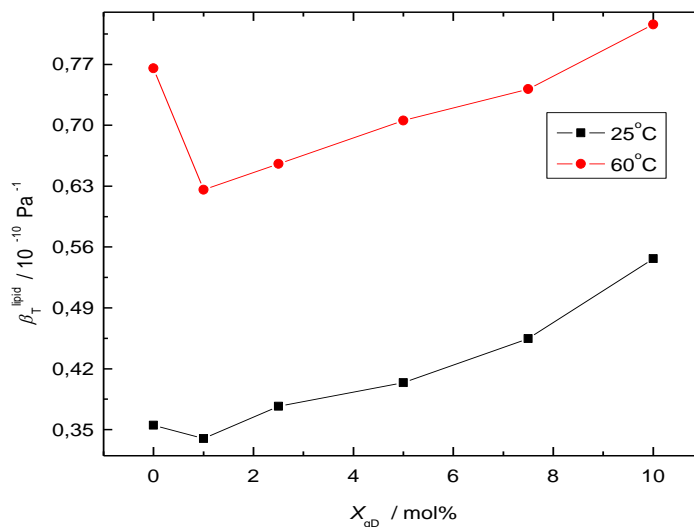
Figure 3.13c: The temperature dependence of the calculated isothermal compressibility coefficient of the lipids, β_T^{lipid}, at 25 and 60 ^{o}C for DPPC-gD mixtures at different gD mole fractions, X_{gD}.

Assuming that the partial specific volume, v^o, is largely determined by the lipid term (see Eqn. 21), i.e. v^o reflects the "real" volume of the lipid molecule, it allows us to modify Eqn. 33b and to convey the relative volume fluctuations given as

$$\sqrt{\frac{\left\langle \Delta V^2 \right\rangle}{V^2}} = \sqrt{\frac{RT\beta_T^{\text{lipid}}}{Mv^o}} \qquad (34)$$

The calculated temperature dependence of the relative volume fluctuations for the DPPC-gD mixtures are displayed in figure 3.13b. The figure clearly shows that the relative volume fluctuations of pure DPPC are drastically increased at the main transition, reaching up to 12 %, and are strongly damped upon addition of gramicidin D to 2.6% at 10 mol% gD. Furthermore, the volume fluctuations in both the gel phase (25 ^{o}C) and in the fluid phase (60 ^{o}C) reveal a continuous and gradual increase with increase in gD concentration between 1 and 10 mol% (Fig. 3.13d). Again, it can be clearly seen that the volume fluctuations are larger in the fluid phase than in the gel phase.
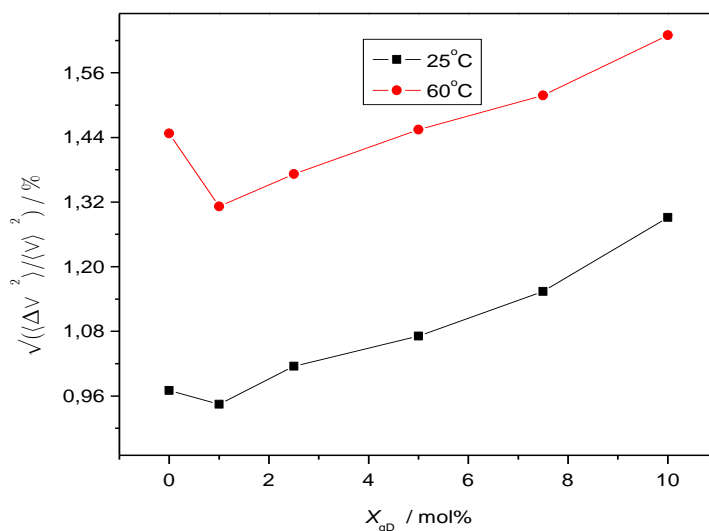
Figure 3.13d: The temperature dependence of the calculated relative volume fluctuations at 25°C and 60°C for DPPC-gD mixtures at different gD mole fractions, X$_{gD}$.

3.2.1.5   Concluding Remarks

In this work we have determined the absolute and relative volume changes, the isothermal compressibility and the volume fluctuations of DPPC – gramicidin bilayer membranes in their different phases by using molecular acoustics (ultrasound velocity and densitometry) and calorimetry (pressure perturbation calorimetry and differential

scanning calorimetry). To the best of our knowledge, this is the first time that such a multi-technique approach has been employed for the study of DPPC – gramicidin interactions.

Our study revealed a considerable influence of gramicidin on the mechanical, volumetric and compressibility properties of the DPPC bilayer. Approaching the transition from either side, thermodynamic fluctuations and response functions have been shown to increase, e.g. the specific heat, the lateral compressibility, the permeability, and the lateral diffusion coefficient [Jahnig 1981].

We observe that fluctuations are maximal at the chain melting transition point, the heat capacity, expansivity, and compressibility are proportional to the local fluctuations in enthalpy and volume, respectively. A further likely effect of large fluctuations of lipids lies in an increased permeability of the membrane, because the likelihood of spontaneous pore formation should be linked to the (lateral) compressibility. Our interpretation of the thermograms seen in figure 3.8 is that gramicidin can still be incorporated beyond the mole fraction of 10%.

It is known from calorimetry that peptides and proteins influence the chain melting transition of lipid membranes. Usually, transition profiles are broadened and/ or shifted to either lower or higher temperature. A shoulder at the low temperature side of the heat capacity profile indicates unfavorable partitioning in the low temperature phase. The calorimetric data therefore indicates that the mixing of gD is less favorable in the gel phase of DPPC. This is reasonable because of the difference in the hydrophobic cores of gramicidin and DPPC bilayer (hydrophobic matching concept).

The asymmetry of the profile results from a change in mixing behavior. The effect of the addition of 10 mol% of the peptide on the heat capacity profile is a symmetric broadening of the heat capacity (Ivanova 2003). This is due to the fact that peptides located between gel and fluid domains lower the cooperativity of the melting transition. However, since the fluid lipids are shorter than the gel lipids, one may expect a better matching of the fluid lipids with gD, and therefore a shift of the C_p-profile to lower temperatures. Upon incorporation of gD into DPPC, it is indeed found in calorimetric experiments that the heat capacity profiles are only very slightly shifted to lower temperatures with a small asymmetry at the low temperature end. Thus the lipid behavior of DPPC membranes

containing gD is very similar to that expected for a peptide that aggregates in both gel and fluid phase, with a slight preference for the fluid phase.

For 2.5 mol% gramicidin concentration, we observe induction of a two phase region, with a more cooperative, higher temperature endotherm superimposed over a less cooperative, lower temperature endotherm. At a concentration of 5 mol%, two endotherms are present in the DSC thermogram, a more cooperative endotherm at 41°C and a less cooperative small endotherm centered at 24 $^{\circ}$C.

The effect of increasing gramicidin concentration on ν° and β_S^{lipid} of the bilayer at T_{m} region, reveals a continuous decrease in ν° and β_S^{lipid} (within the range of concentrations studied) with increase in gD concentration except between 5 and 7.5 %, where we observe a very slight decrease, only. We observe that the isothermal compressibility peak at the main transition drops drastically ($\sim$75%) upon addition of gramicidin concentrations as low as 1 mol%. In addition, we found that at gD concentrations higher than 5 mol%, β_T^{lipid} is greater than β_S^{lipid} in the gel-fluid coexistence region by 10 – 20 % in the whole temperature range covered.

The maximum value of the relative volume fluctuation of 12 % is reached for pure DPPC at the main transition, and is strongly damped upon addition of gD. A gradual decrease in the calculated relative volume fluctuations with gD concentration at T_{m} is observed between concentrations 1 and 10 mol%.

3.2.2   Lipid – Melittin Interaction

3.2.2.1   Calorimetric Measurements on DPPC – Melittin Mixtures

The excess heat capacity (C_{p}-profiles) of multilamellar vesicle (MLV) suspensions of DPPC with different concentrations of melittin added is displayed in figure. 3.14a. The heat capacity trace of pure DPPC displays a maximum at 41 $^{\circ}$C, referred to as the main phase transition temperature, T_{m}. Overall, the heat capacity increase in the transition regime is mainly due to cooperative fluctuations of a large number of lipid molecules.

When the DPPC liposomes are prepared in the presence of melittin concentrations of 1 to 2.5 %, there is no change in the temperatures of the main transition. Addition of 1

mol% melittin leads to a reduction of the lipid pre-transition peak. The peak is not completely abolished; however the temperature of the pre-transition shifts slightly to a lower temperature (32 °C). The pre-transition is completely abolished at a melittin concentration of 1.25 mol% and at this particular concentration there appears a noticeable base peak broadening, a small asymmetry at the low-temperature wing and a reduction in transition profile which continues to increase with increasing melittin concentration. There is a concomitant reduction in the cooperativity of the chain melting transition, which is evidenced by the broadening of the transition profile. A shoulder (a small peak) appears at the low-temperature side (at 39 °C) of the main transition peak for 2.5 % melittin, with a further reduction of the transition profile and cooperativity.

a)   b)
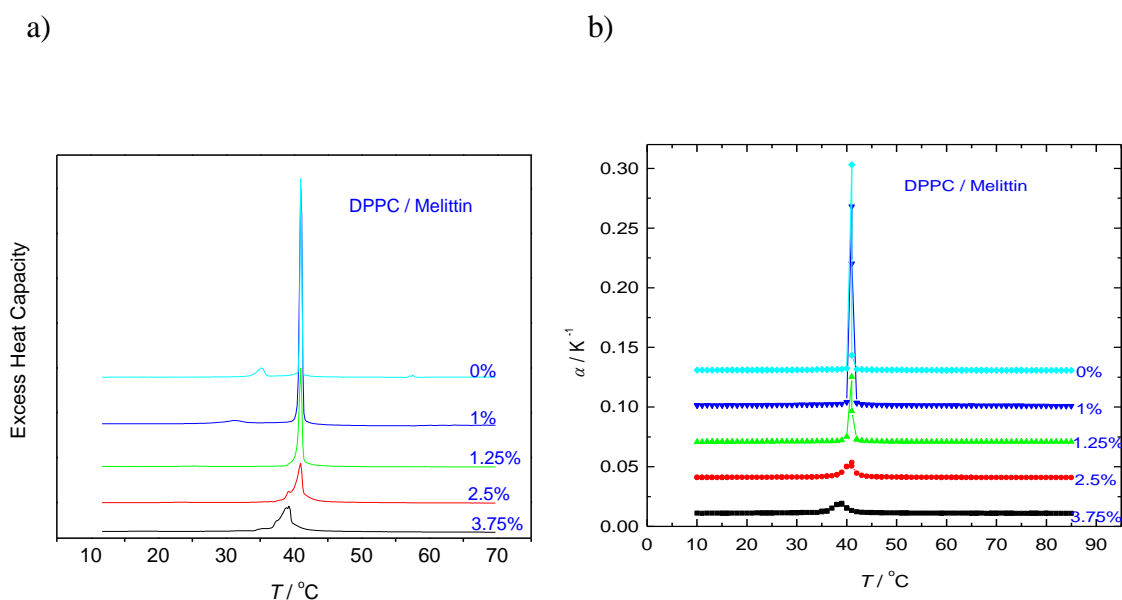
Figure 3.14: Melittin in DPPC lipid bilayers. (a) DSC thermograms (heating scans, only) of melittin in DPPC multilamellar vesicles with 1, 1.25, 2.5, and 3.75 mol% of peptide in excess water. (b) Temperature dependence of the coefficient of thermal expansion, α, of DPPC/melittin mixtures (pH 7.4, 10 mM Tris buffer, scan rate 40°C/h). To ensure clear data representation, plots of different melittin content were shifted along the volume expansion coefficient axis using a constant offset (from bottom to top by 0.02 units).

Additionally, we observe no shift in the main transition temperature up to 2.5 mol% melittin. More than one shoulder is observed at the low-temperature side of the peak for 3.75 mol%, and a slight shift in T_m to 32°C. Oliynyk et al. observed a similar low-

temperature shoulder in the C_p-profile at higher melittin concentrations (Oliynyk 2007), in good agreement with our data.

The PPC stacked plot of the coefficient of thermal expansivity versus temperature curves of the DPPC melittin mixtures is revealed in figure 3.14b. The PPC scans were carried out with solutions of DPPC/melittin in Tris buffer yielding the changes with temperature of the thermal expansion coefficient, α. As stated earlier, the plots can be divided into three temperature regimes. We observe a slight increase in α below the pretransition with increase in melittin concentration, but not in any particular order. For instance, $\alpha = 1.01 \times 10^{-3}$ K^{-1} for 2.5 mol%, and $\alpha = 1.12 \times 10^{-3}$ K^{-1} for 3.75 mol% at 20°C. Above T_m (65 $^{\circ}$C), we observe, just below the pretransition, a very slight increase in α, with increase in melittin concentration (as an example, $\alpha = 0.92 \times 10^{-3}$ K^{-1} and $\alpha = 1.02 \times 10^{-3}$ K^{-1} at 65 $^{\circ}$C for 1.25 % and 2.5 % melittin respectively), whereas the main peak height of α in the transition region decreases and broadens markedly with increase in melittin concentration.

From the integration of α over the temperature range where the main transitions occur, we obtain the relative volume changes, $\Delta V/V$, for the pure DPPC and for each of the DPPC / melittin concentrations. $\Delta V/V = 0.04 \pm 0.007$ (4 %), which corresponds to an absolute volume change of 29 mL/mol, for pure DPPC, $\Delta V/V$ is 0.038 ± 0.001 for 1.25 mol%, 0.029 ± 0.002 for 2.5 mol%, and 0.026 ± 0.002 for 3.75 mol% melittin. The corresponding width of the overall transition, $\Delta T_{1/2}$, increases from about 1 $^{\circ}$C for the main transition of pure DPPC to about 3 $^{\circ}$C for the DPPC / 3.75 mol% melittin mixture.

3.2.2.2   Ultrasound and Density Measurements on DPPC – Melittin Mixtures

The temperature dependent ultrasound velocity number, $[u]$, as a function of temperature for the DPPC–melittin mixtures is displayed in figure 3.15a. As already observed in the DPPC- gD data, at points distant from the lipid main phase transition temperature, a gradual decrease of $[u]$ is observed with increasing temperature, leading to the typical characteristic anomalous dip at the T_m for pure lipid.

Upon addition of melittin to DPPC, we observe, at T_m, a general increase in $[u]$ as compared to the pure lipid. However, we observe that the sample with 3.75 % melittin

has the lowest value of [*u*] compared to the lower melittin concentrations studied. It also exhibits the broadest peak. The dip continues to increase with a decrease in melittin concentration, with the highest value being at 1.25 % and 1 % melittin. This is in contrast to our earlier studied systems lipid-gD and lipid-sterol systems (Krivanek 2008) and might be linked to the lytic property of melittin at higher concentrations, in particular in the lipid phase transition region.
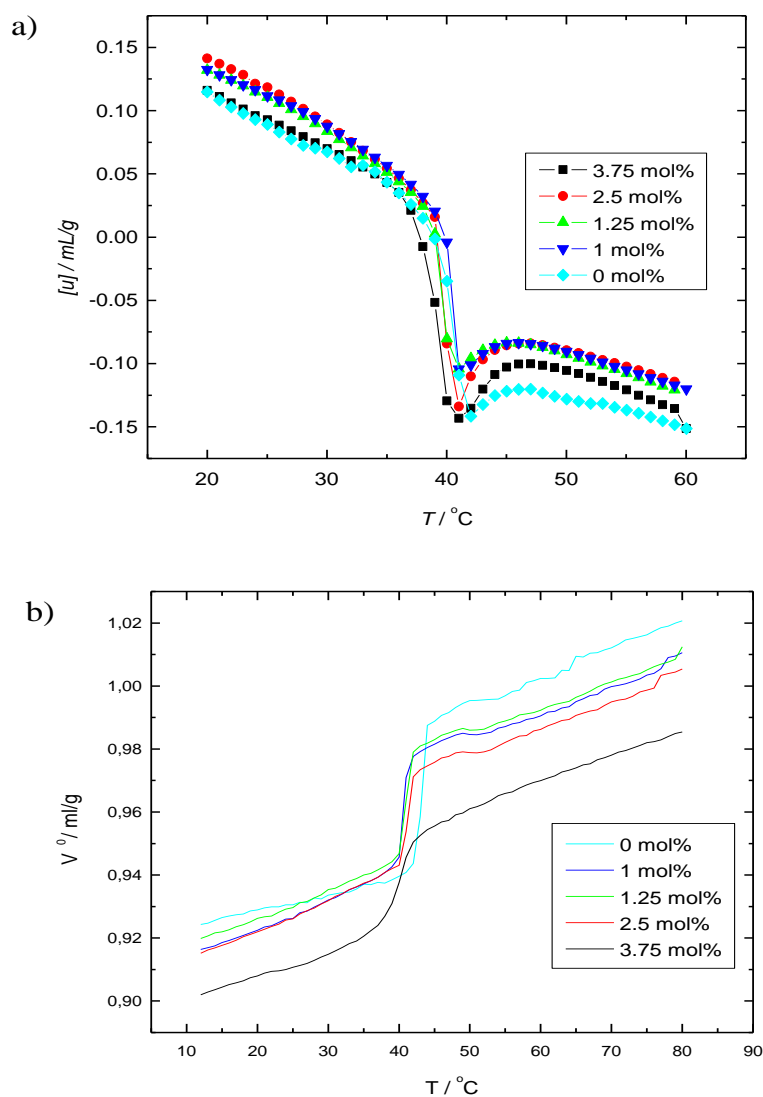
Figure 3.15: The temperature dependence of (a) the ultrasound velocity number, [*u*], and (b) the specific volume, *v*°, for DPPC- melittin mixtures.

We observe that pure DPPC has the least [*u*] both in the gel phase and in the fluid phase region.

In addition, for the DPPC-melittin mixture, both below the pretransition and above the main transition, the sound velocity number is approximately the same for the concentrations 1 %, 1.25 % and 2.5 % melittin. Generally, addition of melittin to DPPC bilayers causes a slight shift of the melting phase transition to lower temperatures.

The temperature dependence of the partial specific volume, v^o, as measured by the densitometer, is shown in figure 3.15b, and an increase of v^o with temperature is observed throughout the whole melting transition regime. A step-like change at the transition temperature T_m is observed for pure DPPC and for DPPC – melittin concentrations up to 2.5 mol%. As already stated above, the changes in [*u*] and v^o with increase in melittin concentration are clearly observed in the T_m region, indicating increased volume fluctuations in this temperature region. The partial specific volume v^o is smaller both below and above T_m for the DPPC – melittin mixtures. A substantial decrease is observed for v^o upon addition of melittin up to 3.75 mol%, which could be attributed to the lytic property of melittin at high melittin concentrations. A more detailed behavior of v^o in the gel phase and in the fluid phase is illustrated in figure 3.15c.
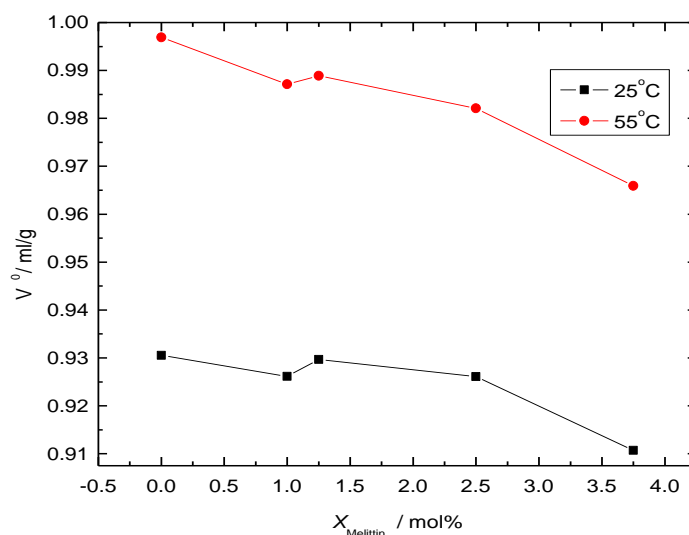
Figure 3.15c: The partial specific volume of DPPC-melittin mixtures as a function of melittin concentration at 25 and 55 ^{o}C.

Figure 3.16a displays the temperature dependent partial specific adiabatic compressibility, k_S^o, of the transitions of both pure DPPC and the DPPC – melittin mixtures, as determined from Equation 23. The k_S^o for pure DPPC has the highest value, increasing from 2.35 mL/gPa at 20°C and abruptly reaching 5.25 mL/gPa (55°C) at T_m, as expected. A slight drop occurs right after T_m, and k_S^o finally continues to increase with increasing temperature to reach the highest level of 5.4 mL/gPa at 60 ^{o}C. Generally, we observe a slight shift to lower temperatures for k_S^o in the melting transition region, just as observed in $[u](T)$. Significant broadening of the transition peak is observed at the 3.75 % concentration. The temperature dependence of β_S^{lipid} for the DPPC – melittin mixtures is displayed in figure 3.16b and exhibits similar shape as $k_S^o(T)$ (Eqn. 25).

a)

b)
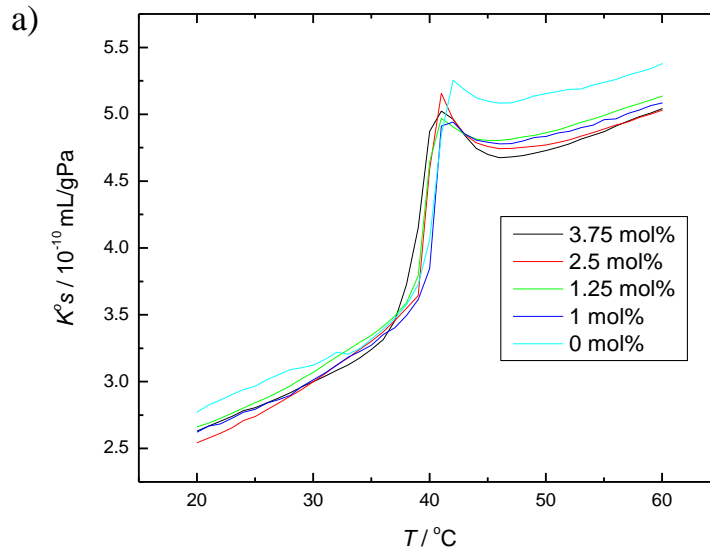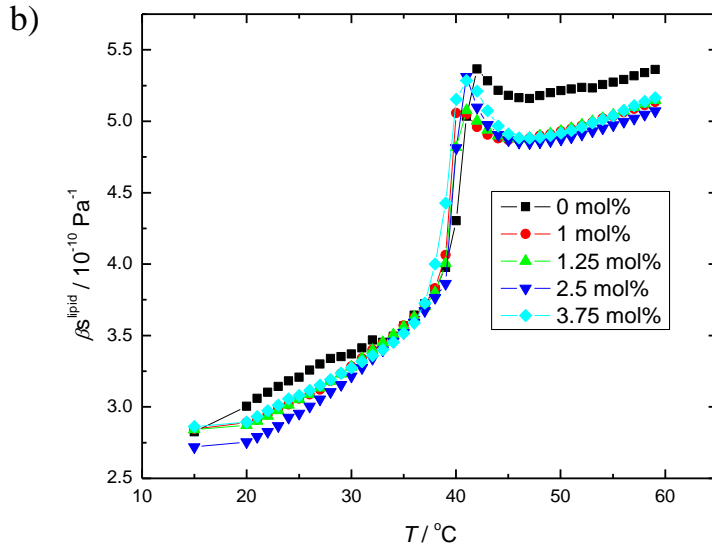
Figure 3.16: The temperature dependence of (a) the partial specific adiabatic compressibility, k_S^o, and (b) the adiabatic compressibility coefficient, β_S^{lipid}, of DPPC-melittin mixtures at various melittin mole fractions.

At 20 and 60 °C, the β_S^{lipid} vales are 3.0 x 10^{-10} Pa^{-1} and 5.4 x 10^{-10} Pa^{-1}, respectively. The value for β_S^{lipid} of 3.4×10^{-10} Pa^{-1} at 30 °C is in good agreement with $\beta_S^{\text{lipid}} = 3.5 \times 10^{-10}$ Pa^{-1} obtained by Mitaku and coworkers (Mitaku 1978). Just as for k_S^o, the anomalous increase of β_S^{lipid} around T_m is still significant at all melittin concentrations. The data for the adiabatic compressibility coefficient of the DPPC-melittin mixtures as a function of melittin concentration at 25 and 55 °C is summarized in figure 3.16c. The plot reveals a gradual decrease in β_S^{lipid} with melittin concentration in both the gel (25 °C) and the fluid phase (55 °C) up to 2.5 mol% melittin. We observe an increase in β_S^{lipid} upon addition of 3.75 mol%, implying a disordering effect (which could be attributed to melittin pore formation) at these higher melittin concentrations.
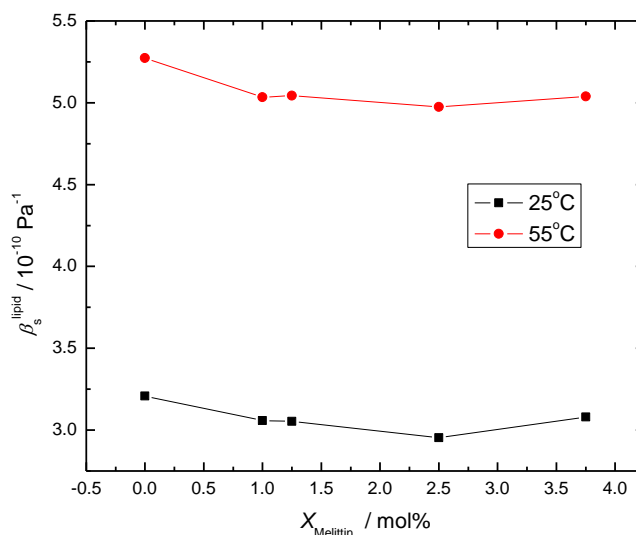
Figure 3.16c: The adiabatic compressibility coefficient of lipid data of DPPC-melittin mixtures as a function of melittin concentration at 25 and 55°C, respectively.

3.2.2.3   Isothermal Compressibility and Volume Fluctuations of DPPC – Melittin Mixtures

Figure 3.17a displays the temperature dependences of the isothermal compressibility of DPPC-melittin LUVs at different melittin concentrations. We observed that the isothermal compressibility peak at the main transition drops drastically ($\sim$ 75 %) upon addition of melittin at concentrations as low as 1 mol%. This decrease in β_T^{lipid} corresponds to a similar strong decrease (80 %) of the thermal expansion coefficient (figure 3.14b), again indicating the close relationship between the corresponding fluctuations ($\langle \Delta V^2 \rangle$ *vs.* $\langle \Delta H \Delta V \rangle$) (52). Furthermore, we observe an increase in β_T^{lipid} with increase in melittin concentrations at the transition temperature (disordering effect at higher melittin concentrations). At all melittin concentrations, β_T^{lipid} is greater than β_S^{lipid} by $\sim$ 20% in the whole temperature range covered. The calculated temperature dependence of the relative volume fluctuations (Eqn. 34) for the DPPC-melittin mixtures is displayed in figure 3.17b.

a)   b)
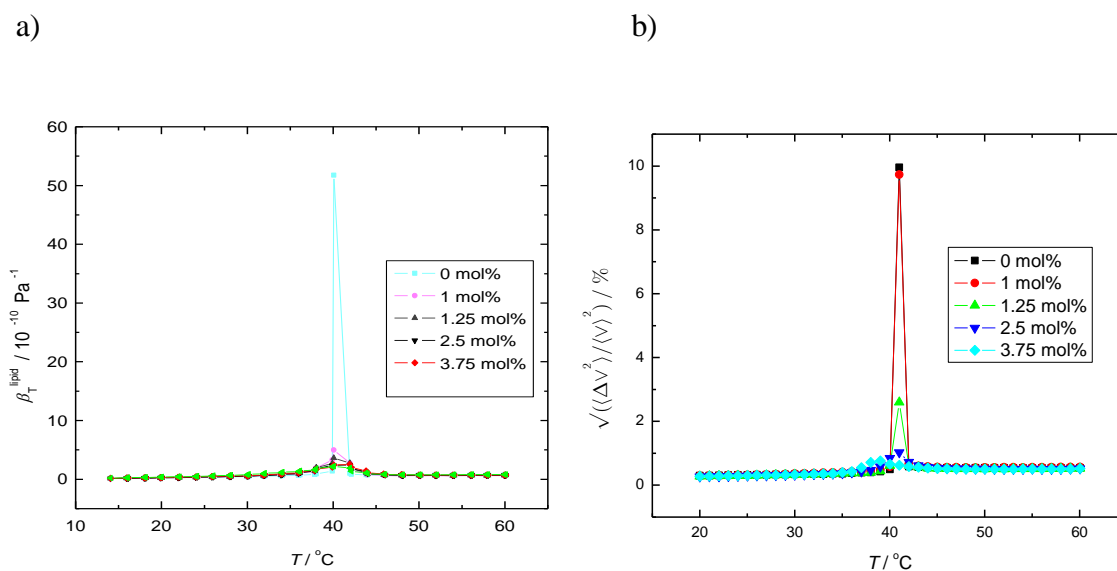
Figure 3.17: The temperature dependence of (a) the isothermal compressibility coefficient of the lipids β_T^{lipid} and (b) the calculated relative volume fluctuations for DPPC-melittin mixtures at different melittin concentrations.

Only a slight decrease in the calculated relative volume fluctuations with melittin concentration is observed between concentrations 0 and 1.0 mol% melittin.

Figure 3.17c: The temperature dependence of the calculated relative volume fluctuations at 25 and 55°C for DPPC-melittin mixtures at different melittin mole fractions X_m.

Above the main transition temperature, basically no change is observed in the calculated relative volume fluctuations for DPPC-melittin concentrations of between 1.25 and 3.75 mol% (figure 3.17c).
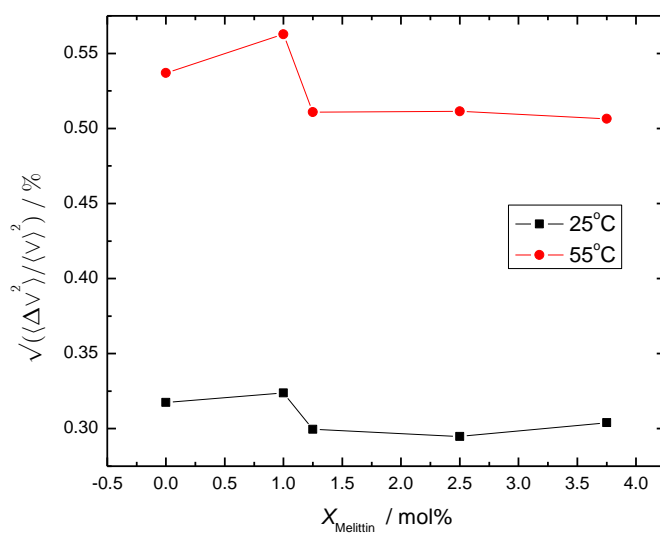
3.2.2.4   Concluding Remarks

In summary, the study has provided further insights into the disruptive effects of melittin on membrane bilayers. In this work we have used molecular acoustics (ultrasound velocity and densitometry) and calorimetry (pressure perturbation calorimetry and differential scanning calorimetry) to determine the absolute and relative volume change, isothermal compressibility and volume fluctuations of DPPC – melittin bilayer membranes in their different phases.

Our study revealed a considerable influence of melittin on the thermodynamic, mechanical, volume and compressibility properties of DPPC bilayers. We have shown that as the concentration of membrane-bound melittin increases, the relative volume change at the main transition of the lipid bilayer decreases. We observe that fluctuations are maximal at the melting point, and that the heat capacity, expansivity, compressibility are proportional to the local fluctuations in the enthalpy and volume, respectively.

From the calorimetric measurements, upon incorporation of melittin into the lipid bilayer up to 1.25 %, we conclude that the pretransition is completely abolished. At this particular concentration, we observe a noticeable base peak broadening and a reduction in transition profile which continues with increase in melittin concentration. The appearance of a small endothermic peak at 39 $^{\circ}$C for 2.5 % melittin could possibly reflect morphological changes of free lipid vesicles in solution. Remarkably, there is no shift in the transition temperature up to 2.5 %, while more than one shoulder was observed at the low-temperature side of the peak for 3.75 %, and a slight shift in T_m to 32 $^{\circ}$C. Oliynyk et al. have demonstrated that melittin incorporation leads to pore formation and the structure of the melittin pores depends on the thermodynamic state of the membrane (Oliynyk 2007). From their AFM images they concluded that at 1 mol% melittin, transmembrane pores are induced in the gel phase of DPPC bilayers. Generally, the peptides in model

and biological membranes can strongly affect the local state of the system, and the effect of peptide may also depend on the overall state of the membrane. Peptides like alamethicin tend to increase the permeability of biological membranes by not only forming water pores, but also by shifting the surrounding bilayer to more disordered states which are more permeable for small molecules. Hence, the state of the membrane can be a regulating factor of the action of antibiotic peptides like melittin, influencing their capability to form transmembrane pores. At the main transition region, the peak height of α decreases and broadens markedly with increase in melittin concentration. Again, at T_m, a general increase in $[u]$ as compared to the pure lipid is observed. However, we observe that 3.75 % melittin induces the broadest peak and lowest value of $[u]$ compared to other melittin concentrations which could be due to changes of hydration of the membrane as a result of the binding process. The dip continued to increase with decrease in melittin concentration, with the highest value being at 1.25 and 1% melitiin.

The melittin concentration effects on v^o and β_S^{lipid} of the bilayer reveals a slight shift of the main transition to lower temperature and a continuous decrease in v^o (within the range of concentrations studied) above the T_m with concentration (except between 1 and 1.25%), as well as a decrease in β_S^{lipid} with decrease in melittin concentration. Again, we observe that the isothermal compressibility peak at the main transition drops drastically upon addition of melittin at concentrations as low as 1 mol% and then increases with increase in melittin concentration. In addition, we found that at all melittin concentrations β_T^{lipid} is greater than β_S^{lipid} in the gel-fluid region by $\sim$ 20%. The maximum value of the relative volume fluctuations of 12 % is reached for DPPC at the main transition, and is strongly dampened upon addition of melittin. Only a slight decrease in the calculated relative volume fluctuations with melittin concentration is observed between concentrations 0 and 1.0 mol%.

SUMMARY

Sterols regulate biological processes and sustain the lateral structure of cellular membranes. The sterol cholesterol, its precursor lanosterol, the plant sterols stigmasterol and ergosterol as well as 7-dehydrocholesterol were added up to 36 mol% to vesicles of the phospholipid 1,2-dipalmitoyl-*sn*-glycero-3-phosphatidylcholine (DPPC). In this study, we have been able to investigate the influence of the sterol side chain and ring structure on the volumetric properties of the lipid bilayer system by using pressure perturbation calorimetry (PPC), a relatively new and efficient technique, to study the thermal expansion coefficient and volumetric properties of biomolecules. The experiments were carried out in the temperature range from 10 to 85 °C, i.e., at temperatures below and above the chain-melting transition temperatures of the lipid mixtures. Additionally, corresponding differential scanning calorimetric (DSC) measurements were carried out.

Recent measurements of the lipid acyl chain order parameter revealed that with increasing side-chain volume of the sterol, the conformational order of the lipid acyl chains decreases, and an increase in alkyl chain volume has the most drastic effect on the condensing capacity of sterols. The introduction of a double bond in the side chain counteracts this effect, owing to the decreased volume fluctuations in the steroid alkyl chain region. Introduction of a double bond in the ring system leads at low and medium high sterol levels (up to ~40 mol%) to a drastic increase in conformational order of the lipid acyl chains (compare, e.g., *trans*-7-dehydrocholesterol with cholesterol), which can indeed be substantially higher than that induced by cholesterol. Additional methyl groups in the ring system of the sterol markedly counteract this rigidifying effect (compare lanosterol with ergosterol). Sterols with the bulkiest unsaturated side chains or sterol nuclei (stigmasterol, lanosterol) induce the smallest order parameter increase of the fluid bilayer at high sterol concentrations (> 30 mol%), and hence are less effective rigidifiers at high sterol levels. The difference might also be due to a different solubility/partitioning in the bilayer. Lanosterol is a sterol precursor. Owing to its additional methyl groups in the ring system, its partitioning is much less effective than that of cholesterol at high sterol levels. An important conclusion has been that cholesterol, with its streamlined molecular structure, interacts more effectively with lipid chains and stabilizes the liquid-ordered

state. Interestingly, from an evolution point of view, cholesterol seems to be very efficient in suppressing the chain-melting transition of the phospholipid bilayer system. A marked limitation of the condensing effect is observed for the stigmasterol system having a rather bulky alkyl chain, which is also reflected in volumetric parameters.

Alterations in the sterol structure are also reflected in their thermodynamic properties. Though the overall thermodynamic features of all sterols besides lanosterol seem to be qualitatively similar, minor differences are found, such as in abolishing the pretransition and in the extension of the phase space of the two-phase regions, as indicated by the differences observed in the corresponding DSC and PPC thermograms. For lanosterol, differences in the miscibility and temperature-concentration phase behavior and hence the thermodynamic functions $C_p(T)$ and $\alpha(T)$ are most obvious when compared to cholesterol and the other sterols. The changes in $C_p(T)$ are found to precisely mirror the corresponding $\alpha(T)$ data, an indication of the membrane enthalpy and volume fluctuations (Eqns. 33a,33c) being governed by the same molecular origin. Increases in $C_p(T)$ and $\alpha(T)$ at phase changes are mainly linked to cooperative fluctuations of large numbers of lipid molecules in their physical state. The sharpness of the transition peaks is related to the correlation lengths of these fluctuations, namely the domain sizes of the coexisting phases. With increasing sterol concentration, the widths of both thermodynamic parameters at the chain-melting transitions increase drastically, indicating coupled enthalpy and volume fluctuations with low amplitude by large correlation lengths over an extended temperature region.

The large cross-sectional area of the steroid ring system of lanosterol makes it a more effective spacer than DPPC molecules in the gel-state bilayer, thus relieving the mismatch in the cross-sectional areas of the acyl chains and the DPPC polar headgroups at lower sterol concentrations more efficient than cholesterol. Also, the rougher surface of the lanosterol molecule would be expected to produce a greater amount of orientational disorder in the adjacent phospholipid's acyl chains, thus further augmenting the expansion of the DPPC gel-state bilayer, and leading to the markedly larger α-values observed for this system.

In another study, gramicidin D (gD) was incorporated into the phospholipid bilayer DPPC at mole fractions up to 10 mol%. Gramicidin insertion into DPPC bilayer has significant influence on the lipid bilayer structure, temperature, and pressure dependence phase behaviour. We have determined the temperature dependence of the coefficient of expansion coefficient, α, the volume fluctuations, and isothermal compressibilities of DPPC – gD bilayer membranes in their different transition phases by using calorimetric (PPC and DSC) and molecular acoustics (ultrasound velocimetry and densitometry) methods. In addition, corresponding differential scanning calorimetric measurements were carried out. The study has revealed a considerable influence of gD on the mechanical, volumetric and compressibility properties of the DPPC bilayer.

The interpretation of the thermograms seen in figure 3.8 is that gramicidin can still be incorporated beyond a mole fraction of 10 mol%. Two endotherms are clearly present in the DSC thermogram at 5 mol% concentration; a more cooperative endotherm at 41 $^{\circ}$C and a less cooperative endotherm centered at 24 $^{\circ}$C. The effect of the addition of 10 mol% of peptide on the heat capacity profiles is a symmetric broadening of the heat capacity. This behavior is due to the fact that peptides located between gel and fluid domains lower the cooperativity of the melting transition. However, since the fluid lipids are shorter than the gel lipids, one may expect a better matching of the fluid lipids with gD, and therefore a shift of the C_{p}-profile to lower temperatures. Upon incorporation of gD into DPPC, the heat capacity profiles are only very slightly shifted to lower temperature with a small asymmetry at the low temperature end. Thus, the behavior of DPPC membranes containing gD is very similar to that expected for a peptide that aggregates in both gel and fluid phase, with a slight preference for the fluid phase.

Both the thermal expansion coefficient peak maxima in the transition region and the relative volume changes decrease with increase in gD concentration. The volume change, Δv^{o}, for pure DPPC at the gel/fluid transition was found to be ~0.045, which corresponds to a 4.5 % increase in bilayer volume. The effects of increasing gramicidin concentration on the partial specific volume, v^{o}, and the adiabatic compressibility coefficient of the lipid, $\beta_{S}^{\mathrm{lipid}}$, of the DPPC bilayer exhibits a gradual decrease in v^{o} and $\beta_{S}^{\mathrm{lipid}}$ with increasing gD concentration. In addition, we found that at gD concentrations higher than 5 mol%, the isothermal compressibility coefficient, $\beta_{T}^{\mathrm{lipid}}$, is greater than

β_S^{lipid} by $\sim 10 - 20$ % in the entire temperature range covered. The maximum value of the relative volume fluctuation of 12 % is reached for DPPC at the main transition, and is strongly dampened upon addition of gD. A gradual decrease in the calculated relative volume fluctuations with gD concentration was observed between concentrations 1 and 10 mol% gD.

A shoulder at the low temperature side of the heat capacity profile indicates unfavorable partitioning in the low temperature lipid phase. The calorimetric data therefore indicate that the mixing of gD is less favorable in the gel phase of DPPC. This is reasonable because of the difference in the hydrophobic cores of gramicidin and the DPPC bilayer (hydrophobic matching concept).

Melittin has been a source of inspiration for the development of novel antiviral and antibacterial agents that act at the membrane level to cause membrane leakage and hence induce cell death. More detailed information on thermodynamic properties of melittin in membranes is therefore important due to the widespread occurrence of the motif in host-defense peptides and membrane proteins.

In this study, we obtained detailed information about the volumetric and mechanical properties of melittin-DPPC bilayers as revealed by calorimetry and molecular acoustics. We have used molecular acoustics and calorimetry techniques to determine, just as for DPPC-gD, the temperature dependence of the coefficient of thermal expansion, α, the volume changes, and the isothermal compressibility of the DPPC – melittin bilayer membrane in its different phases.

We have shown, from the calorimetric measurements, that incorporating melittin (up to 1.25 %) into the lipid bilayer abolishes the pretransition. Remarkably, there is no shift in the transition temperature up to 2.5 % melittin, more than one shoulder is observed at the low-temperature side of the DSC peak for 3.75 %, and a slight shift in T_m to 32°C. It has been demonstrated that the structure of melittin pores depends on the thermodynamic state of the membrane.

At the main transition region, the peak height of α decreases and broadens markedly with increase in melittin concentration. At T_m, a general increase in velocity

number [*u*] as compared to the pure lipid was noticed. However, we observe that 3.75 mol% melittin displays the broadest peak and lowest value of [*u*] compared to the other melittin concentrations, which could be linked to the lytic property of melittin at these high peptide concentrations. The dip continues to increase with decrease in melittin concentration, with the highest value being at 1 and 1.25 mol%. The melittin concentration effects on v^o and β_S^{lipid} of the bilayer shows a slight shift of T_m to lower temperatures and a gradual decrease in v^o above T_m with increase of melittin concentration (except between 1 and 1.25 %). At all melittin concentrations, β_T^{lipid} is greater than β_S^{lipid} by $\sim$ 20 % in the whole temperature range covered.

Generally, the peptides in model and biological membranes can strongly affect the local conformation of the lipid system, and the effect of peptide incorporation may also depend on the overall state of the membrane. Hence, the state of the membrane can be a regulating factor of the action of antibiotic peptides like melittin, influencing their capability to form transmembrane pores.

Zusammenfassung

Sterine regulieren biologische Prozesse und halten die laterale Struktur zellulärer Membranen aufrecht. Das Sterin Cholesterin, sein Ausgangsstoff Lanosterin, die pflanzlichen Sterine Stigmasterin und Ergosterin sowie 7-Dehydrocholesterin wurden zu Vesikeln des Phospholipids 1,2-Dipalmitoyl-*sn*-glycero-3-phosphatidylcholin (DPPC) hinzugefügt, so dass die molare Konzentration 36 % betrug. In dieser Studie wurde der Einfluss der Sterin-Seitenkette und der Ringstruktur auf die volumetrischen Eigenschaften der Lipiddoppelschichten unter Anwendung der Druck-Störungs-Kalorimetrie (engl.: pressure perturbation calorimetry, PPC) untersucht; einer relativ neuen und effizienten Methode, um den thermischen Ausdehnungskoeffizienten sowie volumetrische Eigenschaften von Biomolekülen zu untersuchen. Sämtliche Versuche wurden in einem Temperaturbereich zwischen 10 und 85°C durchgeführt, z.B. bei Temperaturen unter und über den Kettenschmelzübergangstemperaturen der Lipidmischungen. Analog dazu wurden Dynamische Differenz-Kalorimetrie-Messungen (engl.: differential scanning calorimetry, DSC) durchgeführt.

Kürzliche Messungen des Lipid-Acyl-Ketten-Ordnungsparameters haben ergeben, dass die konformative Ordnung der Lipid-Acyl-Kette mit zunehmendem Seitenkettenvolumen des Sterins abnimmt und außerdem einen äußerst drastischen Effekt auf die Kondensationsfähigkeit der Sterine hat. Die Einführung einer Doppelbindung wirkt dem Effekt aufgrund verminderter Volumenfluktuation im Bereich der Alkyl-Ketten des Steroids entgegen. Die Einführung einer Doppelbindung im Ringsystem führt bei niedrigen und mittleren Sterinkonzentrationen (bis zu ~40 mol%) zu einer drastischen Zunahme der konformativen Ordnung der Lipid-Acyl-Ketten (vergleiche z.B. Trans-7-dehydrocholesterin mit Cholesterin). Zusätzliche Methylgruppen im Ringsystem des Sterins wirken diesem Effekt merklich entgegen (vergleiche Lanosterin mit Ergosterin). Sterine mit den grössten ungesättigten Seitenketten oder Sterinkerne (Stigmasterin, Lanosterin) verursachen die geringste Zunahme des Ordnungsparameters der flüssigen Doppelschicht bei hohen Sterinkonzentrationen (>30 mol%) und sind deshalb weniger effektive (Membran-)Stabilisatoren. Der Unterschied könnte auch von einer unterschiedlichen Löslichkeit bzw. Trennung der Doppelschicht herrühren. Lanosterin ist ein Ausgangsstoff

der Sterine. Aufgrund seiner zusätzlichen Methylgruppen im Ringsystem, ist sein Trennvermögen weit weniger effektiv, als das von Cholesterin bei hohen Sterinkonzentrationen. Eine wichtige Schlussfolgerung ist, dass Cholesterin aufgrund seiner schlanken Molekülstruktur effektiver mit den Lipidketten interagiert und den flüssig-geordneten Zustand stabilisiert. Interessanterweise scheint Cholesterin den Kettenschmelzübergang sehr effizient zu unterbinden. Eine deutliche Einschränkung des kondensierenden Effekts wird beim Stigmaterol-System beobachtet, welches eine relativ grosse Alkylkette besitzt. Dieses schlägt sich auch bei den volumetrischen Parametern nieder.

Änderungen in der Sterinstruktur werden auch in den thermodynamischen Eigenschaften widergespiegelt. Obwohl die allgemeinen thermodynamischen Merkmale aller Sterine ausser Lanosterin qualitativ gleich zu sein scheinen, finden sich kleinere Unterschiede, wie z.B. das Verschwinden des Vorübergangs und die Erweiterung des zweiphasigen Bereichs. Darauf deuten die Unterschiede in den entsprechenden DSC- und PPC-Thermogrammen hin. Beim Vergleich mit Cholesterin und den anderen Sterinen sind die Unterschiede in der Mischbarkeit, im Temperatur-Konzentrations-Phasenverhalten und demzufolge in den thermodynamischen Funktionen $C_p(T)$ und $\alpha(T)$ für Lanosterin am auffälligsten. Die Änderungen in $C_p(T)$ spiegeln die entsprechenden $\alpha(T)$- Daten genau wieder; das ist ein Hinweis darauf, dass die Membranenthalpie und -volumenfluktuationen (Gleichungen 33a, 33c) durch die gleiche molekulare Ursache bestimmt werden. Die Zunahme an $C_p(T)$ und $\alpha(T)$ bei Phasenänderungen ist hauptsächlich mit kooperativen Fluktuationen einer grossen Zahl von Lipidmolekülen verknüpft. Die Schärfe der Übergänge ist mit der Korrelationslänge dieser Fluktuationen verknüpft, welches der Grösse der Domänen der koexistierenden Phasen entspricht. Mit zunehmender Sterinkonzentration nehmen die Weiten beider thermodynamischer Parameter bei den Kettenschmelz-Übergängen drastisch zu, was auf gekoppelte Enthalpie- und Volumenfluktuationen mit niedriger Amplitude bei grossen Korrelationslängen über einen erweiterten Temperaturbereich hindeutet.

Die grosse Querschnittsfläche des Steroid-Ringsystems von Lanosterin macht dieses zu einem effektiveren Raumausfüller als DPPC-Moleküle in der Doppelschicht im Gelzustand und gleicht daher die Fehlanpassung zwischen den Querschnittsflächen der

Acyl-Ketten und den polaren DPPC-Kopfgruppen bei niedrigen Sterinkonzentrationen effizienter aus als Cholesterin. Außerdem wäre zu erwarten, dass die rauere Oberfläche der Lanosterin-Moleküle einen größeren Beitrag zur Orientierungs-Fehlordnung in den benachbarten Phospholipid-Acyl-Seitenketten liefert, und somit die Expansion der DPPC-Doppelschicht im Gelzustand noch steigert, welches wiederum zu merklich grösseren α-Werten für das beobachtete System führt.

In einer anderen Studie wurde Gramicidin D (gD) mit molaren Anteilen von bis zu 10% in eine DPPC-Doppelschicht eingebaut. Insertion von Gramicidin in DPPC-Doppelschichten hat einen signifikanten Einfluss auf die Struktur, sowie das Temperatur- und Druck-Phasenverhalten der Lipid-Doppelschicht. Es wurde die Temperaturabhängigkeit des Expansionskoeffizienten α, der Volumenfluktuationen, sowie der isothermalen Kompressibilitäten von DPPC – gD Doppelschichten in deren verschiedenen Übergangsphasen mithilfe von kalorimetrischen (PPC und DSC), sowie molekular-akkustischen (Ultraschall-Geschwindigkeit und Densitometrie) Methoden bestimmt. Zusätzlich wurden entsprechende DSC-Messungen durchgeführt. Hierbei wurde ein erheblicher Einfluss von gD auf die thermodynamischen, mechanischen und Volumen- und Kompressibilitäts- Eigenschaften der DPPC-Doppelschicht festgestellt.

Anhand des Thermogramms, welches in Abb. 3.8 dargestellt ist, wird ersichtlich, dass Gramicidin auch oberhalb des molaren Anteils von 10% in die Membran eingebaut werden kann. Im DSC-Thermogramm sind bei einer Konzentration von 5 mol% zwei endotherme Übergänge deutlich vorhanden: ein eher kooperativer, relativ intensiver Übergang bei 41°C und ein weniger kooperativer Übergang schwächerer Intensität bei ~24°C. Die Zugabe von 10 mol% des Peptids hat einen symmetrisch verbreiternden Effekt auf das Wärmekapazitätsprofil. Dieses kommt dadurch zustande, dass die Peptide, die zwischen den gelartigen und flüssigen Domänen lokalisiert sind, die Kooperativität des Schmelzübergangs erniedrigen. Da die flüssigen Lipide kürzer als die Lipide im Gelzustand sind, wäre nichtsdestotrotz eine bessere Anpassung der flüssigen Lipide an gD zu erwarten, und daher eine Verschiebung des C_p-Profils zu niedrigeren Temperaturen. Wird gD in DPPC-Schichten eingebaut, werden die Wärmekapazitätsprofile jedoch nur geringfügig zu niedrigeren Temperaturen verschoben und enthalten eine kleine Asymmetrie auf der Seite mit der niedrigen Temperatur. Somit

ist das Phasenverhalten von mit gD versetzten DPPC-Membranen einem Verhalten sehr ähnlich, welches für ein Peptid zu erwarten wäre, das sowohl in der Gel-, als auch in der flüssigen Phase aggregiert, mit einer leichten Bevorzugung der flüssigen Phase.

Sowohl das Peakmaximum des thermischen Expansionskoeffizienten im Übergangsbereich als auch die relativen Volumenänderungen nehmen mit steigender gD-Konzentration ab. $\Delta v°$ wurde für reines DPPC beim Gel/flüssig-Phasenübergang auf ~0.045 bestimmt, was einer Zunahme des Volumens der Doppelschicht um ~4% entspricht. Das partielle spezifische Volumen $v°$ und der adiabatische Kompressibilitätskoeffizient des Lipids β_S^{lipid} nehmen zumindest innerhalb des untersuchten Konzentrationsbereichs mit zunehmender Gramicidin-Konzentration kontinuierlich ab. Weiterhin wurde festgestellt, dass im gesamten untersuchten Temperaturbereich bei größeren gD-Konzentrationen als 5 mol% der isotherme Kompressibilitätskoeffizient β_T^{lipid} im gel-flüssig-Bereich ca. 10-20% größer als β_S^{lipid} ist. Der Maximalwert der relativen Volumenfluktuation von 12% wird für DPPC beim Hauptübergang erreicht, und wird bei Zugabe von gD stark reduziert. Bei gD-Konzentrationen zwischen 1 und 10 mol% wurde nur eine graduelle Verminderung der berechneten relativen Volumenfluktuationen beobachtet. Am Schmelzpunkt sind die Fluktuationen maximal, wohingegen die Wärmekapazität, die Expansivität und die Kompressibilität proportional zu den lokalen Fluktuationen sind.

Auf Seite der niedrigen Temperatur des Wärmekapazitätsprofils weist eine Schulter auf eine unvorteilhafte Aufspaltung der Tieftemperaturphase hin. Die kalorimetrischen Daten weisen hingegen darauf hin, dass in der Gel-Phase von DPPC ein Mischen mit gD nachteilig ist. Diese Tatsache liegt in dem Unterschied zwischen den hydrophoben Kernen des Gramicidins und der DPPC-Doppelschicht begründet (Konzept der hydrophoben Anpassung).

Melittin hat sich als Quelle der Inspiration bei der Entwicklung neuartiger antiviraler und antibakterieller Agentien herausgestellt, welche auf Membranebene tödlich für die Erreger wirken, indem sie Löcher hervorrufen. Daher sind aufgrund des weit verbreiteten Auftretens dieses Motivs detailliertere Informationen über die

volumetrischen und thermodynamischen Eigenschaften von Melittin in Membranen von Bedeutung.

In dieser Arbeit wurden detaillierte Erkenntnisse über das volumetrische, thermodynamische und mechanische Verhalten von Melittin-DPPC-Doppelschichten in der Umgebung der Phasenumwandlungstemperatur mithilfe von kalorimetrischen und molekular-akustischen Methoden hinzugewonnen, was einen tieferen Einblick in den molekularen Mechanismus der membranauflösenden Aktivität (Lyse) von Melittin auf DPPC-Membranen zulässt.

Anhand der kalorimetrischen Messungen wurde gezeigt, dass der Einbau von Melittin (bis zu 1.25%) in die Lipid-Doppelschichten den Vorübergang verschwinden lässt. Bemerkenswert ist, dass bis zu 2.5% Melittin keine Verschiebung der Übergangstemperatur stattfindet, aber bei einer Konzentration von 3.75% mehr als eine Schulter auf Seiten der niedrigen Temperatur des Peaks und eine leichte Verschiebung von T_m zu 32 °C hin auftritt. Es wurde gezeigt, dass die Struktur der Melittin-Poren vom thermodynamischen Zustand der Membran abhängt.

Im Hauptübergangsbereich nimmt die Peakhöhe von α mit zunehmender Melittinkonzentration ab und der Peak verbreitert sich merklich. Bei der Schmelztemperatur T_m wurde wiederum eine generelle Zunahme der Geschwindigkeitszahl $[u]$ im Vergleich zu der des reinen Lipids festgestellt. Bei 3.75% Melittin wird jedoch im Vergleich zum reinen Lipid der breiteste Peak und niedrigste $[u]$-Wert beobachtet, was auf die auflösende Eigenschaft des Melittins zurückzuführen sein kann. Das Senkenminimum nimmt mit abnehmender Melittinkonzentration weiterhin zu, und erreicht seinen Höchstwert bei 1.25 mol% und 1 mol%.

Der Melittin-Konzentrations-Effekt auf $\nu°$ und β_S^{lipid} der Doppelschicht äussert sich durch eine leichte Verschiebung zu niedrigen Temperaturen im T_m-Bereich und eine kontinuierliche Zunahme von $\nu°$ (im untersuchten Konzentrationsbereich) oberhalb von Tm mit zunehmender Konzentration, außer zwischen 1 und 1.25%. Gleichermaßen ist eine Abnahme von β_S^{lipid} mit abnehmender Melittin-Konzentration. Es wurde festgestellt, dass der isotherme Kompressibilitäts-Peak beim Hauptübergang bei Zugabe von der niedrigen Melittin-Konzentration von 1 mol% drastisch abfällt und dann mit zunehmender gD-Konzentration wieder ansteigt. Weiterhin zeigte sich, dass β_T^{lipid} bei

allen Melittinkonzentrationen um ~20% grösser als β_S^{lipid} im gel-flüssig-Bereich über den gesamten untersuchten Temperaturbereich ist. Mit zunehmender Melittin-Konzentration wurde nur eine leichte Abnahme der berechneten relativen Volumenfluktuation im Konzentrationsbereich zwischen reinem DPPC und 1.0 mol% Melittin beobachtet.

Generell können Peptide in biologischen sowie in Modell-Membranen den lokalen Zustand des Systems stark beeinflussen, und der Effekt des Peptids kann auch vom Gesamtzustand der Membran abhängen. Deshalb kann der Zustand der Membran ein regulierender Faktor der Aktivität von antibiotischen Peptiden wie Melittin sein, da sie deren Fähigkeit beeinflussen, Transmembranporen auszubilden.

REFERENCES

Allende D.; S. A. Simon and T. J. McIntosh. 2005. Melittin-induced bilayer leakage depends on lipid material properties: evidence for toroidal pores. *Biophys J.* 88:1828-1837.

Bachar, M. and O. Becker. 2000. Protein-induced membrane disorder: A molecular dynamics study of melittin in a dipalmitoylphosphatidylcholine Bilayer. *Biophy. J.* 78:1359-1375.

Bacia, K.; P. Schwille and T. Kurzchalia. 2005. Sterol structure determines the separation of phases and the curvature of the liquid-ordered phase in model membranes. *Proc. Natl. Acad. Sci. USA.* 102:3272-3277.

Baghian, A.; J. Jaynes; F. Enright and K. Kousoulas. 1997. An amphipatic $\propto$-helical synthetic peptide analogue of melittin inhibits herpes simplex virus-1 (HSV-1)-induced cell fusion and virus spread. *Peptides*, 18:177-183.

Baker K. J.; J. M. East and A. G. Lee. 1995. Mechanism of inhibition of the Ca2+-ATPase by melittin. *Biochemistry,* 34:3596-3604.

Baumgart, T.; S. T. Hess and W. W. Webb. 2003. Imaging coexisting fluid domains in biomembrane models coupling curvature and line tension. *Nature*, 425:821-824.

Bechinger, B. 1997. Structure and functions of channel-forming peptides: Magainins, cecropins, melittin and alamethicin. *J. Membr.Biol.* 156:197-211.

Bernsdorff, C. and R. Winter. 1996. The effect of temperature and pressure on structural and dynamic properties of phospholipids/sterol: A steady-state and time-resolved fluorescence anisotropy study. *Z. Phys. Chem.* 193:151-173.

Bernsdorff, C.; A. Wolf and R. Winter. 1997. Effect of hydrostatic pressure on water penetration and rotational dynamics in phospholipid-cholesterol bilayers. *Biophys. J.* 71:1264 -1277.

Bernsdorff, C. and R. Winter. 2003. Differential properties of the sterols cholesterol, ergosterol, β-sitosterol, *trans*-7-dehydrocholesterol, stigmasterol and lanosterol on DPPC bilayer order. *J. Phys. Chem. B.* 107:10658-10664.

Bloch, K. 1985. *Cholesterol, evolution of structure and function. In:* Biochemistry of Lipids and Membranes, Eds. J. E. Vance and D. E. Vance, Benjamin/Cummins Pub. Co. Inc., New York, pp. 1-24.

Bourinbaiar, A. S. and C. F. Coleman. 1997. The effect of gramicidin, a topical contraceptive and antimicrobial agent with anti-HIV activity, against herpes simplex viruses type 1 and 2 in vitro. *Arch Virol.* 142:2225-2235.

Böttner, M. and R. Winter. 1993. Influence of the local anesthetic tetracaine on the phase behavior and the thermodynamic properties of phospholipid bilayers. *Biophys. J. 65*:2041-2046.

Bradrick, T. D.; A. Philippetis and S. Georghiou. 1995. Stopped-flow fluorometric study of the interaction of melittin with phospholipid bilayers: Importance of the physical state of the bilayer and the acyl chain length. *Biophys. J.* 69:1999-2010.

Bradshaw, J. P.; C. E. Dempsey and A. Watts. 1994. A combined x-ray and neutron diffraction study of selectively deuterated melittin in phospholipid bilayers: Effect of pH. *Mol. Membr. Biol.* 11:79-86.

Brown, D. A. and D. London. 1998. Functions of lipid rafts in biological membranes. *Annu. Rev. Cell Dev. Biol.*, 14:111-136.

Burkhart, B. M. 1999. Gramicidin D conformation, dynamics and membrane ion transport. *Biopolymers* 51:129-144.

Cevc, G. and D. Marsh. 1987. *Phospholipid Bilayers*, John Wiley and Sons, New York.

Chalikian, T. V. 2003. Volumetric Properties of Proteins. *Annu. Rev. Biophys. Biomol. Struct.* 32:207-235.

Chattopadhyay, A.; S. S. Rawart; D. V. Greathouse; D. A. Kelkar and R. E. Koeppe II. 2008. Role of tryptophan residues in gramicidin channel organisation and function. *Biophys. J.* 95:166-175.

Clague M. J. and R. J. Cherry. 1988. Comparison of p25 presequence peptide and melittin. Red blood cell haemolysis and band 3 aggregation. *Biochem J.* 252:791-794.

Cooper, A. 1984. Protein fluctuations and the thermodynamic uncertainty principle. *Prog. Biophys. Molec. Biol.* 44:181-214.

DeGrado W. F.; G. F. Musso; M. Lieber; E. T. Kaiser and F. J. Kezdy.1982. Kinetics and mechanism of hemolysis induced by melittin and by a synthetic melittin analogue. *Biophys J.* 37:329-338.

Demel, R. A. and B. de Kruyff. 1976. The preferential interaction of cholesterol with different classes of phospholipids. *Biochim. Biophys. Acta* 457:109-132.

Dempsey, C. E. 1990. The actions of melittin on membranes. *Biochim. Biophys. Acta.* 1031:143-161.

Dzwolak, W.; R. Ravindra; J. Lendermann and R. Winter. 2003. Aggregation of Bovine Insulin Probed by DSC/PPC Calorimetry and FTIR Spectroscopy. *Biochemistry* 42:11347-11355.

Ebel, H.; P. Grabitz and T. Heimburg. 2001. Enthalpy and volume changes in lipid membranes I. The proportionality of heat and volume changes in the lipid melting transition and its implication for the elastic constants. *J. Phys. Chem.* 105:7353-7360.

Edidin, M. 2003. The state of lipid rafts: From model membranes to cells. *Ann. Rev. Biophys. Biomol. Struct.* 32:257-283.

Eggers, F. and K. Kustin. 1969. Ultrasonic methods. *Methods Enzymol*. 16:55-80.

Eggers, F. and T. Funk. 1973. Ultrasonic measurements with millilitre liquid sample in the 0.5 – 100 MHz range. *Rev. Sci. Instr*. 44:969-978.

Eisenberg, D. and A. D. McLachlan. 1986. Solvation energy in protein folding and binding. *Nature (London)*. 319:199-203.

Eisenblätter, J. and R. Winter. 2006. Pressure effects on the structure and phase behaviour of DMPC-Gramicidin lipid bilayers: A synchrotron SAXS and ^{2}H-Nmr spectroscopy study. *Biophys. J*. 90:956-966.

Eyster, K. M. 2007. The membrane and lipids as integral participants in signal transduction. *Adv. Physiol. Edu*. 31:5-16.

Faucon, J-F.; J-M. Bonmatin; J. Dufourcq and E. Dufourc. 1995. Acyl chain length dependence in the stability of melittin-phosphatidylcholine complexes. A light scattering and 31P-NMR study. *Biochim. Biophys. Acta*. 1234:235-243.

Finegold, L.1993.*Cholesterol in Membrane Models*, CRC Press, Boca Raton, Florida.

Ge, M. T. and J. H. Freed. 1999. Electron spin resonance study of aggregation of gramicidin in dipalmitoylphosphatidylcholine bilayers and hydrophobic mismatch. *Biophys. J*. 76:264-280.

Glowka, M. L.; A. Olzzak; J. Bojarska; M. Szczesio; W. L. Duax; B. M. Burkhart; W. A. Pangborn; D. A. Langs and Z. Wawrzak. 2005. Structure of gramicidin D-Rbcl complex at atomic resolution from low–temperature synchrotron data: interactions of double-stranded gramicidin channel contents and cations with channel wall. *Biological crystallography* 61:433-441.

Grabitz, P.; V. P. Ivanova and T. Heimburg. 2002. Relaxation kinetics of lipid membranes and its relation to the heat capacity. *Biophys. J*. 82:299-309.

Habermann, E. 1972. Bee and wasp venoms. *Science*. 177:314-322.

Haines, T. H. Do. 2001. sterols reduce proton and sodium leaks through lipid bilayers? *Prog. Lipid Res.*, 40:299-324.

Heerklotz, H. and J. Seelig. 2002. Application of pressure perturbation calorimetry to lipid bilayers. *Biophys. J*. 82:1445-1452.

Heerklotz, H. and A. Tsamaloukas. 2006. Gradual change or phase transition - characterization of fluid lipid-cholesterol membranes on the basis of thermal volume changes *Biophys. J*. 91:600-607.

Heimburg, T. 1998. Mechanical aspects of membrane thermodynamics. Estimation of the mechanical properties of lipid membranes close to the chain melting transition from calorimetry. *Biophys. Biochim. Acta*. 1415:147-162.

Heimburg, T. and D. Marsh. 1996. Thermodynamics of the interaction of proteins with lipid membranes. *In* Biological Membranes: A Molecular Perspective from Computation and Experiment. K. M. Merz, and B. Roux. editors. Birkhauser, Boston. 405-462.

Hianik, T. and V. I. Passechnik. 1995. Bilayer Lipid Membranes: Structure and Mechanical Properties, Kluwer Academic, Dordrecht/ Boston/London.

Higashino, Y.; A. Matsui and K. Ohki. 2001. Membrane fusion between liposomes composed of acidic phospholipids and neutral phospholipids induced by melittin: A differential scanning calorimetric study. *J. Biochem.* 130:393-397.

Hill, T. L. 1960. An Introduction to Statistical Thermodynamics. Dover, New York.

Hsueh, Y. –W.; K. Gilbert; C. Trandum; M. Zuckermann and J. Thewalt. 2005. The effect of ergosterol on dipalmitoylphosphatidylcholine bilayers: A deuterium NMR and calorimetric study *Biophys. J*. 88:1799-1808.

Hui S. W.; C. M. Stewart and R. J. Cherry. 1990. Electron microscopic observation of the aggregation of membrane proteins in human erythrocyte by melittin. *Biochim Biophys Acta* 1023:335-340.

Ipsen, J.; O. G. Mouritsen and M. Bloom. 1990. Relationships between lipid membrane area, hydrophobic thickness, and acyl-chain orientational order. The effects of cholesterol. *Biophys. J*. 57:405-412.

Israelachvili, J. N.; S. Marcelja and R. G. Horn. 1980. Physical principles of membrane organization. *Q Rev Biophys*, 13(2):121-200.

Ivanova, V. P. and T. Heimburg. 2001. Histogram method to obtain heat capacities in lipid monolayers, curved bilayers, and membranes containing peptides. *Phys. Rev.,* E63:1914-1925.

Ivanova, P. T.; S. B. Milne; M. O. Byrne; Y. Xiang and H. A. Brown. 2007. Glycerophospholipid identification and quantitation by electrospray ionization mass spectrometry. *Meth. Enzymol.* 432:21-57.

Ivanova, V. P.; I. M. Makarou; T. E. Schäffer and T. Heimburg. 2003. Analysis, heat capacity profile of peptide containing membranes cluster formation of gramicidin A. *Biophys. J.* 84:2427-2439.

Iwadate M.; T. Asakura and M. P. Williamson.1998. The structure of the melittin tetramer at different temperatures. An NOE-based calculation with chemical shift refinement. *Eur J. Biochem* 257:479-487.

Jahnig F. 1981. Critical effects from lipid-protein interaction in membranes. *Biophys. J.* 36:329-345.

Kaatze, U.; B. O'Driscoll, E. Hanke, M. Jäger, and V. Buckin. 2006. Ultrasonic calorimetry of membranes. *Pharmaceutical Technology Europe.* 01 September: 1-5.

Kharakoz, D. P.; A. Colotto; K. Loher and P. Laggner. 1993. Fluid-gel interphase line tension and density fluctuations in dipalmitoylphosphatidylcholine multilamellar vesicles: an ultrasonic study. *J. Phys. Chem*. 97:9844-9851.

Killian, J. A. 1992. Gramicidin and gramicidin-lipid interactions. *Biochim Biophys. Acta* 1113:391-425.

Kratky, O.; H. Leopold and H. Stabinger. 1973. The determination of partial specific volume of protein by the mechanical oscillator technique. *Methods Enzymol*. 27:98-110.

Krivanek, R.; P. Rybar; E. J. Prenner and R. E. McElhaney. 2001. Interaction of the antimicrobial peptide gramicidin S with dimyristoyl-phoshatidyl choline bilayer membranes: A densitometry and sound velocimetry study *Biochim. Biophys. Acta* 1510:452-463.

Krivanek, R.; L. Okoro and R. Winter. 2008. Effect of cholesterol and ergosterol on the compressibility and volume fluctuations of phospholipid-sterol bilayers in the critical point region – A molecular acoustic and calorimetric study. *Biophys. J*. 94:3538-3548.

Kujawa, P. and F. M. Winnik. 2001. Volumetric studies of aqueous polymer solutions using pressure perturbation calorimetry: A new look at the temperature-induced phase transition of poly(N-Isopropylacrylamide) in water and D_2O. *Macromolecules* 34:4130.

Kusumi, A.; M. Tsuda; T. Akino; O. Ohnishi and Y. Terayama. 1983. Protein-phospholipid-cholesterol interaction in the photolysis of invertebrate rhodopsin. *Biochemistry*, 22:1165-1170.

Lad, M.; F. Birembaut; L. Clifton; R. Frazier; J. Webster and R. Green. 2007. Antimicrobial Peptide-Lipid Binding Interactions and Binding Selectivity. *Biophys. J.* 92:3575-3586.

Ladokhin, A., and S. White. 1999. Folding of amphiphilic $\propto$-helices on membranes:

Energetics of helix formation by melittin. *J. Mol. Biol*. 285:1363-1369.

Lewis, R. N. A. H.; E. J. Prenner; L. H. Kondejewski; C. R. Flash; R. Mendelsohn; R. S. Hodges and R. N. McElhaney. 1999. Fourier transform infrared spectroscopic studies of the interaction of Antimicrobial peptide Gramicidin S with micelles and with lipid monolayer and bilayer membranes. *Biochemistry.* 38:15193-15203.

Lin, J-H. and A. Baumgaertner. 2000. Stability of a Melittin Pore in a Lipid Bilayer: A Molecular Dynamics Study. *Biophys. J.* 78:1714-1724.

Lin, L. N.; J. F. Brandts; J. M. Brandts and V. Plotnikov. 2002. Determination of the volumetric properties of proteins and other solutes using pressure perturbation calorimetry. *Anal. Biochem.* 302:144-160.

MacDonald, R. C.; R. I. MacDonald; B. P. M. Menco; K. Takeshita; N. K. Subbarao and L.-R. Hu. 1991. Small-volume extrusion apparatus for preparation of large unilamellar vesicles. *Biochim. Biophys. Acta.* 1061:297-303.

Mannock, D. A.; R. N. A. H. Lewis and R. N. McElhaney. 2006. Comparative calorimetric and spectroscopic studies of the effects of lanosterol and cholesterol on the thermotropic phase behavior and organization of dipalmitoylphosphatidylcholine bilayer membranes. *Biophys. J.* 91:3327-3340.

Matsuzaki K.; S. Yoneyama and K. Miyajima. 1997. Pore formation and translocation of melittin. *Biophys J.* 73:831-838.

McMullen, T. P. W.; R. N. A. H. Lewis and R. N. McElhaney. 1994. Comparative differential scanning calorimetric and FTIR and 31P-NMR spectroscopic studies of the effects of cholesterol and androstenol on the thermotropic phase behavior and organization of phosphatidylcholine bilayers. *Biophys. J.* 66:741-752.

McMullen, T. P. W. and R. N. McElhaney. 1995. New aspects of the interaction of cholesterol with dipalmitoylphosphatidylcholine bilayers as revealed by high-sensitivity differential scanning calorimetry. *Biochim. Biophys. Acta* 1234:1025-1035.

McMullen, T. P. W.; R. N. A. H. Lewis and R. N. McElhaney. 1993. Differential scanning calorimetric study of the effect of cholesterol on the thermotropic phase behavior of a homologous series of linear saturated phosphatidylcholines. *Biochemistry* 32:516-522.

Melchior, D. L.; F. J. Scavitto and J. M. Steim. 1980. Dilatometry of dipalmitoyllecithin-cholesterol bilayers. *Biochemistry* 19:4828-4834.

Miao, L.; M. Nielsen; J. Thewalt; J. H. Ipsen; M. Bloom; M. J. Zuckermann and O. G. Mouritsen. 2002. From lanosterol to cholesterol: Structural evolution and differential effects on lipid bilayers. *Biophys. J.* 82:1429-1444.

Mitaku, S.; A. Ikegami and A. Sakanishi. 1978. Ultrasonic studies of lipid bilayer phase transition in synthetic phosphatidylcholine liposomes. *Biophys. Chem.* 8:295-304.

Mitaku, S. and T. Data. 1982. Anomalies of nanosecond ultrasonic relaxation in the lipid bilayer transition. *Biophys. Biochim. Acta*. 688:411-421.

Mitra, L.; N. Smolin; R. Ravindra; C. Royer; R. Winter. 2006. Pressure perturbation calorimetric studies of the solvation properties and the thermal unfolding of proteins in solution: experiments and theoretical interpretation *Phys. Chem. Chem. Phys.* 8:1249-1265.

Monette, M. and M. Lafleur. 1995. Modulation of melittin-induced lysis by surface charge density of membranes. *Biophys. J.* 68:187-195.

Monette, M., and M. Lafleur. 1996. Influence of lipid chain unsaturation on melittin-induced micellization. *Biophys. J.* 70:2195-2202.

Morrow, M. R.; J. Davis; F. Sharom and M. Lamb. 1986. Studies on the interaction of human erythrocyte band 3 with membrane lipids using deuterium nuclear magnetic resonance and differential scanning calorimetry. *Biochim. Biophys. Acta*. 858:13-20.

Mouritsen, O. G. and M. J. Zuckermann. 2004. What's so special about cholesterol? *Lipids* 39:1101-1113.

Munro, S. 2003. Lipid rafts: elusive or illusive? *Cell*, 115(4): 377-88.

Orädd, G., and G. Lindblom. 2004. Nmr studies of lipid lateral diffusion in the DMPC/gramicidin D/water system: peptide aggregation and obstruction effects. *Biophys. J.* 87:980-987.

Okoro, L. and R. Winter. 2008. Pressure Perturbation Calorimetric Studies on Phospholipid-Sterol Mixtures. *Z. Naturforsch.* 63b:769-778.

Oliynyk, V.; U. Kaatze and T. Heimburg. 2007. Defect formation of lytic peptides in lipid membranes and their influence on the thermodynamic properties of the pore environment. *Biochim. Biophys. Acta* 1768:236-245.

Osdol, V. W. W.; M. L. Johnson; Q. Ye and R. L. Biltonen. 1991. Relaxation dynamics of the gel to liquid-crystalline transition of phosphatidylcholine bilayers. Effects of chain length and vesicle size. *Biophys. J.* 59:775-785.

Osdol, V. W. W.; R. L. Biltonen, and M. L. Johnson. 1989. Measuring the kinetics of membrane phase transition. *J. Bioenerg. Biophys. Methods*. 20:1-46.

Pawlak, M.; S. Stankowski and G. Schwarz. 1991. Melittin induced voltage-dependent conductance in DOPC lipid bilayers. *Biochim. Biophys. Acta.* 1062:94-102.

Privalov, P. L. 1980. Scanning microcalorimeters for studying macromolecules. *Pure Appl. Chem.* 52:479-497.

Raghuraman, H. and A. Chattopadhyay. 2004. Interaction of melittin with membrane cholesterol: A fluorescence approach. *Biophys. J.* 87:2419-2432.

Raghuraman H. and A. Chattopadhyay. 2005. Cholesterol inhibits the lytic activity of melittin in erythrocytes. *Chem Phys Lipids.* 134:183-189.

Rapaport D.; R. Peled; S. Nir and Y. Shai. 1996. Reversible surface aggregation in pore formation by pardaxin. *Biophys J.* 70:2502-2512.

Ravindra, R. and R. Winter. 2003. On the temperature-pressure free-energy landscape of proteins. *ChemPhysChem.* 4:359-365.

Raynor R. L.; B. Zheng and J. F. Kuo. 1991. Membrane interactions of amphiphilic polypeptides mastoparan, melittin, polymyxin B, and cardiotoxin. Differential inhibition of protein kinase C, Ca2+/calmodulindependent protein kinase II and synaptosomal membrane Na,K-ATPase, and Na+ pump and differentiation of HL60 cells. *J Biol Chem.* 266:2753-2758.

Rex S. 1996. Pore formation induced by the peptide melittin in different lipid vesicle membranes. *Biophys Chem* 58:75-85.

Rice, D. and E. Oldfield. 1979. Deuterium nuclear magnetic resonance studies of the interaction between dimyristoylphosphatidylcholine and gramicidin A. *Biochemistry.* 18:3272-3279.

Risley, J. M. 2002. Cholesterol Biosynthesis: Lanosterol to Cholesterol. *J. Chem. Ed.*, 79:377-384.

Rudenko S. V. and S. V. Patelaros. 1995. Cation-sensitive pore formation in dehydrated erythrocytes. *Biochim Biophys Acta* 1235:1-9.

Russell, D. W., and K. D. Setschell. 1992. Bile acid biosynthesis. *Biochemistry*, 31:4737-4749.

Sankaram, M. and T. E. Thompson 1991. Cholesterol-induced fluid-phase immiscibility in membranes. *Proc. Natl. Acad. Sci. USA,* 88:8686-8690.

Schoonjans, K.; C. Brendel; D. Mangelsdorf and J. Anxwerx. 2000. Sterols and gene expression: Control of affluence. *Biochim. Biophys. Acta*, 1529:114-125.

Seeger, H. M.; M. L. Gudmundsson and T. Heimburg. 2007. The influence of anaesthetics, neurotransmitters and antibiotics on the reaction process in lipid membranes. Physics. *J. Phys. Chem B*. 111:13858-13866.

Seemann, H. and R. Winter. 2003. Volumetric properties, compressibilities and volume fluctuations in phospholipid-cholesterol bilayers. *Z. Phys. Chem.* 217:831-846.

Sessa, G.; J. H. Freer; G. Colacicco and G. Weissmann. 1969. Interaction of a lytic polypeptide, melittin, with lipid membrane systems. *J. Biol. Chem*. 244:3575-3582.

Schrader, W.; H. Ebel; P. Grabitz; E. Hanke; T. Heimburg; M. Hoeckel; M. Kahle; F. Wente and U. Kaatze. 2002. Compressibility of Lipid mixtures studied by calorimetry and ultrasonic velocity measurements. *J. Phys. Chem*. 106:6581-6586.

Short, K. W.; B. A. Wallace; R. A. Myers; S. P. A. Fodor and A. K. Dunker. 1987. Comparison of lipid/gramicidin dispersion and co-crystals by Roman scattering. *Biochemistry*. 26:557-562.

Silvius, J. R. 2003. Role of cholesterol in lipid raft formation: lessons from lipid model systems. *Biochim. Biophys. Acta*, 1610:174-183.

Simons, K., and D. Toomre. 2000. Lipid rafts and signal transduction. *Nature Rev. Mol. Cell Biol.*, 1:31-39.

Smirnovas, V.; R. Winter; T. Funck and W. Dzwolak. 2006. Protein Amyloidogenesis in the Context of Volume Fluctuations: A Case Study on Insulin *ChemPhysChem* 7:1046-1049.

Spiller, G. A. 2006. Handbook of Lipids in Human Nutrition, Boca Raton: CRC Press.

Stanley, H. E. 1971. Introduction to Phase Transitions and Critical Phenomena. Oxford University Press, NY.

Stuehr, J., and E. Yeager. 1965. The Propagation of Sound in Electrolytic Solutions. *In* Physical Acoustics. Vol. 2A. W. P. Mason. editor. Academic Press, NY.

Szule, J. A., and R. P. Rand. 2003. The effects of gramicidin on the structure of phospholipid assemblies. *Biophys. J.* 85:1702-1712.

Teng, Q., and S. Scarlata. 1993. Effect of high pressure on the association of melittin to membranes. *J. Biol. Chem.*, 268:12434-12442.

Terwilliger, T.; L. Weissman and D. Eisenberg. 1982. The structure of melittin in the form I crystals and its implication for melittin's lytic and surface activities, *Biophys. J.* 37:353-361.

Tosteson M. T. and T. C. Tosteson. 1981. The sting. Melittin forms channels in lipid bilayers. *Biophys J.* 36:109-116.

Tosteson, M. T.; S. J. Holmes; M. Razin and D. C. Tosteson. 1985. Melittin lysis of red cells. *J. Membr. Biol.* 87:35-44.

Troiano, G. C.; K. J. Stebe; R. M. Raphael and L. Tung. 1999. The effects of gramicidin on electroporation of lipid bilayers. *Biophys. J.* 76:3150-3157.

Unger, T.; Z. Oren and Y. Shai. 2001. The effect of cyclization of magainin 2 and melittin analogues on the structure, function, and model membrane interactions: Implication to their mode of action. *Biochemistry*, 40:6388-6397.

Vance, D. E. and H. Van den Bosch. 2000. Cholesterol in the year 2000. *Biochim. Biophys. Acta* 1529:1-8.

Vist, M. R. and J. H. Davis. 1990. Phase equilibria of cholesterol/ dipalmitoylphosphatidylcholine mixtures: ^{2}H-nuclear magnetic resonance and differential scanning calorimetry. *Biochemistry* 29:451-464.

Wang, X. 2004. Lipid signalling. *Curr. Opin. Plant Biol.* 7 (3): 329-36.

Wilcox W. and D. Eisenberg. 1992. Thermodynamics of melittin tetramerization determined by circular dichroism and implications for protein folding. *Protein Sci* 1:641-653.

Wilson, A. H. 1957. Thermodynamics and statistical mechanics. Cambridge University Press, Cambridge.

Winter, R.; A. Gabke; C. Czeslik and P. Pfeifer. 1999. Power-law fluctuations in phase-separated lipid membranes. *Phys. Rev.* E. 60:7354-7359.

Woolf, T. B. and B. Roux. 1994. Molecular dynamic simulations of the gramicidin channel in a phospholipid bilayer. *Proc. Natl. Acad. Sci. USA*. 91:11631-11635.

Woolf, T. B. and B. Roux. 1996. Structure, energetics and dynamics of lipid-protein interactions: a molecular dynamics study of the gramicidin A channel in a DMPC bilayer. *Proteins* 24:92-114.

Yeagle, P. L. 1985. Cholesterol and the cell membrane. *Biochim. Biophys. Acta* 822:267-287.

Zein, M. and R. Winter. 2000. Effect of temperature, pressure and lipid acyl-chain length on the structure and phase behaviour of phospholipid-gramicidin Bilayers", *Phys. Chem. Chem. Phys.* 2:4545-4551.

Zhang, Y.-P.; R. N. A. H. Lewis; R. S. Hodges and R. N. McElhaney. 1995. Peptide models of helical hydrophobic transmembrane segments of membrane proteins. 2. Differential scanning calorimetric and FTIR studies of the interaction of Ac-K_2-$(LA)_{12}$-K_2-amide with phosphatidylcholine bilayers. *Biochemistry.* 34:2362-2371.

Zhao, O., and P. L. Polavarapu. 2001. Vibrational circular dichroism of gramicidin D in vesicles and micelles. *Biopolymers (Biospectroscopy).* 62:336-340.

Zuckermann, M. J.; J. H. Ipsen; L. Miao; O. G. Mouritsen; M. Nielsen; J. Polson; J. Thewalt; I. Vattulainen and H. Zhu. 2004. Modelling lipid-sterol bilayers: Application to structural evolution, lateral diffusion and rafts. *Methods in Enzymology* 383:198-229.

List of Abbreviations / Symbols

DSC	Differential Scanning Calorimetry
PPC	Pressure Perturbation Calorimetry
LUV	Large Unilamellar Vesicles
MLV	Multilamellar Vesicles
DPPC	1,2-dipalmitoyl-*sn*-glycero-3-phosphatidylcholine
7-DHC	7-Dehydrocholesterol
Chol	Cholesterol
Lan	Lanosterol
Ergos	Ergosterol
Stg	Stigmasterol
gD	Gramicidin D
AFM	Atomic Force Microscopy
URT	Ultrasonic Resonator Technology
ΔV	Absolute volume change
$\Delta V/V$	Relative volume changes
Eqn	Equation
α	Coefficient of thermal expansion
c	Concentration
C	Molar concentration
M	Mass
Tm	Melting temperature
β_S^{lipid}	Adiabatic compressibility coefficient of lipid
k_S^{o}	Partial specific adiabatic compressibility
$[u]$	Velocity number,
ν^{o}	Partial specific volume
β_T^{lipid}	Isothermal compressibility coefficient of lipid
ΔH	Enthalpy change

Lebenslauf

Persönliche Daten

Name: Linus Okoro

Geburtsdaten: 07.02.1973

Nationalität   Nigerianish

Schulausbildung

09/1979 – 07/1985	Gruppe Schule, Umuokrika
09/1985 - 08/1991	Gymnasium USTS, Ekwerazu, Mbaise

Studium

02/1993 - 08/1998	Chemiestudium an der FUT, Owerri, Nigeria
10/2000 - 03/2002	Masterstudiengang, Universität Ibadan, Nigeria
04/2003 - 07/2005	Masterstudiengang, TU Braunschweig
10/2006 - z. Z	Promotion bei Prof. Dr. Winter an der Technischen Universität Dortmund

Berufspraxis

08/2005 – 08/2006	wissenschaftlicher Assistent an der Technischen Universität Dortmund
10/2006 - 12/2008	wissenschaftlicher Angestellte an der Technischen Universität Dortmund

Publikationen

- Roland Krivanek, <u>Linus Okoro</u>, Roland Winter. Effect of Cholesterol and Ergosterol on the compressibility and volume fluctuations of Phospholipid - Sterol bilayers in the critical region: A molecular acoustic and calorimetry study. *Biophys*. *J*. **2008**, 94: 3538 – 3548.

- <u>Linus Okoro</u>, Roland Winter. Presssure Perturbation Calorimetry Studies on Phospholipid – Sterol Mixtures. *Z. Naturforsch*. **2008**, *63b*: 769 - 778.